EVALUATION OF THE MECHANICAL BEHAVIOR OF A METAL–MATRIX DISPERSION FUEL FOR PLUTONIUM BURNING

A Thesis
Presented to
The Academic Faculty

By

Lee Van Duyn

In Partial Fulfillment
Of the Requirements for the Degree
Master of Science in Mechanical Engineering

Georgia Institute of Technology
November 2003

EVALUATION OF THE MECHANICAL BEHAVIOR OF A METAL–MATRIX DISPERSION FUEL FOR PLUTONIUM BURNING

Approved by:

Dr. Said I. Abdel–Khalik, Advisor

Dr. W. Jack Lackey

Dr. Suresh K. Sitaraman

Date Approved: 11 / 05 / 2003

DEDICATION

I'd like to dedicate this thesis to everyone that has been there to encourage me and help me along the way in the non-technical areas of this work. The perseverance and motivation that was required to complete this work in a timely manner was very much needed, and without you I could not have done it.

Thank you Mom, and Dad, and Ryan, and Bruce and Dawn. You will all be an important part of my life. I hope that this work, and all my future endeavors, as I was once taught, follow the words of Colosians 3:23 – very important words I need to live by.

I would also like to dedicate this to all those who devote their lives to making sure that the great power of nuclear reactions are used only for good, and not by evil. May the world never experience a nuclear holocaust as a result of this amazing technology.

Most importantly, "Thanks be to God for his indescribable gift!" (II Cor. 9:15).

ACKNOWLEDGEMENTS

I would like to thank a number of people for making this thesis research and graduate program possible. First, and foremost, I'd like to thank the United States Department of Energy who sponsors the Advanced Fuel Cycle Initiative University Fellowship program, of which I am so fortunate to be a part of. I did not know how lucky I was when I first was awarded the fellowship, and for it I am truly grateful, for without the available funds, this research and graduate degree would not have been possible.

I would also like to thank Mitch Meyer and Steve Hayes for allowing me to spend the summer working with them in Idaho, for I learned much more with them than I could have on my own. I also thank all the others there at ANL-W that assisted me in my research, especially Steve Hemingray for his PYTHON language skills, and the other interns that made it an experience I will not soon forget.

I am also grateful for the constant assistance that my advisor Prof. Abdel-Khalik provided whenever I ran into problems, or needed someone to comment on my written documents. His willingness to advise me was much appreciated.

I also want to thank Prof. Lackey and Prof. Sitaraman for further advising me on this thesis and further developing my skills professionally in their classes.

There are many others that deserve recognition that I can not fit on this page, so to them, you know who you are, thank you for your help, criticism and guidance in this research work.

TABLE OF CONTENTS

LIST OF TABLES

LIST OF FIGURES

SUMMARY

Recent nuclear proliferation concerns and disarmament agreements have encouraged the U.S. to decrease the excess amount of weapons-grade and reactor-grade plutonium. Continued use of nuclear power without a permanent solution for waste disposition has also led to the need for a reliable method by which the "waste" products, specifically plutonium, can be utilized or destroyed. One possible solution to plutonium destruction is achieved by manufacturing it into small microspheres and embedding it within an inert metal matrix, then placing it inside a conventional nuclear reactor. This process would burn some of the plutonium while producing electricity. PuO_2–Zr dispersion fuel has been proposed for such a purpose. Prior to its use, however, this non-fertile metal matrix dispersion fuel must be shown to be mechanically stable in the reactor environment.

The internal mechanical interactions of dispersion fuel were modeled using finite element analysis. The results were used to assess the stability of PuO_2–Zr dispersion fuel inside a reactor. Several parameters, including fuel particle size, volumetric loading, temperature, and burnup, were varied to determine the maximum amount of plutonium that can be burned while maintaining fuel integrity. Earlier experiments using UO_2 – stainless steel dispersion fuels were used to validate the model and establish a failure criterion. The validated model was then used to determine the parameter space over which PuO_2–Zr dispersion fuel can be successfully used. These results show that PuO_2–Zr dispersion fuel is robust and may offer a reliable method for plutonium disposal in current reactors.

CHAPTER 1 – INTRODUCTION

Nuclear power has been a reliable source of energy since it first began in the United States in 1951. Since then many changes have happened within the industry, and many of the components of reactors have evolved. Currently, nuclear power produces approximately 20% of the total power generated in the United States. Even though nuclear power has been successfully providing electricity over many years, the United States has yet to implement a permanent solution to the disposal of nuclear waste. In addition, recent nuclear proliferation concerns and disarmament agreements have encouraged the United States to decrease the inventory of weapons-grade and reactor-grade plutonium levels. As a result, this has led to the necessity of understanding how to effectively dispose of the "waste" plutonium. Many solutions have been proposed, from deep burial of the fuel in remote locations, to the recycling of the fuel materials. One potential solution to the problem of plutonium disposition is to burn the plutonium by using a metal-matrix dispersion fuel inside commercial nuclear reactors. This is accomplished by manufacturing the plutonium into small microspheres and embedding it within an inert metal-matrix, then placing it inside a conventional nuclear reactor (see figure 1.1). This process using a dispersion type metal-matrix nuclear fuel, specifically zirconium (Zr) as the matrix material (because of its low neutron capture cross-section), has the potential to burn most of the plutonium while producing electricity. A dispersion type nuclear fuel is similar in structure to a cermet or metal-matrix composite. The objective of this research is to evaluate the mechanical behavior of this type of fuel, and

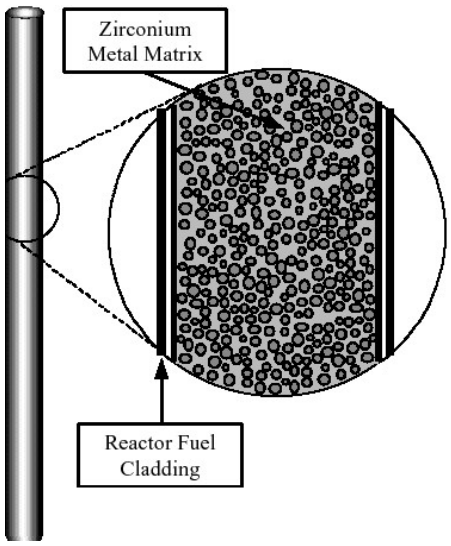

Figure 1.1 Example of a dispersion nuclear fuel [35]

to analyze the mechanical stability of this fuel when used in the proposed plutonium disposition application.

A finite element analysis computer code, ABAQUS, is used to model mechanical interactions within the fuel inside the reactor. To obtain an accurate analysis on this fuel, fuel burnup phenomena such as swelling, fission gas release, fission fragment damage, radiation embrittlement, and other interactions must be completely modeled. These characteristics can be simulated by using ABAQUS; however, several simplifying assumptions need to be made. Further details of the model and its assumptions are described in chapter 3. Once the model is completed, it must be verified by comparing it to previous experimental data and to the analytical solutions quantifying the effect of different nuclear fuel parameters (described in chapter 4). The primary variables that will be considered in the analysis of the mechanical behavior are: the stress and strain (including plastic strain), fuel swelling, and temperature profiles. Some of the variables that affect the stability of the fuel are: the burnup (fission density), the operating

temperature of the fuel, and the geometry of the fuel microspheres pertaining to the loading percentage, coating, and overall size and distribution within the matrix.

Thorough analysis of previous experimental data has led to the definition of a stability threshold that determines when this fuel type might fail inside a reactor. In the late 1950's and early 1960's, a great deal of research was conducted on various dispersion fuel forms, but primarily uranium dioxide in a stainless steel matrix (UO_2 – S.S.) [19]. More details of previous research in this area and an explanation of the benefits and drawbacks of dispersion fuels are discussed in chapter 2. Many of these tests were conducted using plate-type geometry for the dispersion fuel, a type of fuel that is currently used in a number of research reactors around the country. Since the overall geometry and failure mode of a plate-type fuel element differs from a cylindrical rod-type, much of the plate-type fuel experimental data is not usable for the current analysis. Figure 1.2 shows a cross-section of a plate-type fuel element. The drastic differences between the plate-type cross-section and the circular pellet-type cross-section can be seen.

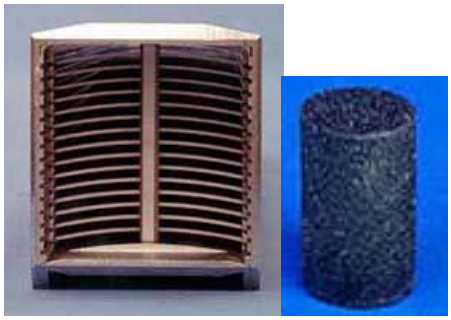

Figure 1.2. Comparison of Plate-type fuel vs. Pellet fuel

Although much of the experimental data for plate-type fuel elements is not applicable to current commercial reactor fuel designs, a few experimental tests have been done on the pellet-type geometry using UO_2 – S.S. that are useful in this proposed fuel study. In order to determine a failure criterion for the plutonium dioxide – zirconium (PuO_2 – Zr) dispersion fuel, the data points pertaining to pellet dispersion fuel are modeled under the same conditions as is described in the experiments in the literature. The stress, strain and swelling results from this model are the primary results analyzed. Using the experimental data from both the stable and unstable dispersion fuels in the finite element model, a comparison can be done between the results to determine the conditions that are the probable cause of fuel failure. From these results, a failure criterion is determined. Further details on the development of the failure criterion and the numerical results generated by the model are presented in section 5.1. Using this failure criterion allows prediction of the burnup and temperature range required for fuel stability within a reactor. Combining this failure criterion with the parametric studies described in section 5.2 allows for the optimization of this fuel and determination of what the operating limits of a fuel of this type might be. A more in depth explanation of PuO_2 – Zr dispersion fuel and the modeling results from that fuel are shown in section 5.3.

Further discussion and analysis of the modeling data from the PuO_2 – Zr fuel are included in section 5.4 while the final recommendations and conclusions of this research are found in chapter 6. This final chapter also addresses questions that are left open by the research and recommendations for future modeling work and experiments.

CHAPTER 2 – BACKGROUND

During the early days of nuclear energy development, a great deal of fuel-related research was conducted with the objective of determining the most desirable fuel form for commercial use [12]. The dispersion type nuclear fuel form was one of the fuels that was heavily studied in the late 1950's and early 1960's. With the resurgence of interest in potential new nuclear reactor types and nuclear waste transmutation, there has been a renewed interest in the dispersion fuel form. A dispersion nuclear fuel is defined to be "a solid nuclear fuel used in nuclear reactors distinguished by having a fissionable material dispersed as small particles through a nonfissionable matrix of metal, ceramic or graphite" [24]. The nonfissionable material is referred to as the matrix. The primary concept behind this fuel is to gain the combined benefits of the high strength, radiation stability, and thermal conductivity of the matrix (either metals, ceramics or graphite) in a radioactive and high temperature environment, while retaining the fissioning characteristic required to produce heat for nuclear reactors.

The environment inside of a nuclear fuel is very demanding; combining the effects of thermal and radiation enhanced diffusion, fission gas generation, high power density, and neutron, alpha, gamma, and heavy ion irradiation. If the fuel loses its integrity, fission products may be released into the reactor resulting in contamination. Preventing failure is a primary concern for nuclear fuel elements, and must be focused on in the design. This design of the fuel elements involves many complex interactions within the fuel that must be considered. A number of them are described in the next section.

2.1. General Fuel Phenomena

The fissioning that occurs inside a nuclear reactor is responsible for generating the heat that is subsequently transformed into electricity. On the other hand, it is also responsible for the harsh environment that the fuel must withstand, because it produces fission fragments, energetic neutrons, gamma rays and other types of radiation. The fission fragments and neutrons exchange this energy with the lattice atoms until they come to rest. The fission fragments, which are highly ionized (+20), move rapidly through the fuel material with a range of about 7 – 10 microns. Over this path, it excites atoms in a radius up to a 100-angstroms from the path center, consequently raising temperatures to thousands of degrees locally. This phenomenon is called a fission spike. Within each spike, many atoms are displaced from the lattice positions producing vacancies and interstitials. Studies indicate that about 55% of fission fragment energy goes toward ionization and excitation of atoms while 45% goes toward displacement damage [12].

The fission fragments consist of numerous different atoms and isotopes (for example: Mo, Tc, Rh, Ru, Pd, Cs, I, Br, Te, Xe, Kr and others) that cause many different problems. The most troublesome are the xenon and krypton, because these gases cause fuel swelling. These gases migrate (due to a temperature gradient) and build up within the fuel resulting in an overall expansion of the fuel. Fission gas release from the fuel occurs, and is a function of fuel type, temperature, fission rate, grain size and other variables. This gas release causes an additional pressure to be exerted on the cladding, causing it to rupture under extreme operating conditions or with poorly designed fuel.

Another problem is caused by fission product elements such as cesium, tellurium and oxygen that reduce the thermochemical stability of the outer cladding by corrosion and intergranular attack [38].

The generation of fission products results in an overall effect on fuel such that considerable stresses are produced. They are produced by the high temperatures and temperature gradients, the static and dynamic loads, fuel expansion, fission gas pressure, radiation embrittlement, and changes in other physical properties [44]. These complex interactions and internal stresses are difficult to model and understand on an atomistic scale, but can be adequately simulated as macroscopic effects on a more global scale. The way in which these interactions are modeled for the PuO_2–Zr fuel is described in chapter 3. Overall, some fuel types are better suited to withstand this type of environment than others; fortunately, the dispersion fuel type is a particularly well-suited candidate fuel.

2.2. Benefits and Drawbacks of Dispersion Fuel

There are many benefits to dispersion fuels in comparison to current commercial reactor fuel. Commercial fuel consists of uranium dioxide (UO_2) pellets encased in zirconium alloy cladding. The problem with a solid oxide fuel pellet is that the ceramic has a low thermal conductivity resulting in large temperature gradients, on the order of a thousand of degrees per centimeter, within the small pellet. The large temperature gradient causes migration of atoms and gas bubbles, resulting in structural changes in the fuel. The temperature gradients are responsible for cracking in the fuel, which further reduces the effective thermal conductivity. Figure 2.1 is a micrograph of the cross-

section of an irradiated porous oxide UO_2 fuel pellet showing multiple cracks and a central void. Metal-matrix dispersion fuel has a great advantage over the solid oxide fuel because it has many microspheres of oxide fuel particles spread throughout the metal-matrix pellet. These spheres are surrounded by a highly conductive metal, so the temperature gradients within the fuel are only on the order of tens of degrees per centimeter compared to the thousand of degrees per centimeter in solid oxide fuel pellets.

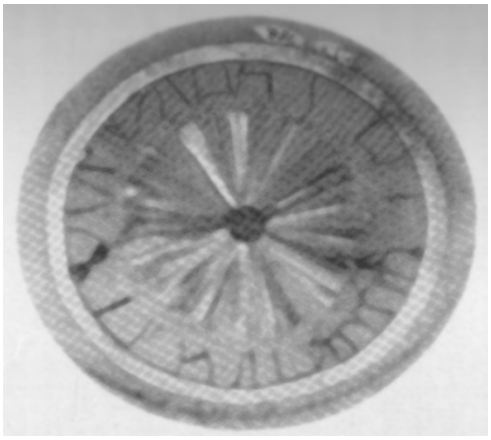

Figure 2.1. Cross-section of a solid oxide UO_2 fuel pellet [23]

Figure 2.2 shows thermal profiles of a typical solid oxide fuel pellet versus a metal-matrix dispersion (cermet) fuel pellet. The metal-matrix fuel is capable of much more efficient heat transfer within the fuel due to a much higher overall thermal conductivity than the solid oxide fuel pellet. The lower operating temperature and temperature gradient result in more robust fuel performance.

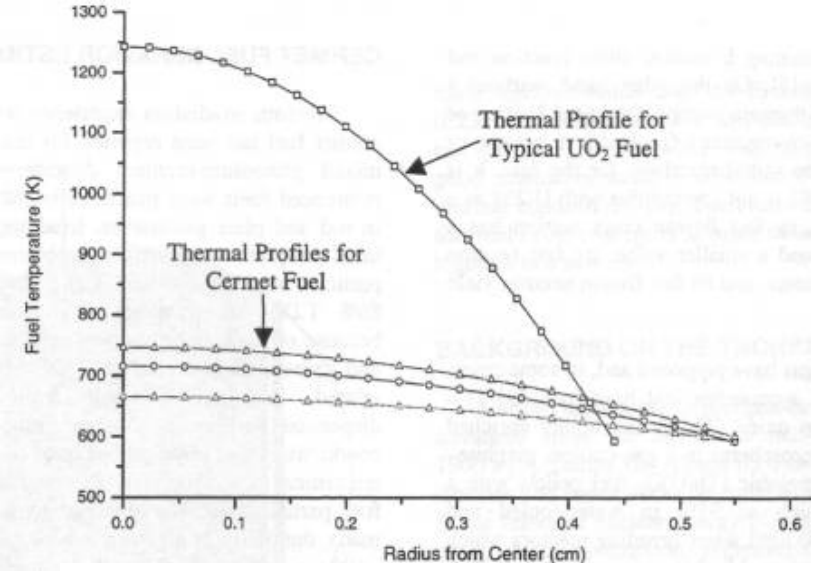

Figure 2.2 Comparison of Thermal Profiles [35]

Another fuel characteristic to consider is that in the solid oxide fuel pellet, fissions are occurring within the material, leading to fission fragment damage (and all the problems that accompany it) throughout the entire fuel pellet. In contrast, in the dispersion fuel, fissions are contained within the tiny microspheres that are scattered throughout the matrix, resulting in fission fragment damage that is localized within the microspheres, extending to only a small ring around the spheres with a length equal to the range of fission fragments within a material (often 7 – 10 microns). Figure 2.3 shows the ring of fission fragment damage in a stainless steel matrix surrounding the UO_2 particle. Also, as figure 2.1 shows a large central void, figure 2.3 shows smaller voids that have formed in the small dispersed particles. These much smaller voids are also localized within the fuel particles and do not contribute to the degradation of properties of the metal matrix.

Due to localization of fission damage there exists a portion of the matrix that is completely interconnected, and undamaged. This connected, undamaged matrix material

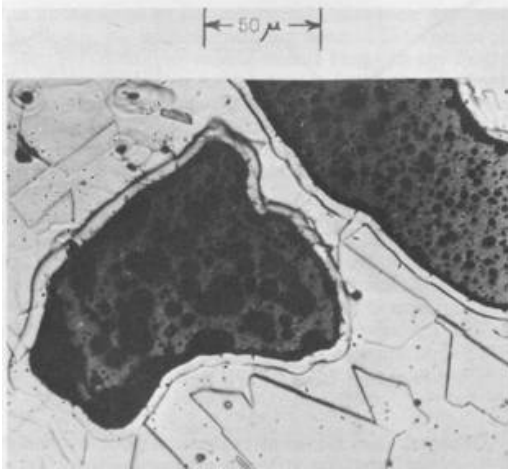

Figure 2.3. Zone of fission fragment damage in a dispersion fuel [24]

is the backbone for greater structural and dimensional stability, corrosion resistance and an overall higher strength [24]. Much of the emphasis in the design of dispersion fuels is thus directed at attempting to maximize the amount of undamaged matrix material. Further details in this area will be presented later.

Another one of the benefits of this fuel type is the flexibility in the choice of matrix material. The matrix material can be chosen to reflect reactor operating conditions. Choices can range from a metal like stainless steel, to a ceramic like alumina to the high temperature resistant graphite. The fissionable particles can also be selected on the basis of desirable properties, for example, uranium, plutonium or thorium metal alloys, oxides, carbides or nitride ceramic microspheres. This flexibility allows the fuel to be designed according to the requirements of each application. Homogeneous nuclear fuels do not allow this flexibility. These numerous favorable properties of dispersion fuels make them superior to most other forms of nuclear fuel.

Although there are many advantages, the dispersion fuel form does have a few disadvantages. Since the fuel is in a more complex structural form, it is more expensive and more difficult to fabricate than a homogenous solid UO_2 fuel pellet fuel. The presence of a large amount on non-fuel matrix may also complicate fuel recycling, since this material must be dissolved in order to expose the fuel particles. This may be a difficult and expensive process, and the best application of this fuel may be to use it to burn the fissionable material to as low of levels as possible, then directly dispose of it. Despite these disadvantages, the dispersion fuel form has many characteristics that merit further consideration in certain present and future nuclear reactor applications.

2.3. Dispersion Fuel Theory

Most of the theory pertaining to dispersion fuels has come from the contributions of Weber and Hirsch [54], Weber [55] and White, Beard and Willis [58]. These papers have focused on a few of the important fuel parameters, and methods to optimize these parameters so that it is possible to design a stable fuel. The primary variables include the size of the fissionable particles, the volumetric loading of fissionable particles within the matrix, and the fission fragment distance in both the matrix and particle materials. The theory is only partially applicable to the fuel, because it uses the idealized assumption that all the fissionable particles are uniformly distributed spheres [24].

As was seen in figure 2.3, a ring of fission fragment damage surrounds each fissionable particle. The radius of this ring depends on the characteristics of the matrix material. For example, the theoretical range of fission fragments from U^{235} is: 6.9 microns (μ) in uranium metal, 9.4 μ in UO_2, 9.1 μ in zirconium, 6.6 μ in iron, and 13.8 μ in aluminum. Since this range of fission fragments is nearly constant in each material, it can be concluded that for a given volume fraction of fuel particles, the smaller the particle size, the more likely will overlapping of the damaged fission fragment regions occur. In addition, if the volume fraction of particles is increased while maintaining a constant particle size, the fraction of damaged matrix material will increase. Figure 2.4 shows an example of an idealized dispersion fuel complete with the fission fragment damage zones and the matrix. Figure 2.4b demonstrates that small particle size leads to overlapping damage zones (with constant volume fraction), while comparison of figure

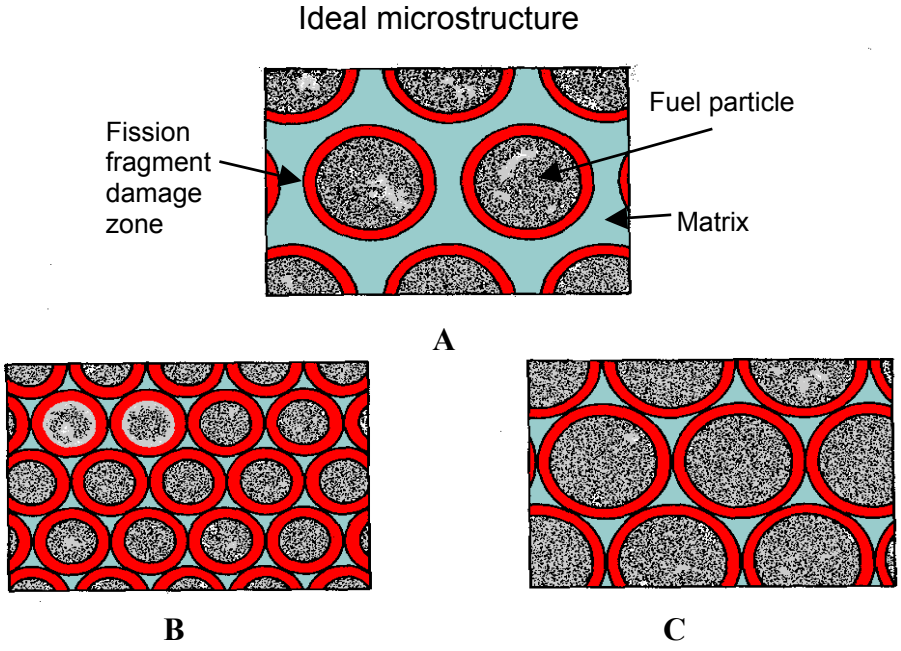

Figures 2.4a,b,c. Different combinations of particle distributions [55]

2.4a and figure 2.4c demonstrates that higher particle volume loading also leads to overlapping damage zones (with constant particle size). The primary goal is to be sure that there is a continuous network of undamaged matrix to maintain structural integrity [55].

The fraction of undamaged matrix (V_m) is related to the volume fraction of particles (V_f), their diameter (D) and the range of fission fragments in the matrix (λ_m).

The equation relating them is:

$$V_m = 1 - \frac{V_f}{(1 - V_f)} * \left[\left(1 + \frac{1}{D/(2 * \lambda_m)} \right)^3 - 1 \right]. \qquad (2.1)$$

Figure 2.5 shows a plot of the effect of particle size on the fraction of undamaged matrix material for varying volume fractions. It uses the equation stated above [58].

In figure 2.5, the thicker, black line going through the middle is the boundary for where the damage zones of the particles are touching. It is desirable to design the

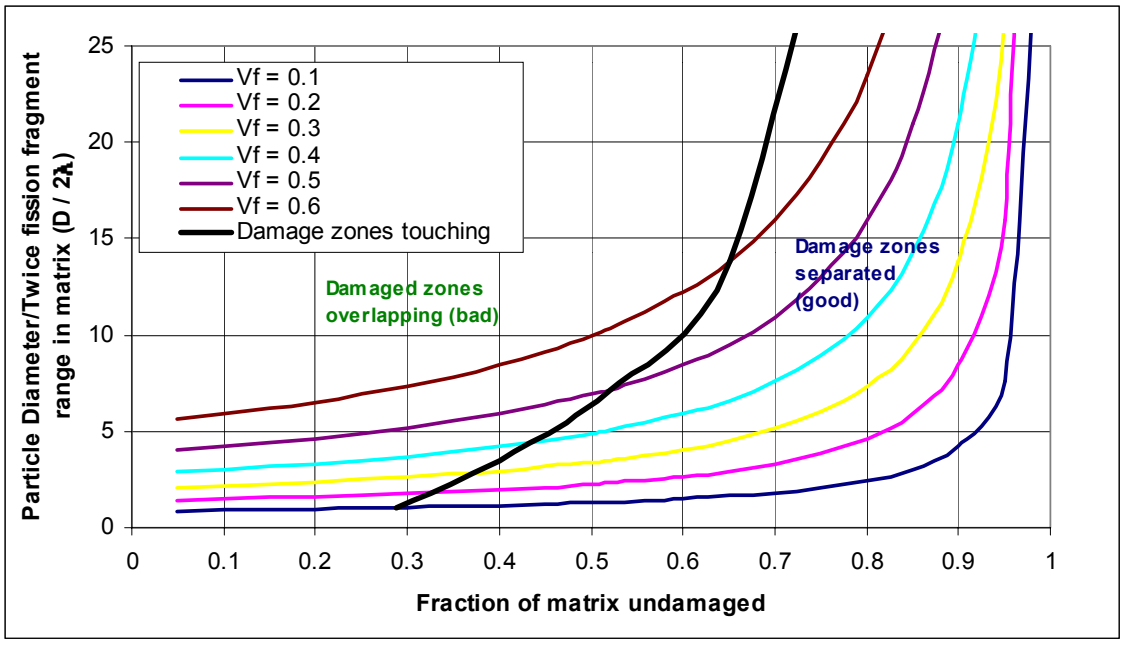

Figure 2.5. Effect of particle size on fraction of undamaged matrix for varying V_f [58]

dispersion fuel such that the damage zones are separated, resulting in an interconnected undamaged matrix, as represented in area to the right of the line. Other geometrical analyses have been done with regard to fission fragment damage zones. Some of these studies are in regard to the fission fragment concentration within the matrix [58], and the distribution of fission fragments in the matrix [55]. However, the details of these discussions will be omitted here due to the lack of ability of the finite element computer model to specifically take these microscopic interactions into account.

Not only is the proper manufacturing of the fuel important so that there remains a continuous undamaged matrix network, but the materials and conditions under which it is used also have a major impact on the fuel and the stress it experiences. Some of these sources of stress in a dispersion fuel are discussed in references 58 and 44. The principal sources of stress in a typical fuel element are the thermal stresses due to the thermal gradients produced by the heat transfer throughout the fuel. These stresses depend on the power density and thermal conductivity of the fuel. There are also local thermal stresses coming from the heterogeneous nature of the different heat generating spheres inside the fuel. Local stresses are also generated by the mismatch of thermal expansion between the particles and the matrix materials. Another source of stress is from the fuel particle volume change resulting from driven swelling. Local fission gas release also results in matrix stress. These stresses can be minimized by reducing the thermal gradients, and choosing a combination of materials that have similar mechanical properties. The particular dispersion fuel (PuO_2 – Zr) that is being investigated in this study, attempts to make use of some of these facts. The numerous previous experiments that were conducted on dispersion fuels tried to take advantage of the information gathered from

these design studies in order to learn more and understand where further problems might arise in this fuel form.

2.4 Previous Experiments and Current Use of Dispersion Fuel

A wide range of research on dispersion fuels has been conducted since the 1950's. A majority of the tests that were completed included some type of uranium – metal alloy, or a UO_2 – metal matrix type structure. During early nuclear research, some of the alloy fuels like U–Mo, U–Al, and other U-refractory metal alloys were investigated [12, 17, 24]. The primary result from this research has been the use of U-Al alloy fuel in many of the civilian research and test reactors around the United States, including small university reactors. Other dispersion fuel combinations that have been researched include carbides like UC and (U,Pu)C in a graphite matrix [11] as well as a ceramic – ceramic type dispersion fuel like Al_2O_3 – UO_2 [24]. The unique ZrH – UO_2 dispersion fuel for the space nuclear auxiliary power (SNAP) program and TRIGA reactors was also investigated in the mid-sixties [24]. Many variants of metal-matrix type dispersion fuels have been tested; these include: UO_2–Mo, UO_2–Nb, UO_2–Cr [28], UO_2–Fe [30], $(Th,U)O_2$–Zr [35], UN–stainless steel, and UC–stainless steel [44]. The combination of UO_2 in a stainless steel matrix was the fuel type most extensively tested.

Since the most extensive database has been generated for UO_2–stainless steel dispersions, the focus of the experimental data analysis in this research will involve this dispersion fuel type. One challenge in the application of nuclear fuel in general is being able to predict when it might fail. Keller [29] attempted to do this by compiling numerous experimental data points plotting them on a graph of U^{238} burnup in atom

percent versus the fuel surface temperature, for a 25 weight percent UO_2 fuel. This plot is shown in figure 2.6. In the plot, the blue circular data points represent the experimental tests in which the fuel was stable throughout the entire test. The red, square data points represent the experimental tests where the fuel had failed prior to the end of the test. The yellow shaded region to the left encompasses the conditions under which a dispersion fuel would likely remain stable throughout reactor operation. The blue shaded area on the right represents the conditions that would likely result in dispersion fuel failure. The gray region in the middle is the region where it is difficult to predict whether or not the fuel will remain stable. From this plot, the large dependence of fuel performance on the fuel surface temperature can be seen. Therefore, as a part of the PuO_2–Zr study, temperature sensitivity was considered.

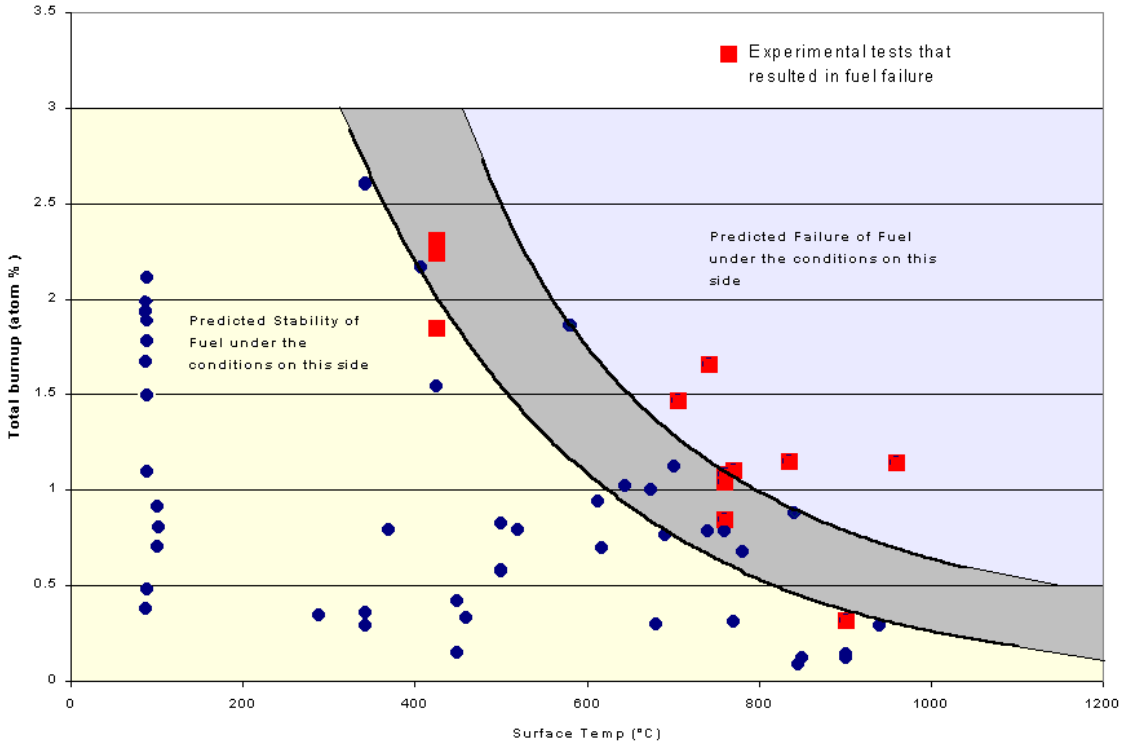

Figure 2.6. Burnup performance of UO_2 – stainless steel dispersion fuel [29]

In figure 2.6 the majority of the dispersion fuel data points are for plate-type fuel. Since the proposed dispersion fuel is of the pin type, it must be determined if plate type fuel data can be extrapolated to determine the performance of pin-type fuel. The geometry of the fuels are quite different (as seen in figure 1.2); these differences lead to different failure mechanisms for each fuel type. Figure 2.7 shows the typical failure mechanism of the plate-type fuel. Figure 2.8 shows a pin-type fuel element failure due to cracking through the cladding often extended from internal fuel cracks. Since the fuels have different failure modes, the experimental data pertaining to the plate fuel cannot be applicable to the pellet type fuel. The plate fuel is long and narrow it can much more easily fail by a slight bulge or crack, while a fuel pellet is more robust and can withstand cracking and some swelling in a reactor. Considerable effort was expended locating useable pin-type dispersion fuel data, which is scarce in comparison to plate-type fuel data. Further specific details about the data that were used to help build the dispersion fuel model will be presented in chapter 5

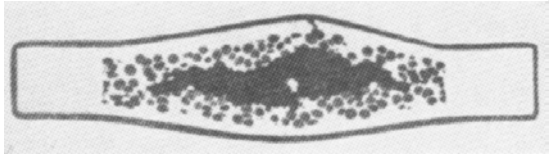

Figure 2.7. Typical plate-type failure mechanism [12]

Additional comparison of the two fuels further shows that the processing differences are also very significant, for the fabrication techniques used to manufacture each fuel type are quite dissimilar [12, 36, 24]. This further adds to the overall differences between the fuel types

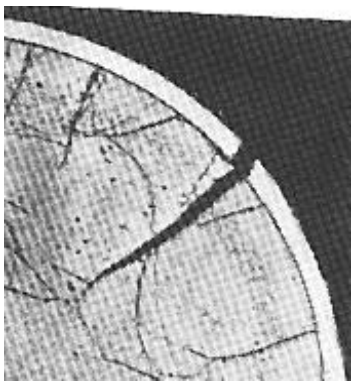

Figure 2.8. Failure in a pin-type fuel element due to cladding cracking [12]

Finally, theories describing dispersion fuel performance were formulated prior to development of modern computational abilities. Current computational capabilities make possible the accurate description of the complex stress state present in a dispersion fuel through the use of finite element analysis. This was not previously possible using strictly analytical methods. This ability allows further progress in the design and understanding of this fuel, exploiting the advantages it has over current generation fuels. The next chapter will describe in more detail how the interactions are modeled, and describe overall the functioning of the finite element model.

CHAPTER 3 – MODEL DESCRIPTION

In this chapter, the details of the finite element model used to analyze the performance of rod-type dispersion fuel will be presented along with the assumptions underlying the model. In order for the model to properly represent the behavior of the fuel as a whole, each of the parts of the model must be physically realistic and act in a manner consistent with known behavior. However, the modeling of a few of the specific behaviors raise substantial issues in model formulation. This chapter describes how the physical behaviors within the component parts of the fuel are represented and combined into the finite element model.

3.1. Geometry

A rod-type geometry is typical of LWR fuel, and is adopted for application of this dispersion fuel concept. As is often done in finite element analysis, the use of symmetry is to reduce computational time. Two models were considered, a quarter section of the pellet with multiple layers of fuel particles and a quarter section with a single layer of particles. Figure 3.1 shows what a quarter pellet cylinder with full depth would look like geometrically in the finite element program. Obviously, the geometry is very complicated and involved. Inclusion of numerous surfaces in the model results in large computational time. This geometry limits the ability to vary parameters and run numerous test cases. Therefore, a simpler model was selected. This model is composed of a single layered slice from the larger model. Figure 3.2 shows an example of the quarter pellet slice geometry for an eleven volume percent loading of particles. The

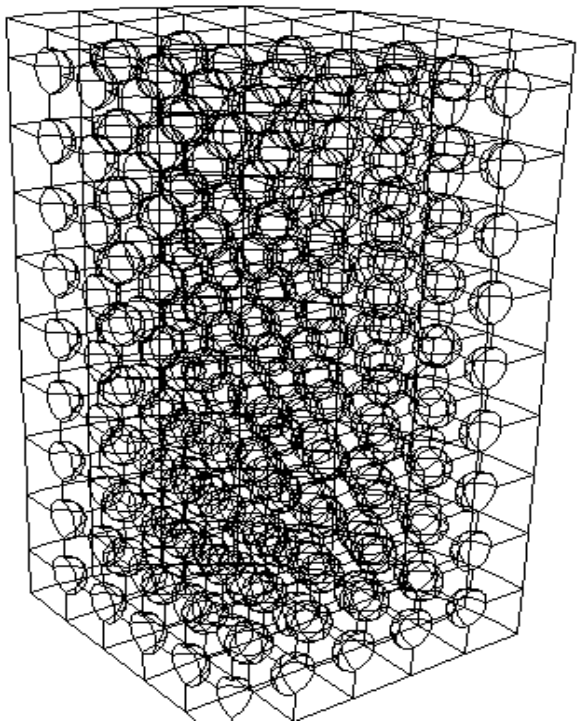

Figure 3.1. Wire frame of the full quarter pellet geometry

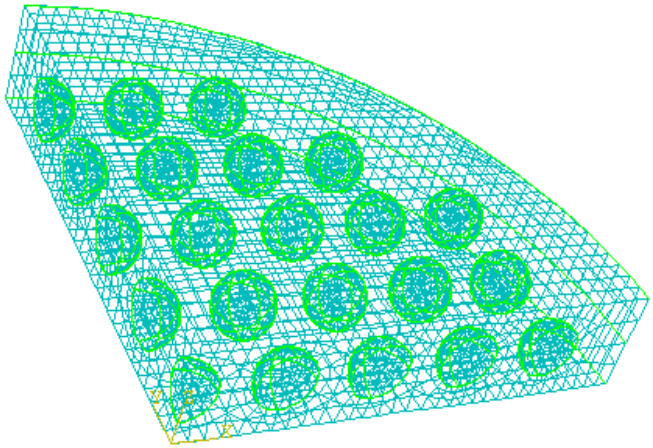

Figure 3.2. Dispersion fuel slice geometry

idealized geometry of perfectly spherical particles in a cubic array embedded within the matrix is used to represent the fuel.

The finite element model was built using the scripting ability of ABAQUS with the PYTHON computer programming language. The easiest way in which to generate the model of spheres embedded within the matrix using ABAQUS is by first forming a solid slice of matrix material. The 'cutting feature' in the software was used to remove the matrix material where the spheres would be located. Spheres of fuel material were reinserted into the matrix in the locations where voids had been created. All the nodes in the model were forced into coincidence. The PYTHON scripting code was subsequently used to vary the number of spheres in the matrix, the diameter of the spheres, the spacing of the spheres, the separation of the spheres from the outer edge of the pellet, and the pellet outer dimensions. An example of the PYTHON scripting code is found in Appendix A.

The use of this ideal geometry produces best-case fuel performance predictions and assumes that fuel can be fabricated as modeled. There were a number of improvements in manufacturing capabilities during the 1960's that make this assumption valid. Figure 3.3 shows a 20 volume percent loading of UO_2 in a stainless steel matrix with an average particle size in the figure of 350 microns. Figure 3.3 is an example from 1962 that demonstrates the ability at that time to make and evenly distribute the spherical particles in a steel matrix. More recent advances in sol–gel processes for spherical particle fabrication and advances in composite forming technology indicate that this work can be reproduced.

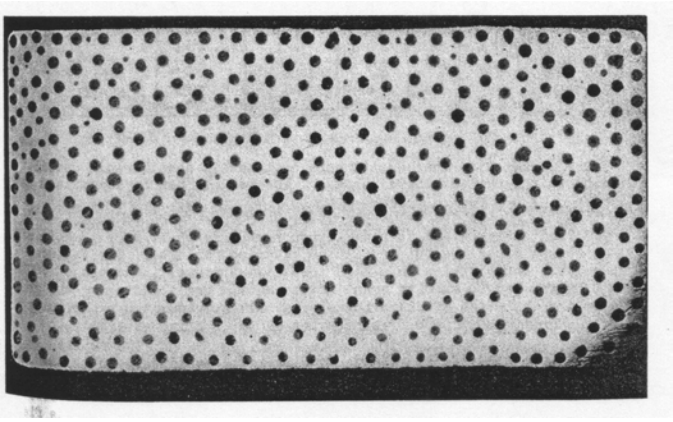

Figure 3.3. Spherical particles within a UO_2 – stainless steel dispersion fuel [13]

3.2. Fission Gas Release

The primary challenge in building this model is in properly simulating the loads applied to the matrix under the conditions resulting from fissioning. As was mentioned in chapter two, an important problem to account for is fission gas release from the fuel particles. Fission gas (primarily Xe and Kr) is produced in the fuel lattice due to fissions. This gas is not soluble in the lattice and tends to precipitate as clusters of atoms. Many of these clusters are redissolved in the lattice by fission spikes. However, statistically, some of the gas clusters survive the fissions and grow to a size where they cannot be redissolved. These bubbles then further grow, due to diffusion of gas, inside of grains in the fuel. Eventually, small bubbles coalesce into larger bubbles, and often tend to be trapped at the grain boundaries. Finally, these bubbles join along the grain boundaries forming a connected 'pipeline' for gas release to the surface. Because of this fission gas production, the bubbles that migrate through the fuel cause an increase in the overall internal pressure of the fuel [10, 36].

A great deal of research has been done in this area; research continues since the presence of fission gases is often a large contributor to the failure of nuclear fuel [21, 34, 38, 37]. Figure 3.4 is a micrograph showing fission gases migrating due to the temperature gradient. Streaking trails from the gases can be seen to show they are moving to the right. One way that this effect can be lessened is by manufacturing microspheres of a lower density. Porosity contained within these spheres acts as a free space (plenum) for gas accumulation, lowering the pressure–driven matrix stress.

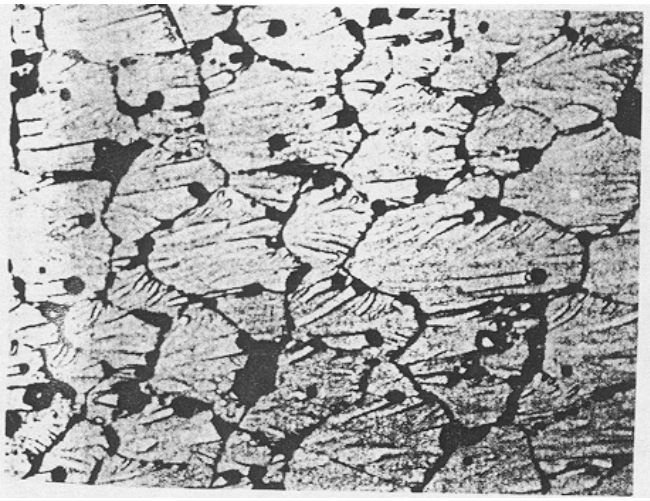

Figure 3.4. Fission gases migrating through a $(U,Pu)O_2$ fuel [12]

The method by which this phenomenon is implemented in the dispersion fuel model is by exerting a pressure, due to the released gases, on the matrix surface that surrounds the microspheres. The pressure force that is input into the ABAQUS model uses several equations relating the amount of gas produced per fission with the amount of gas released for a specific fuel density. From these equations, the number of moles of gas

is calculated, and then the simple ideal gas law relates the moles of gas to the resulting pressure. The equations used to calculate the fission gas driven stress are detailed below.

First a conversion from the burnup units: MWd/kgHM to percent burnup of uranium atoms is required.

$$Bu\left(\frac{MWd}{kgU}\right)*\frac{10^{6}\left(\frac{J}{s}\right)}{MW}*86400\,\frac{\sec}{day}*\frac{1MeV}{1.6*10^{-13}(J)}*\frac{1fission}{200MeV}*\frac{0.238\_kgU}{6.02*10^{23}atomsU}=U\%$$

where: Bu = Burnup in MWd / kgHM (megawatt days per kilogram of heavy metal)

MW = megawatts

U% = the percent burnup of uranium atoms

This conversion is required so that the fission gas release correlation of Manzel [34] can be used in the subsequent calculations.

The number of moles of gas produced is calculated using the following equations [57]:

$$n_{Xe}=0.865*\left(\frac{4}{3}\right)*\pi*r_{sphere}^{3}*\rho_{\%}*N*\frac{U\%}{100} \qquad (3.1)$$

$$n_{Kr}=0.135*\left(\frac{4}{3}\right)*\pi*r_{sphere}^{3}*\rho_{\%}*N*\frac{U\%}{100} \qquad (3.2)$$

where [57]:

$$N = 4\times10^{-27}\frac{moles\ gas}{atoms\ U\ in\ 1\%\ burned\ fuel} * 2.46\times10^{22}\frac{atoms\ U}{cm^3\ of\ UO_2}$$
$$= 9.7\times10^{-5}\frac{moles\ gas}{cm^3\ \%U\ burned}$$

r_{sphere} = *radius of spheres in fuel*

$\rho_{\%}$ = *percent theoretical density of* UO_2 *in spheres*

The coefficients of 0.865 and 0.135 in equations 3.1 and 3.2 respectively, are used because approximately 86.5% of the gases produced in the fission process are xenon isotopes, and 13.5% are krypton isotopes. Once the number of moles of gas produced is calculated, the actual number of moles of gas that are released and exerted on the matrix are found by using this equation:

$$n_{FGR} = (n_{Xe} + n_{Kr}) * FGR\% \tag{3.3}$$

where FGR% = the percent of fission gas released as a function of burnup as shown in the plot in figure 3.5 from Manzel [34]. Conversion of the number of moles of gas released to pressure is done using the ideal gas law.

$$P = \frac{n_{FGR} * R * T}{V_{sphere} * \%_{porosity}} \tag{3.4}$$

where: R = 8.314 J/mol-K

T = the assumed temperature within the fuel

V_{sphere} = Volume of the sphere

$\%_{porosity}$ = the percentage of porosity in the microspheres

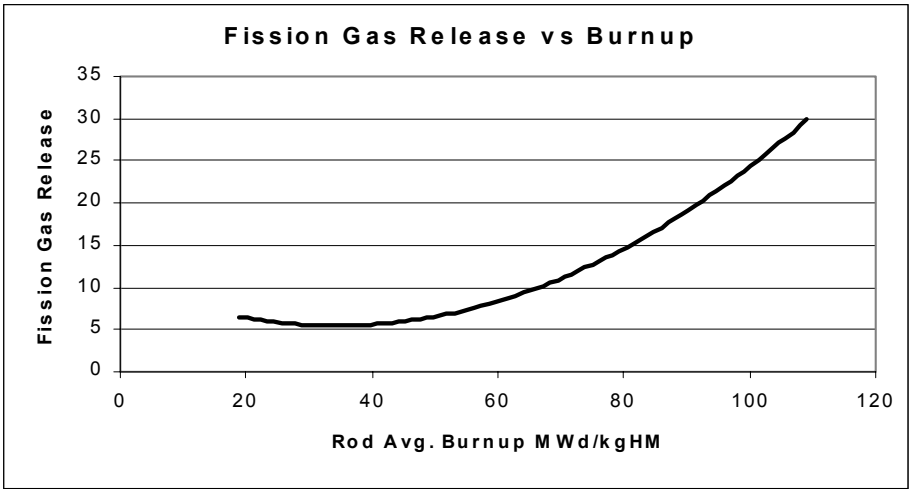

Figure 3.5. Plot of fission gas release vs. Burnup [34]

Once the pressure has been calculated, it is input into the computer model to account for the pressure driven matrix stress. The methodology of calculating this pressure has been checked with the neutronics computer code WIMS. WIMS is an extensive and versatile neutronics code with the latest JEF2.2 validated nuclear data libraries that has the ability to solve most problems associated with thermal reactor physics [26]. The comparison was conducted at 260 MWd/kgHM using a fuel with particles of radius 300 microns, theoretical density of 90%, and the geometry of a typical Westinghouse 17 x 17 reactor core. The methodology mentioned above calculated $2.74*10^{-9}$ moles of fission gas (Xe and Kr) produced, while WIMS calculated $2.94*10^{-9}$ moles of Xe and Kr produced. The comparison between the two methodologies in calculating how much fission gas is produced varies slightly since the WIMS code took into account a number of other factors, but the final results between the two calculations are quite similar.

3.3 Fissioning to Produce Heat

Another result of the fissioning process in the nuclear fuel is that thermal energy is generated due to fission. The best way in which to model the creation of heat via fissioning, is by using the heat generation function of ABAQUS. Each microsphere within the matrix has the ability to generate heat. The heat generation in each sphere is correlated to the power density of the reactor. The process that was used to calculate the particle heat generation rate, needed as input into the ABAQUS model, is given below.

Since the primary application of this fuel type is for plutonium burning in current commercial reactors, the calculation is based on a typical Westinghouse 17 x 17 pressurized water reactor (PWR) core. A typical core power density for a PWR is 105 kW/L [52]. The linear heat rates for fuel can vary substantially inside a reactor depending on the location. The peak linear heat rate for a PWR is 42.7 kW/m; the average value is 17.8 kW/m [52]. A reference value of 20 kW/m was used for most calculations, but can be varied depending on the reactor and fuel type. Typical values for power generation within nuclear fuel materials are in the hundreds of MW/m^3 range.

$$Volumetric\ Heat\ Generation\ in\ fuel\ rod = \frac{LHR}{A} \tag{3.5}$$

where: LHR = Linear Heat Rate (kW/m)

A = area of the fuel rod ($\pi * r^2$)

r = radius of the fuel rod (0.00475 m) [14]

3.4. Materials and Properties

A further result of the fissioning that occurs in the fuel is that the many energetic particles interact with the fuel and matrix materials, resulting in changes to physical and

thermal properties. For example, neutron radiation affects the mechanical properties of metals in the form of loss of ductility. Ceramic fuel particles are heavily damaged by fission fragments. In order to effectively model this fuel, an accurate representation of the irradiated material properties of the four primary materials that were being studied (UO_2, PuO_2, stainless steel, and zirconium) had to be developed.

The properties used by the model include; thermal conductivity, density, thermal expansion coefficient, Young's modulus, Poisson's ratio, specific heat, swelling, and yield stress. These properties are listed in the table in appendix B. A number of these property values contain significant uncertainty since there is not a great deal of irradiation data available for some materials. The best values were tabulated after searching through a number of different references [41, 33, 18, 7, 51, 32, 49, 53, 47].

3.5. Assumptions / Limitations

Since there are so many different processes occurring within the dispersion fuel, and all are not well understood, it is not possible to model every detail. The capabilities of ABAQUS also impose a few limitations on the detail that can be incorporated into the model. Therefore, a number of simplifying assumptions were made.

The first assumption is that the radial power distribution within the fuel is uniform. In reality the power distribution within the fuel is a function of radial position due to self-shielding of the interior of the fuel rod by the fuel material at the periphery of the fuel rod. Since neutron flux is lower in the center of the fuel rod, there are less fissions, resulting in a lower power density than that on the periphery of the fuel [27]. This is true in the dispersion fuel, but the affect is not accounted for in the finite element

model. Instead, the average of the radial power throughout the fuel pellet is implemented [27]. Therefore, the profile of the radial power gradient is flat.

Another assumption that has been made is that the creep within the ceramic microspheres does not operate to relieve matrix stresses. A large amount of research has been conducted concerning creep of ceramic nuclear fuel materials [40, 45, 46]. Analysis of this data makes it clear that fuel particle creep is only a concern under very high temperatures and high pressures. Figure 3.6 shows a plot of the creep rates of UO_2 as a function of temperature and pressure. The rates at lower pressures and temperatures are not shown because they are very small, less than 10^{-6} hr^{-1}. It can be seen from figure 3.6 that fuel creep occurs at significant rates only for a temperature regime above 1500° C. The calculated temperature for the proposed PuO_2–Zr is approximately 700° C. Therefore, the decision to neglect the effects of creep of the microspheres in the model, and consequent relaxation of matrix stress, is valid.

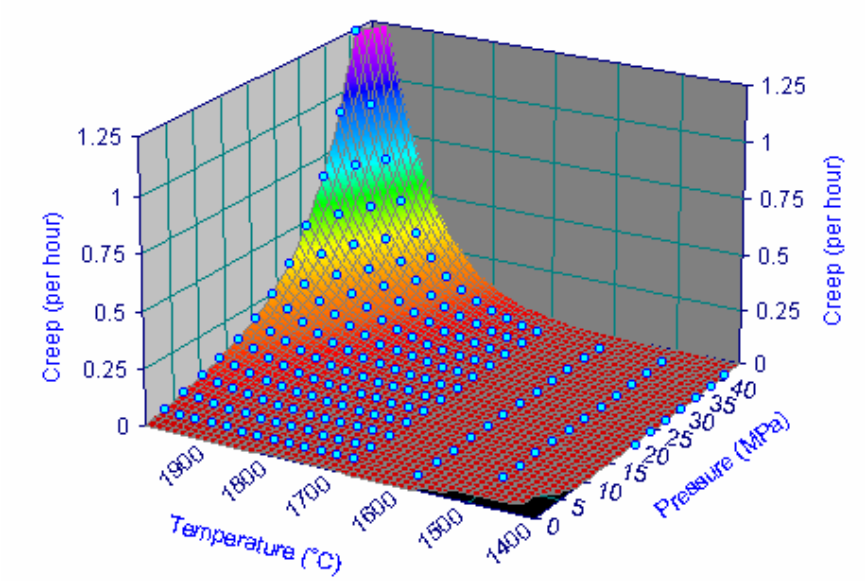

Figure 3.6. 3-D Creep Curve of UO_2 under different pressures and temperatures [46]

It has further been assumed that the creep of the matrix is neglected since the creep function of ABAQUS is not used. However, the ABAQUS function calculating the overall plastic deformation of the materials is implemented to take into account the plastic deformations in the matrix and fuel. Creep of zirconium has been studied in depth and a few equations have been developed for a range of temperatures and pressures [3]. A solution to one of the equations shows that for an operating temperature of 550°C and stress of 150 MPa, the resulting creep is $3.38*10^{-4}$ hr^{-1}. The matrix creep is greater than the creep for the particles, but it will not significantly influence the overall fuel behavior unless the fuel is in the reactor for a very long time. Some uncertainty in the model is acknowledged due to the lack of matrix creep; however, the irreversible strain in the dispersion fuel is accounted for by utilizing yield data and activating the ABAQUS solver to include plastic deformation in the overall solution.

Material property data for PuO_2 is scarce, so it is assumed that the mechanical behavior of PuO_2 is similar UO_2. For example, since there is no data available for the yield stress of PuO_2, it has been assumed that the yield stress of UO_2 is comparable to that of PuO_2. Likewise, there is no recorded data on the swelling of pure PuO_2 as a function of burnup, and thus swelling data for UO_2 has been used.

Further improvements to the model depend both on expanding capabilities of the software to handle more complex burnup dependent property relationships and expanding the material property database.

3.6. Finite Element Analysis Boundary Conditions

The geometry for the dispersion fuel is a quarter slice of a rod, chosen to exploit the advantages of symmetry to reduce computation time. The boundary conditions that are required for this symmetry are shown in figure 3.7. The red colored edges denote surfaces constrained by a boundary condition of zero displacement in the "one" direction for the edge in the background and the same for the "two" direction on the edge in the foreground, according to the coordinates shown. The central bottom corner (shown in blue) is a fixed point constrained in all directions.

Since nuclear fuel is cooled by the flow of coolant through the reactor, cooling must also be implemented into the computer model. This cooling is achieved by convection along the outer boundary of the fuel. The temperature of the coolant and the convection coefficient were selected in accordance with acceptable actual operating conditions within a reactor [52]. After inputting these boundary and convection conditions, the model is fully described.

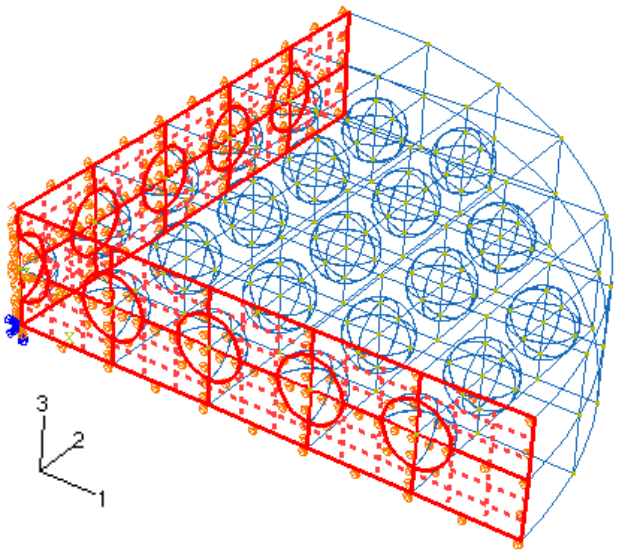

Figure 3.7 Boundary conditions and partitions included in the FEA model

Initially, the geometry of the model was not conducive to meshing. The partitions completed directly through the middle of each sphere in both the "one" and "two" directions, seen in figure 3.7, allowed for adequate meshing.

Once the model was meshed (see figure 4.7), a three-dimensional thermally coupled linear brick element (C3D8T) was used homogeneously throughout the entire model The C3D8T element consists of a brick with eight nodes, and four degrees of freedom (x, y and z displacements $\{u_x, u_y, u_z\}$ and temperature). This element calculates displacements and temperatures using a linear integration method. In addition to the C3D8T element, the twenty node, thermally-coupled brick C3D20T element was also tested. This element calculates displacement using a quadratic integration, and uses linear integration to solve for the temperature [1]. The C3D8T brick was used for the majority of the calculations, because it requires less computation time, and provided the same results as the twenty node brick element. The two element types were compared by

running a number of cases with identical conditions, the only difference being the element type. Results from the comparison between the eight node brick and the twenty node brick are shown in figures 3.8 and 3.9. The two different elements generally result in solutions within 0.5 % of each other. Overall, the C3D8T element works well in calculating displacements, temperatures and other associated variables.

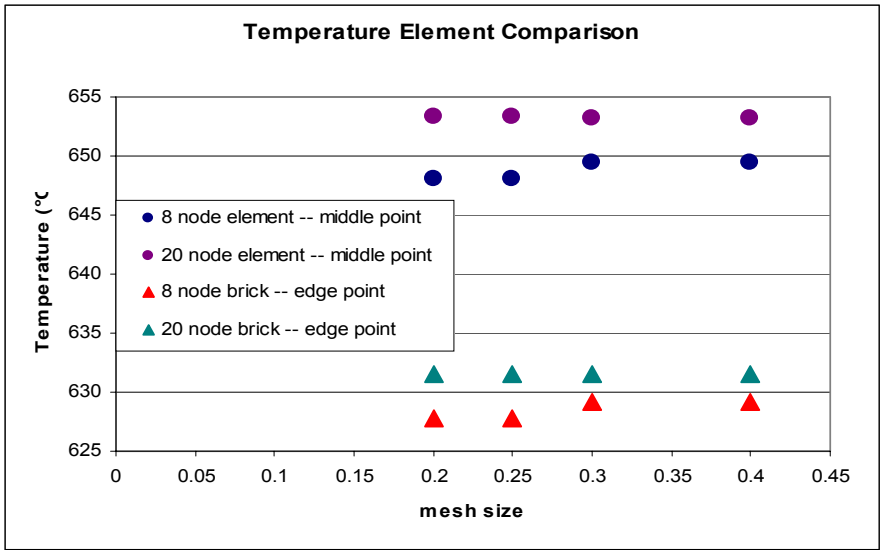

Figure 3.8 Element comparison for various temperature values

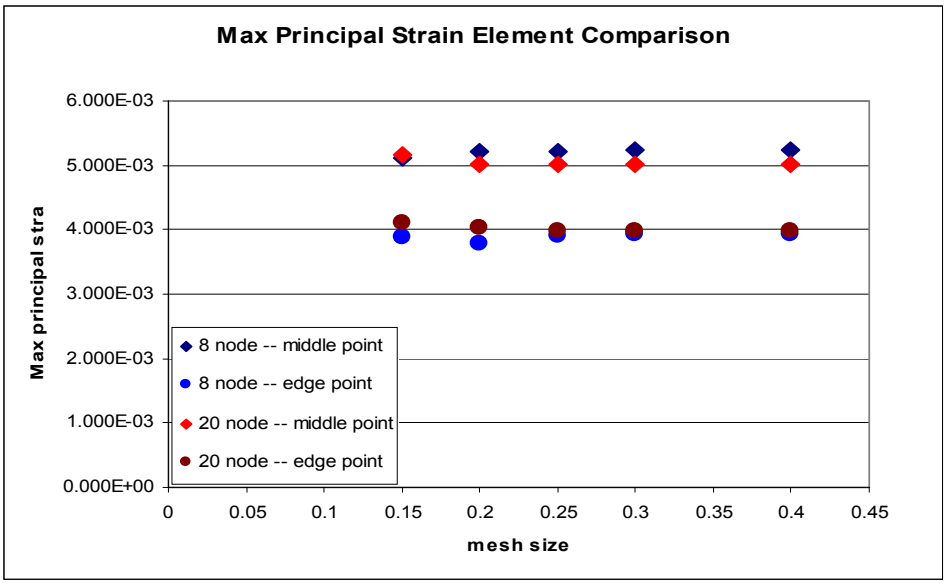

Figure 3.9 Element comparison for the maximum principal strain values

In this chapter, the various components that are involved in building the finite element model of the metal-matrix dispersion nuclear fuel have been described. The modeling of fission gas release, fission heat, and radiation embrittlement has been described. The simplifying assumptions made necessary by the lack of irradiated material property data, measured creep data, and code limitations have been stated. The analysis element and boundary conditions were also described. Chapter 4 explains the process and data used to validate the finite element analysis model.

CHAPTER 4 – MODEL VALIDATION AND EXPERIMENTAL CORRELATIONS

In order to assure that the results obtained from the computer model are realistic, the model must be benchmarked. Confidence must also be established in the components within the model so that it can be assured that the various solutions to the different cases are consistent with reality. This confidence is demonstrated by performing a series of benchmarking and validation studies. The model was benchmarked by comparing the computational results to the experimental database for rod-type dispersion fuel.

Validation of thermal calculations, and stress calculations was also carried out. The thermal results from the model were compared with an analytical solution for a typical fuel element. The thermal results were also compared to the results of a different finite element computer code model to further establish the model's accuracy. Values of stress generated by the finite element model were compared to an analytical solution for the stresses in a pressurized sphere. Finally, the stability of the solutions was demonstrated by performing a mesh convergence study and other stability checks. Validation calculations for the mechanical, thermal and computational aspects of the model in comparison to other solutions are shown in the subsequent sections.

4.1. Temperature Validation

The thermal aspects of this model are validated in two different ways. The first comparison is with an analytical solution of the temperature in a fuel rod. The second comparison is with an ALGOR solution. ALGOR is a finite element computer code that was also used to thermally model the dispersion fuel form. These validations help

demonstrate a confidence in the overall model, so that it can be assured that it is a reasonable simulation of the real situation.

Heat conduction through the dispersion fuel form involves the heat transfer through the matrix, then a microsphere, then through the matrix again, and so on. A simple conduction correlation for the heat transfer in cylindrical fuel elements was used for validation of the finite element results [9]. For a fuel pellet with uniform volumetric heat generation and constant thermal conductivity:

$$\Delta T_{fuel} = \frac{q''' * r_{pellet}^2}{4 * k} \tag{4.1}$$

where: ΔT_{fuel} = temperature drop across the fuel element (°C)

q''' = the volumetric heat generation rate within the fuel (W/m^3)

r_{pellet} = the radius of the pellet (mm)

k = the thermal conductivity of the fuel element material (W/m°C)

This equation includes two assumptions in the derivation. First, it neglects axial conduction of heat. This assumption is valid because the temperature gradient in the radial direction is several orders of magnitude larger than the axial temperature gradient. The second assumption is that the equation is for a completely homogeneous fuel. Though dispersion fuel is heterogeneous, this equation can be used with an effective thermal conductivity for the heterogeneous material. The effective thermal conductivity for metal-matrix composites is defined in equation 4.2. This equation is a variant of the Maxwell equation describing the thermal conductivity of a two-phase system. This equation is often referred to as the Maxwell-Euken equation [48].

$$k_{effective} = k_m * \left[\frac{2 * k_m + k_f - 2 * b * (k_m - k_f)}{2 * k_m + k_f + b * (k_m - k_f)} \right] \tag{4.2}$$

where: $k_{effective}$ = the effective thermal conductivity for metal matrix composites

k_m = the conductivity of the matrix material

k_f = the conductivity of the fissionable material

b = volume fraction of matrix material:

$$b = \frac{V_m}{V_m + V_f} \tag{4.3}$$

V_m = total volume of the matrix

V_f = total volume of the fissionable particles

Since the heat generation rate defined in the finite element model refers to that in the microspheres, the entire equation must be multiplied by the volumetric loading of fissionable material, since only the spheres contribute to the heat generation. This results in the following equation that can be used to predict what the solution for the temperature drop in a dispersion fuel should be, given the heat generation, pellet radius, and volumetric loading.

$$\Delta T_{fuel} = \left(\frac{q''' * r_{pellet}^2}{4 * k_{effective}} \right) * (1 - b) \tag{4.4}$$

The second comparison was done by creating a similar finite element model of the dispersion fuel using the ALGOR finite element analysis code. The particular version of the software used was only able to perform a thermal analysis. The comparison was done by generating the exact same geometry, i.e. the same number of spheres, the same pellet radius, and the same volume loading of spheres. Once the two models were shown to be identical, the thermal analysis in each pellet was conducted.

Multiple thermal analyses case studies were performed to validate the thermal model, but the results of only one specific comparison will be discussed. For this specific

case, the fuel was a UO_2 – Zr type dispersion fuel. The pellet radius was 5 mm; the radius of the spheres was 300 microns; the fuel had a 28 volume percent loading, and the heat generation within each sphere was 100 MW/m^3. The final solution for this case resulted in a temperature difference from center to surface of 14.5° C for the ABAQUS model, 13.70° C for the ALGOR model, and 14.1° C for the analytical solution. Even with the assumptions that are made in the analytical solution and the differences in the ALGOR model, these results are all within a 5% error band. The results show that the thermal analysis portion of the model is accurate. Figure 4.1 shows the geometry and thermal profile of the fuel for the described case.

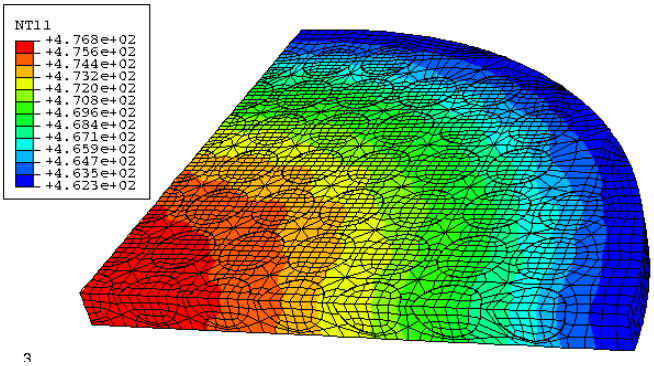

Figure 4.1. Results from the validation case for thermal analysis

Another verification of the thermal analysis was conducted to investigate the thermal profiles within the fuel on a local scale. Since the microspheres are made of a ceramic with low thermal conductivity, and the matrix is made of a metal, it is intuitive that the temperatures within the microspheres would be larger than that of the surrounding matrix. Figure 4.2 shows the thermal profile across the dispersion, for a

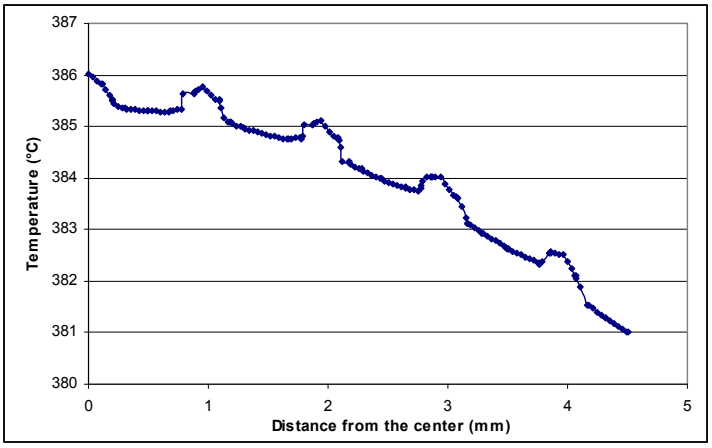

Figure 4.2. Thermal Profile of a dispersion fuel showing local heating within the microspheres

PuO_2 – Zr fuel with a particle loading of 5%. The bumps on the curve indicate the locations of the heat generating spheres.

These multiple validation techniques indicate that the thermal component of the finite element model is valid, and can be used to predict the temperatures within the dispersion fuel.

4.2. Stress Validation

There no analytical solution in the literature that solves for the stresses in the dispersion fuel geometry, due to the complex nature of the body to body interactions across the matrix. Since there is no analytical solution available in this situation, model simplifications were required in order to use an analytical validation.

The analytical solution that most resembles the dispersion fuel situation is that for a thick-walled spherical pressure vessel. In this solution, the thick-walled pressure vessel represents the matrix surrounding the spherical particle. The stress equations for the thick-walled spherical pressure vessel written for a fuel sphere are listed below [60].

$$\sigma_{Tangential} = \frac{P \cdot R_{fuel}^3}{2 \cdot R_{stress}^3} \cdot \frac{R_{matrix}^3 + 2 \cdot R_{stress}^3}{R_{matrix}^3 - R_{fuel}^3} \tag{4.5}$$

$$\sigma_{Radial} = \frac{-P \cdot R_{fuel}^3}{R_{Stress}^3} \cdot \frac{R_{matrix}^3 - R_{stress}^3}{R_{matrix}^3 - R_{fuel}^3} \tag{4.6}$$

where: $\sigma_{tangential}$ = the tangential stress within the pressure vessel wall at an arbitrary location (MPa)

σ_{radial} = the radial stress within the pressure vessel wall at an arbitrary location (MPa)

P = uniform internal pressure exerted on the walls (MPa)

R_{fuel} = the outer radius of the spherical particle (mm)

R_{matrix} = the outer radius of the pressure vessel wall (mm)

R_{stress} = an arbitrary location within the pressure vessel wall (mm)

The above equations reasonably approximate the dispersion fuel situation, because the microspheres in the matrix build up pressure from the fission gases, and exert that pressure onto the matrix, similar to a thick-walled spherical pressure vessel. Figure 4.3 shows how the geometry of the analytical solution compares to the finite element model. This solution does not take into account the interaction between multiple spherical particles that are present in the dispersion fuel, therefore, these equations are not strictly valid for the typical dispersion fuel geometry. The simple model is a reasonable approximation of the finite element solution in the limit of low volume fraction, and a second simplification can be made to make these equations valid for comparison to the dispersion fuel model. This simplification involves removing all of the microspheres within the matrix except one, in order to eliminate interaction of the stress fields between particles. Since the analytical solution does not take into account any

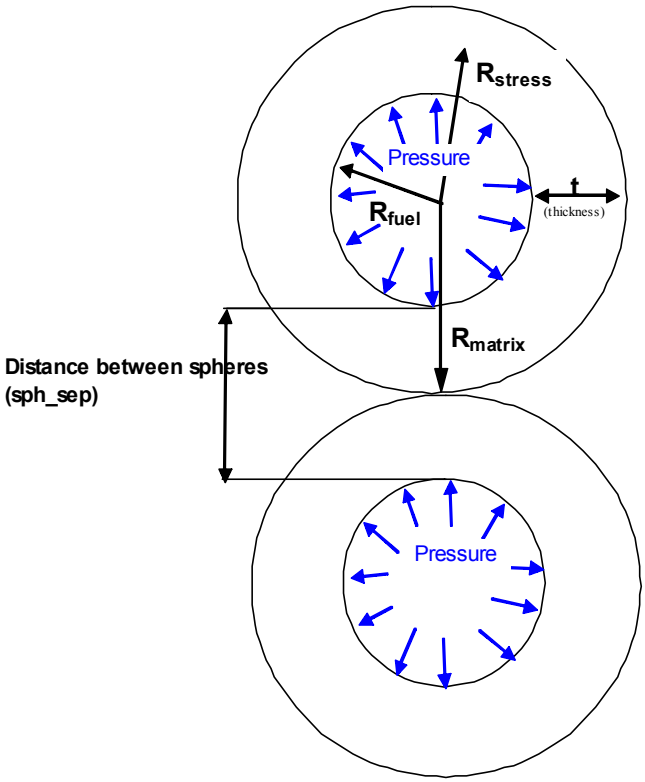

Figure 4.3. Geometrical representation of the analytical solution for the FEA model

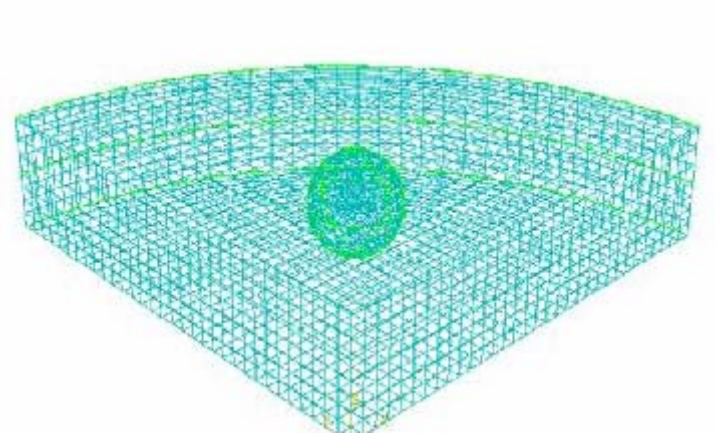

Figure 4.4. Required geometry for comparison to the analytical solution

temperature gradients within the spherical pressure vessel, the finite element model was also further simplified by removing the heat generation and convective cooling components. Fuel swelling was also not considered in the stress validation test, to simplify comparison of results. Figure 4.4 above shows the finite element geometry used to compare the model with the analytical solution for a thick-walled spherical pressure vessel.

The tangential stress found using equation 4.5 corresponds to stress tensor components σ_{22} and σ_{33}, the principal stresses in the 2-2 and 3-3 directions respectively. The radial stress found in equation 4.6 corresponds to the σ_{11} stress tensor that is solved for in the finite element model. The comparison between the analytical solution and the finite element solution is shown graphically in figures 4.5 and 4.6. The internal pressure in this test case was set to be 250 kPa, the microsphere radius was 1 mm, and the pellet radius 6 mm. Figures 4.5 and 4.6 show the tangential stress within the matrix

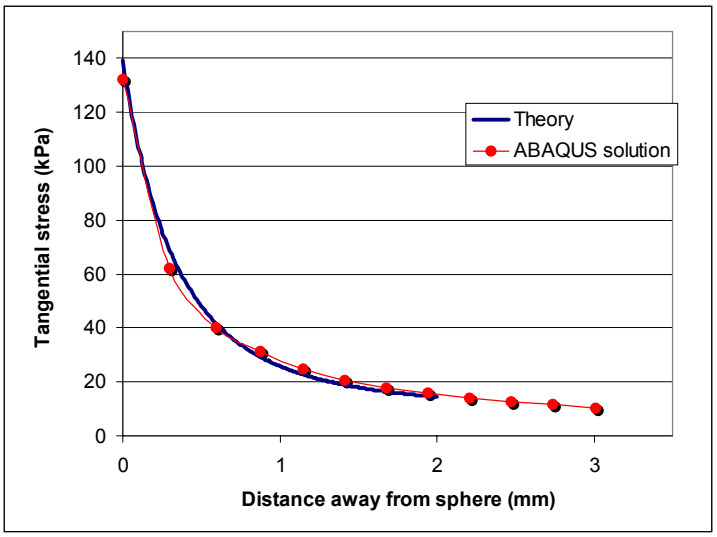

Figure 4.5. Tangential stress comparison of theory to FEA model

surrounding the particle to be positive (in tension), while the radial stress in the matrix surrounding the particle is negative (compression). The similarity between the finite element solution and the analytical solution in figures 4.5 and 4.6, show that matrix stress generated by the finite element analysis is consistent with analytical results.

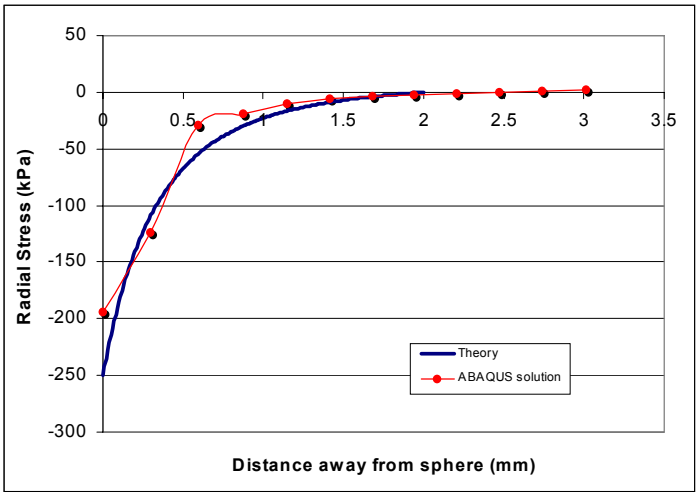

Figure 4.6. Radial stress comparison of theory to the FEA model

The tangential and radial stresses within the matrix are found to coincide with the analytical solution. From the results shown in figures 4.5 and 4.6, the validation of the finite element results is reasonable with regard to stress and strain, since one is dependent upon the other, as proven by the linear elastic model and Hooke's Law [5].

4.3. Swelling Validation

The fuel swelling that occurs within the fuel element, as a result of fission gases, is one of the modeled parameters. The number of valid experimental data points for UO_2–stainless steel dispersion fuels is small; only four well-documented data points have been found in the literature. More discussion about these data are presented in section

5.1. Of these four data points, only two include data on volume change during irradiation.

A simulation of the experimental data for the UO_2–stainless steel dispersion fuel was conducted using the finite element model. The primary variable of interest in this validation study was the overall volume change ($\Delta V/V$). The two studies focusing on this variable are required in order to show the validation of the finite element model in regard to swelling. Table 4.1 below shows the comparison between the conditions under which the experiments were performed, as well as the recorded swelling results and model conditions [31]. In the table, EXP refers to experimental data and results, while CPU refers to the results of the computational model.

Table 4.1. Comparison of experimental data to model data for swelling results [31]

Test Name	Dispersion Fuel Type	Volume percent of UO_2	Surface Temperature (°C)	Burnup (units in % of U^{235} atoms)	Overall Volume Change (%) [swelling]
EXP – 1	UO_2 – S.S.	40	470 – 625	6.8	2.62
CPU – 1	UO_2 – S.S.	39.77	528.15	6.83	2.51 – 2.77
EXP – 2	UO_2 – S.S.	30	430 – 525	9.2	2.33
CPU – 2	UO_2 – S.S.	29.72	434.32	9.233	2.22 – 2.39

A simple calculation analyzing the contribution of thermal expansion in the overall swelling shows that it only accounts for a small portion. The temperature drop across the pellet is less than 20°C and the effective coefficient of thermal expansion for a metal-matrix composite [25] is on the order of $1.5*10^{-5}$ $°C^{-1}$. Simple multiplication shows that the volume change due to thermal expansion is only on the order of tenths of a

percent. Therefore, it can be concluded that the majority of the swelling in this case is due to plastic deformation and swelling strain.

Looking at Table 4.1 , the ability of the finite element model to simulate the conditions of the two experiments is good. The swelling results generated by the model agree well with the actual recorded values for each case. The swelling results from the finite element model include a small range of values, because the swelling is a calculated value based on the changes in position of the nodes from the initial to the final state. This shows that the model can successfully simulate the global swelling behavior of the fuel.

4.3. Finite Element Analysis Model Stability

Validation of the finite element model was conducted to check the stability of the calculated results as a function of mesh size. Knowing that the model remains consistent for varying mesh size around the chosen mesh size indicates that the chosen mesh is appropriate for the problem.

In order to confirm that mesh size did not have an impact on the dispersion model results, the model was meshed more densely, step by step, until the limit of available computational resources was reached (due to memory error). Figure 4.7 shows the evolution, from a very large mesh to a much smaller, more dense mesh. Figures 4.8 and 4.9 show the evolution of stress and displacement as a function of mesh size for a dispersion fuel test case. These results show that very little variation occurs in the predicted stress and displacement values of the model as a function of mesh size. Both figures follow the progress of two specific nodes within the finite element model. One of the nodes is located within a sphere and one is located within the matrix. Figure 4.8 is a

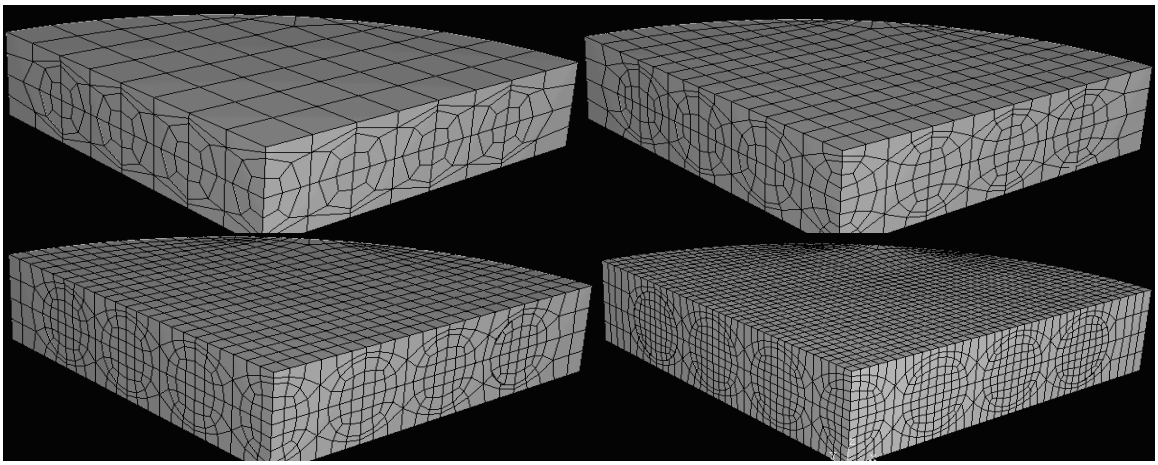

Figure 4.7. Evolution of the mesh sizes in the mesh convergence study

plot of maximum principal stress in the model versus the mesh size, while figure 4.9 is a plot of the total node displacement within the model versus mesh size. Additional examples of mesh stability plots are shown in figures 3.8 and 3.9. These plots showed the stability of the solution for temperature and strain as a function of mesh size. They also include the comparison of a solution for a linear element versus a quadratic element as a function of mesh size. The test case for these studies consisted of a pellet of radius 5 millimeters, a thickness of 0.705 millimeters, and a particle radius of 500 microns. The four plots 3.8, 3.9, 4.8 and 4.9 combined show the overall stability of the model with regard to mesh size.

The overall accuracy and stability of the model is verified by these validations. The thermal component of the model was compared to both an analytical solution and an alternate finite element model. This comparison demonstrated that the model correctly simulates the heat transfer mechanisms. The mechanical stress within the dispersion fuel as calculated by the finite element model was compared to the analytical solution for the thick-walled spherical pressure vessel. This study confirmed the ability of the model to

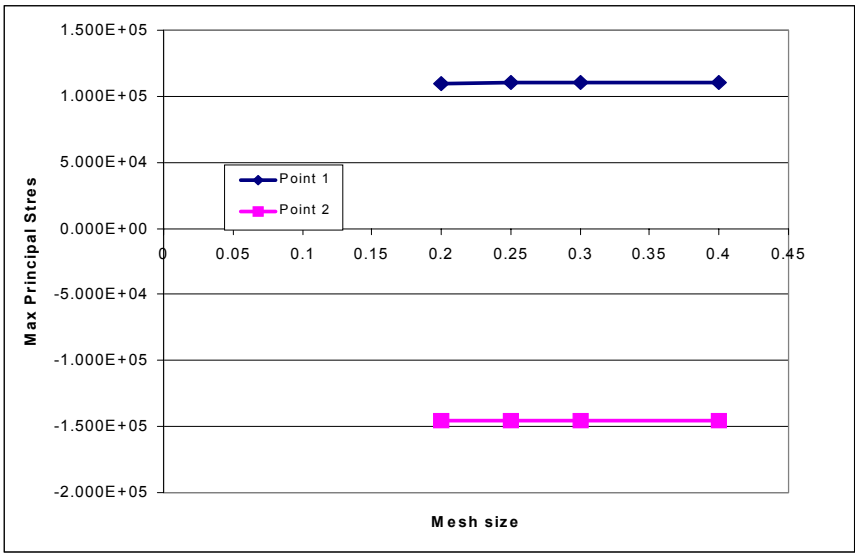

Figure 4.8. Maximum Principal Stress vs. Mesh size – showing mesh stability

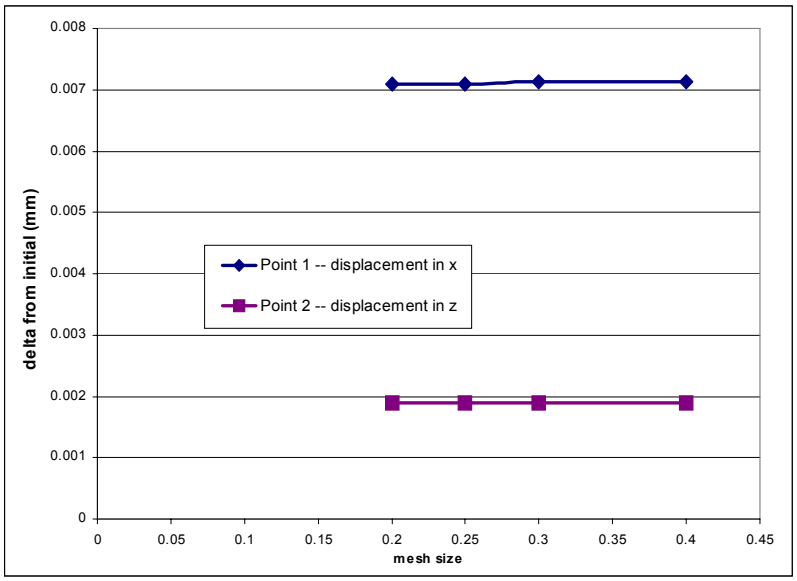

Figure 4.9. Total Node displacement vs. Mesh size – showing mesh stability

accurately simulate stresses that are generated due to gas pressure within the matrix. Model results were compared to experimental data to validate the ability to simulate the overall swelling of the fuel. The recorded swelling data was successfully predicted by the finite element model. Lastly, the model results were shown to vary only slightly as the mesh size and element type were changed. The results of these validation and benchmark studies prove the validity of this model with regard to the thermal and stress behavior of dispersion nuclear fuels.

CHAPTER 5

PLUTONIUM DIOXIDE–ZIRCONIUM DISPSERSION FUEL EVALUATION

In order to properly evaluate the proposed fuel, stability and failure regimes as a function of operating conditions must be determined. This is accomplished by selecting a failure criterion based on comparison between the model characteristics and experimental data. Once the failure criterion has been adequately defined, parametric studies are performed to gain an understanding of how operating variables affect fuel stability. These parametric studies are described in this chapter; results are presented both numerically and visually and analyzed for relevance to the in-service behavior of dispersion fuel.

5.1. Predicting fuel failure

Being able to predict failure of the fuel using the model is an important part of the overall understanding of the behavior of dispersion type nuclear fuel. Predicting how and when a failure occurs in a fuel of this type requires a thorough understanding of the experimental data that is currently available for dispersion fuels. As mentioned in chapter two, much of the research on dispersion fuels was done in the late 1950's and early 1960's. Some of the data are difficult to interpret; additionally, a great deal of the early research was classified, since some of the studies were conducted on fuels for use in defense applications. Because the breadth of experimental data is limited, the general applicability of the failure criterion may also be limited.

The largest database is available for UO_2 – stainless steel dispersion fuel. This data was discussed in chapter 2.4 and pointed to the fact that a great deal of the experimental data pertains to plate-type geometry. Unfortunately, none of this plate-type data can be applied to the study of the proposed fuel because it is a pellet-type geometry, and the pellet fuel likely fails in a very different way in comparison to the plate fuel (see figures 2.7 and 2.8). Therefore, the amount of UO_2-stainless steel dispersion fuel experimental data on which to benchmark the model is limited. Table 5.1 shows the primary data that were taken from three main references. The table also shows the conditions under which the experiments were run and whether or not the fuel failed, along with the amount of swelling which may have occurred. In the table, the test is labeled as a failure if swelling, cracking, or fission product release, resulted from the irradiation [19]. The data from reference 29 did not include the post-irradiation measurement of swelling. The data from reference 44 used $(U,Pu)O_2$ instead of only UO_2 data for the embedded fissionable particles. This discrepancy may impact the fuel response, since it is a slightly different fuel, but mechanically, UO_2 and $(U,Pu)O_2$ are quite similar, so that the differences should be negligible. Nevertheless, careful attention should be taken when comparing to this data. In addition, the swelling measurements for this data seem to be inconsistent, since two tests with identical conditions (30 volume percent loading and 635° – 645°C), produced significantly different swelling measurements of 8.6% and 5.3%.

Table 5.1. Complete UO_2 – Stainless steel pin-type fuel experimental data

UO_2 content volume %	Average particle size (microns)	Fuel Surface Temperature (°C)	Burnup % (atom % of U^{235})	Burnup % (of all atoms in the fuel)	Results: Failure? (swelling or vol. increase % - in parentheses)
[ref. 29]			Tests conducted by NDA (1954 – '56) [19]		
17.8	n/a	460	6.7	0.33	No failure (n/a)
18.6	n/a	500	16	0.82	No failure (n/a)
18.6	n/a	450	3	0.15	No failure (n/a)
18.6	n/a	450	8.2	0.42	No failure (n/a)
23.7	n/a	500	8.9	0.58	No failure (n/a)
			Tests conducted by KAPL (1953 – '56) [19]		
19.1	n/a	573	18	0.94	No failure (n/a)
22.4	n/a	573	18	1.13	No failure (n/a)
22.4	n/a	484	12	0.75	No failure (n/a)
23.7	44 – 74	425	28	1.85	1 of 2 failed (n/a)
23.7	44. – 74	425	34	2.24	1 of 2 failed (n/a)
23.7	44 – 74	425	35	2.31	Fully ruptured (n/a)
[ref. 13].					
50	n/a	440 – 565	4.7	n/a	No failure (0.85%)
40	n/a	470 – 625	6.8	n/a	No failure (2.62%)
30	n/a	430 – 525	9.2	n/a	No failure (2.33%)
[ref 44] – note: this data is for $(U,Pu)O_2$ –stainless steel fuel, pellet dia. = 2.5 – 3 mm					
50	100 – 350	585 – 595	8.8	n/a	No failure (3.9 %)
30	100 – 350	585 – 595	11.4	n/a	No failure (3.9 %)
40	100 – 350	585 – 595	9.2	n/a	No failure (2.4 %)
40	100 – 350	635 –645	4.1	n/a	No failure (3.6 %)
30	100 – 350	635 – 645	4.2	n/a	No failure (8.6 %)
30	100 – 350	635 – 645	4.2	n/a	No failure (5.3%)
40	100 – 350	635 – 645	4.3	n/a	No failure (5.2%)

The primary goal of analyzing this experimental data is to validate the formulation of the failure criteria. Of the experimental data listed in table 5.1, only one test fully failed. Therefore, this particular test (35% burnup, conducted by KAPL) is an obvious choice for inclusion in the evaluation. In addition to these two data points, four more data points were selected to be modeled; the two data points with the highest burnup from reference 13 were used, as well as the two highest burnup data points from reference 44. Even though the data from reference 44 uses fuel embedded with $(U,Pu)O_2$ instead of pure UO_2, the two fuels have similar properties overall, especially for small amounts of Pu [23, 59], so they remain valid.

The primary limitation in the use of this data to validate the failure criterion is that only one recorded test case actually failed. It is true that two others failed as well, but retesting using the identical conditions of those two points later resulted in no failure. Therefore, those two data points were inconsistent and not used in this study. Additional background research was conducted on this data point to ensure that this failed test did not occur due to negligence, improper test setup, or accidental local heating. The Oak Ridge National Laboratory report [19] from 1958 by Haynes, Neill, and Schaffer shows that this test was successfully conducted and has no indication of faulty conditions under which the fuel test was performed.

Table 5.2 shows the experimental conditions for the chosen tests as compared with the modeled parameters. The six tests that are listed in table 5.2 correlate with the highlighted experimental data points in table 5.1. For the tests in which the particle size was not given, an assumption was made based on similar data for these fuels. For the

Table 5.2. Comparison of Experimental conditions vs. Modeling conditions

Experiment or Computer calculation?	Particle loading content (vol %)	Particle size (microns)	Surface Temperature (°C)	Burnup % (atom % of U^{235})
Experiment – 1	18.6	n/a	500	16
CPU calc – 1	19.1	250	500.7	16.0
Experiment – 2	40	n/a	470 – 625	6.8
CPU calc – 2	39.77	250	471.5	6.83
Experiment – 3	30	n/a	430 – 525	9.2
CPU calc – 3	29.72	200	434	9.23
Experiment – 4	30	100 – 350	585 – 595	11.4
CPU calc – 4	28.62	225	592.1	11.42
Experiment – 5	40	100 – 350	585 – 595	9.2
CPU calc – 5	43.84	225	583.5	9.23
Experiment – 6	23.7	44 – 74	425	35
CPU calc – 6	23.70	59	425.0	35.22

tests that had a large range of surface temperatures, the assumption was made that the operating temperature was conducted within 1.5% of the minimum recorded temperature in the range. The material properties of the particles and matrix that were used to model these test cases are tabulated in appendix B, applied at each specific operating temperature.

Simulations of the experimental tests were input into ABAQUS. Computational time was typically in the range of one to seven hours per run. The length of time that it took to obtain a solution was directly related to the complexity of the geometry, specifically the number of surfaces and parts in the model. Figure 5.1 shows the geometry that was used in the model for the six different experimental tests.

The experimental test #1 is obviously the test with the lowest volumetric loading of particles. Tests #2 and #5 have the highest volumetric loading; the spheres in these two cases are nearly touching. Experimental test #6 differs in that it uses a distribution of

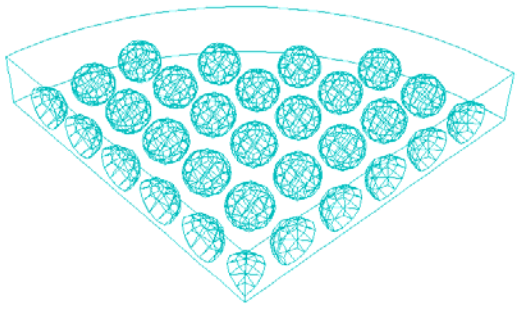

Experiment Model #1

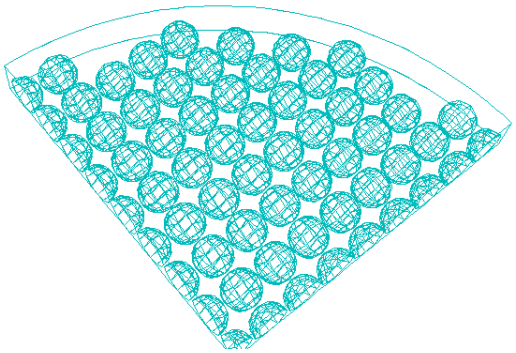

Experiment Model #2

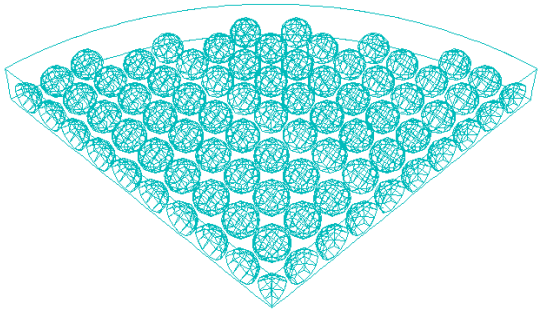

Experiment Model #3

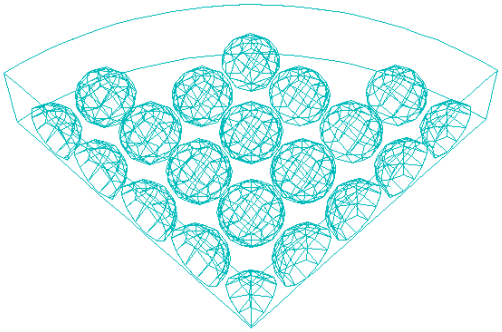

Experiment Model #4

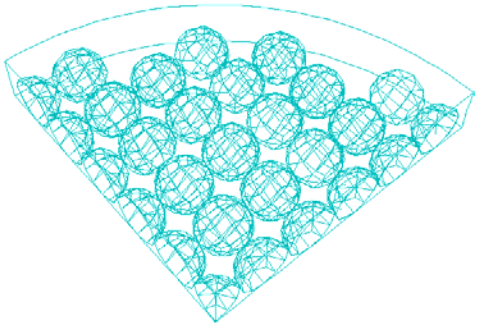

Experiment Model #5

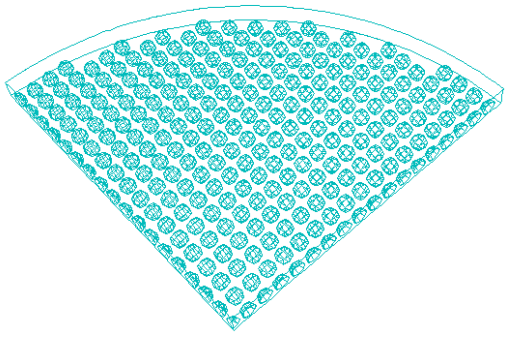

Experiment Model #6

Figure 5.1. Various modeled geometries for the experimental test simulations.

small particles. These small particles affect this experimental case quite differently than the larger particle sizes common to the other experimental cases.

The finite element model calculates solutions at every node or element within the model. Since there are thousands of nodes and elements in each geometrical model, this results in thousands of individual data points each having an individual solution. A difficulty lies in trying to select the data most relevant from the array of finite element solution values. Since a primary part of this research is focused on predicting fuel failure, it makes sense to select locations of maximum stress and strain. Data at surface interfaces, i.e. between the matrix and the particle, was also selected for analysis. The way in which these important areas were selected for analysis was by defining a 'path' within the model.

The 'path' can be viewed as a line cutting through the nodes and elements that records the solutions of the individual data points through which it intersects. Two paths were defined for each test case. The locations of these pathlines are shown in figure 5.2. Both of the paths were located in the z-direction (depth) to be exactly at the midpoint of

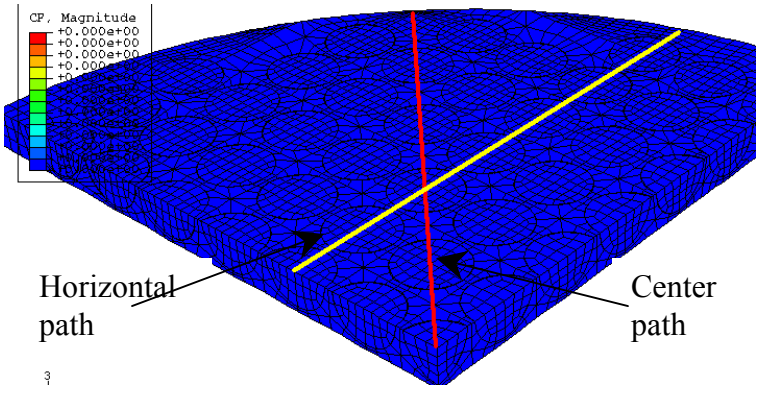

Figure 5.2. Pathlines used to gather the solution values at each data point

the slice, which cuts directly through the middle of the spheres, and through the center of the pin. The reason for locating the line in the middle is that the matrix experiences the greatest loads at this location. With a depth at the mid-plane, one of the pathlines follows directly through the center of the pellet from radius equal zero to the final outer radius. The second pathline is also at the mid-plane depth, but tracks horizontally through the center of a row of spheres.

Post-processing of the data was done by looking at the overall trends in the model using the ABAQUS post-processing program, as well as investigating each of data points along the pathlines. The matrix material stresses and strains are most relevant to this analysis, since this fuel type relies on matrix integrity to ensure long life; therefore, most of the data analysis is focused on mechanical behavior in the matrix. The primary focus of data analysis includes the maximum principal stresses, the maximum principal strains, the plastic strains, and swelling.

Some of the sources for these stresses, as stated in section 2.3, are thermal expansion mismatch, gas pressure, thermal gradients, and particle swelling. A simple stress comparison calculation was done calculating the thermal stress, swelling stress and stress due to fission gases. From this simple calculation, it was found that over 50 percent of the stresses experienced by the fuel are due to thermal stresses. The calculation focused on only one particle within the entire fuel pellet. The stress due to the pressure from fission gases was calculated using the tangential stress from the thick-walled spherical pressure vessel approximation. The swelling stress was calculated using the swelling factor, as determined in the literature for a particle, as a function of burnup [32]. Lastly, the thermal stress was calculated with using the simple thermal expansion

value. The conditions of the fuel for which this calculation was completed include: a sphere radius of 200 microns, 10 micron fission fragment range, 20 volume percent loading, burnup of 150 MWd/kgHM, and an operating temperature of 400°C. The results of these calculations show that the fission gas contributes 0.8 MPa of stress, the irradiation fuel swelling contributes 0.1 MPa, and the thermal stress contributes 1.18 MPa. Clearly, the thermal stress is an important aspect of the overall stress state of these fuels, and so temperature must be taken into account carefully in the development of the failure criterion.

When determining the failure criterion, a close look at the failure modes of the fuel pellet, and the stresses mentioned above, were considered. The most probable mode of fuel pellet failure is due to cladding rupture; therefore the development of the failure criterion took this into account. Failure could occur due to local stress (or strain), but many of the failures initiate due to microstructural flaws, fuel restructuring or internal chemical attack [38]. Microstructurally, a number of large pores, or holes, form within the fuel particles due to the segregation of fission gas bubbles. These plastically deform the fuel particles due to its internal pressure [31]. These local failure modes are very difficult for a finite element model, based on the mechanical behavior, to predict. Therefore, a different definition of the failure mode, as applicable to the finite element model, is required.

The local stress and strain profiles in each modeled case were investigated. A plot of the stress profile in a typical dispersion fuel element as generated by the ABAQUS model is shown in figure 5.4. The total strain and elastic strain profiles in a typical dispersion fuel element are shown in figure 5.3. These profiles represent the

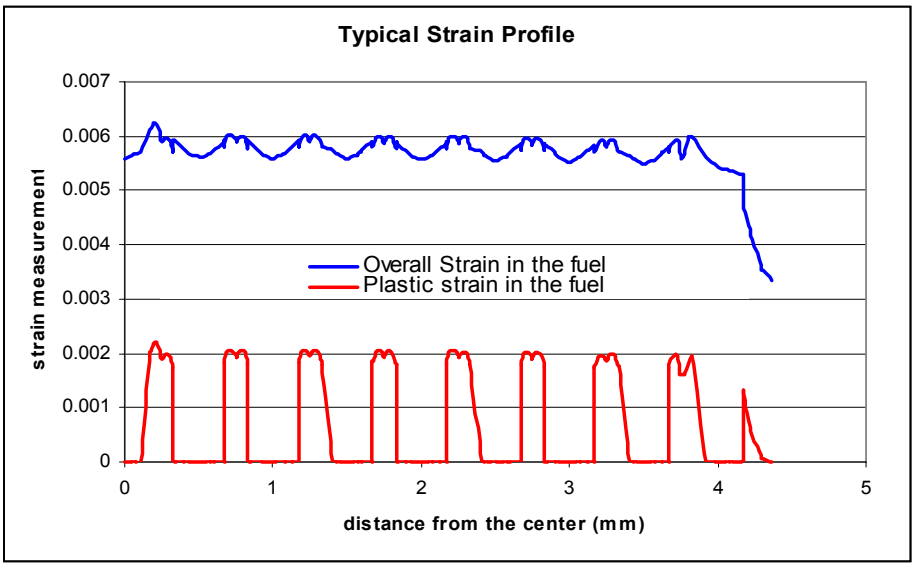

Figure 5.3. Typical Strain profile results from the FEM model

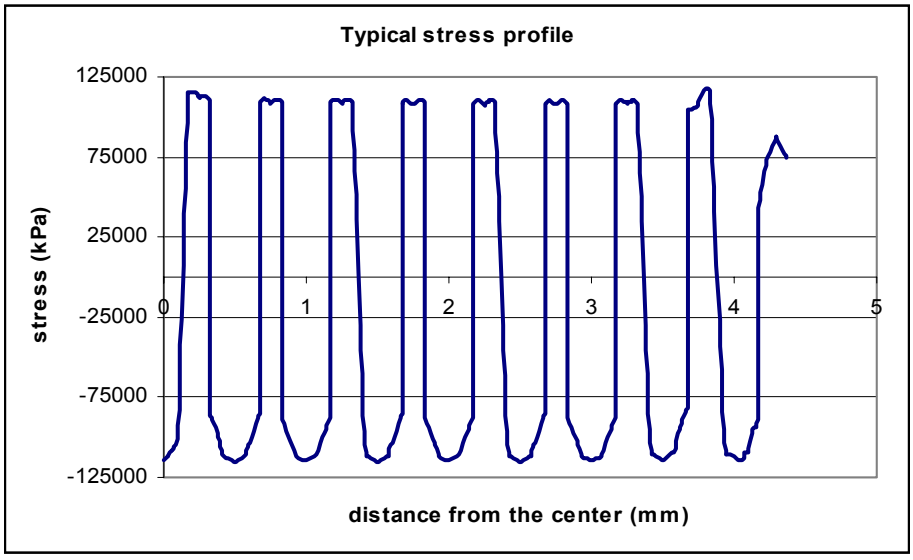

Figure 5.4. Typical Stress profile results for a dispersions fuel

details of the stress state within both the particles and the matrix. These profiles were taken from the pathline from a model with parameters: pellet radius of 4.5 millimeters, particle radius of 200 microns, volumetric loading of 20 percent, a burnup of 25 percent, and a power of 175 MW/m^3 per particle resulting in a surface temperature of 457°C.

The overall stress state of the fuel changes for the different test cases in a couple of ways. First, obviously, the values of stress and strain vary depending on what type of conditions are put on the fuel. Second, when the volumetric loading is higher (or lower), there are more (or less) peaks and valleys corresponding to the number of spheres within the matrix. If there are too many particles, the profiles would have many peaks and valleys due to the lack of matrix material present between the particles. Notice in figure 5.3 that the plastic strain is indicated only in the matrix material. The place where the plastic strain is zero is within the ceramic microspheres. The plastic deformation in the matrix is one variable that is looked at in developing the failure criterion. Figure 5.4 shows the stress state of the fuel where the matrix material has a positive stress associated with it while the particles have a negative stress. This is what should be expected since the matrix material is expanding around the spheres pushing on them in order to try to relieve the matrix.

Another feature that is seen in the profiles is that, since the volumetric loading is still relatively small, the stress (and strain) decreases slightly in the middle of the region of matrix material that is equidistant from the edges of the particles. This matrix region is more relaxed than the other regions because it is not completely adjacent to the particle – matrix interface. However, as the particles move closer together, a strain similar to figure 5.5 is experienced. As the particles approach, the stress and strain greatly increases causing local maximums. This demonstrates that the maximum calculated stresses and strains in the fuel are primarily a function of the proximity of the spheres. The stress and strain profiles are useful to understand the local phenomena occurring in the fuel, but on a global scale, the overall average is more applicable because it is not geometry dependent.

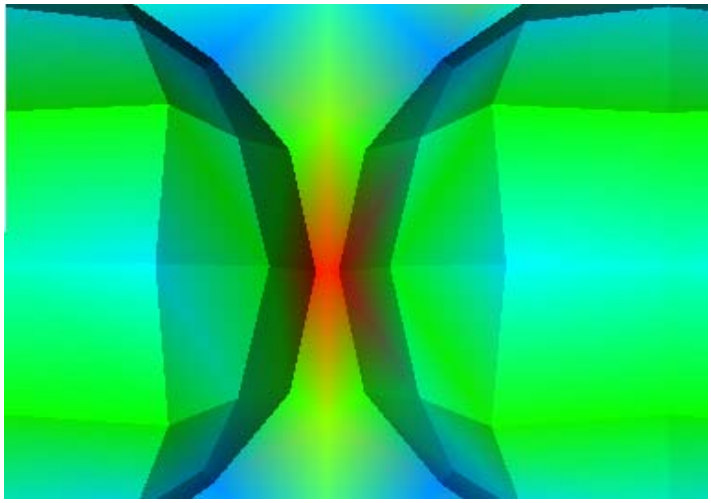

Figure 5.5. Strain contours in the matrix between two particles in close proximity

In general, the fuel is likely to fail once it becomes weak. This will occur due to microstructural interactions. Since the finite element model cannot sufficiently model all the small local interactions, the best prediction it can make is in the overall stress state of

the fuel. Therefore, when the overall stress state of the fuel approaches the yield stress, then the fuel throughout will be weak. The matrix in the fuel will be near permanent plastic deformation. When the overall stress state becomes fully plastic, the matrix is very weak and cannot withstand loads, so it will fail. This is the failure mode that is simulated by the finite element model.

The variables that were investigated to coincide with the failure mode as potential failure limits include:

- Maximum and average principal stress
- Maximum and average principal strain
- Maximum and average Von Mises stress
- Ratio of total stress to yield stress
- Ratio of total strain to yield strain
- Ratio of elastic strain to total strain
- Maximum and average swelling
- Maximum and average plastic strain
- Total stress compared to yield stress, ultimate tensile strength, or fracture toughness

Upon extensive evaluation, the determining variable on which the failure criterion has been based, while taking into account the failure mode, is the maximum principal stress value calculated by ABAQUS. The average of this value as recorded by the center pathline is the variable of interest.

Examination of the average stress within the matrix for each experimental case shows that the experimental data point with failed fuel had the highest average stress

calculated among all the experimental data points. Further consideration of this average stress within the rod led to a comparison of this average stress to the yield stress of the matrix material at the specific operating temperature of the experiment. The temperature at which this yield stress was calculated, was taken to be the surface temperature of the fuel model. The surface temperature yield stress value was used since that was the only temperature given and recorded in the experimental data, therefore, the most consistent in determining a failure criterion. Additionally, the temperature gradient across the fuel pellet is small. Figure 5.6 shows the comparison of the yield stress and average stress within the matrix for each of the experimental cases that were modeled. The cases are identified using the scheme in table 5.2 and figure 5.1. As seen from figure 5.6, the data from the experimental case that had failed is distinctly different from the other cases; in

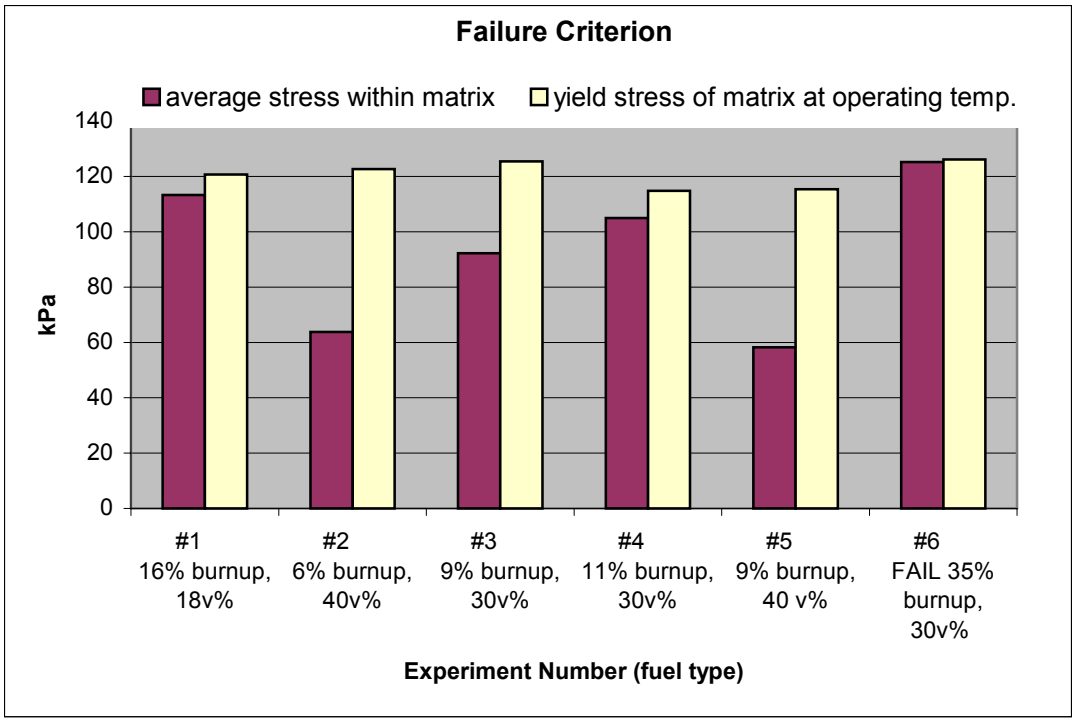

Figure 5.6. Comparison of average stress in the matrix to yield stress of the matrix

this case the matrix yield stress value and the average stress value within the matrix are essentially equal. In cases #1 and #4, the average stress is slightly lower than the yield stress. The average stress within the matrix for the other cases is far from approaching the yield stress. Using this trend, the overall data, and the defined failure mode, leads to the conclusion that a reasonable failure criterion can be developed based on comparison of the yield stress to average calculated stress. The failure criterion applied throughout this analysis is that failure occurs when the average principal stress in the matrix is equal or greater than the yield stress calculated at the surface temperature.

This failure criterion suggests that when the matrix material begins to plastically deform, locally, failure occurs. This is not the case since the successful experimental tests (#1 – 5) all experience some local plastic strain. In fact, some of the successful experimental tests experience a maximum plastic and elastic strain higher than the failed test. The key to the failure criterion is that the comparison is done using the average stress within the matrix along the center pathline. When the entire matrix, on average, is plastically deforming, failure occurs.

Since the tests are quite different in terms of total burnup, geometry and overall operating conditions, the failure criterion was based on a variable that is consistent throughout each of the tests examined. Averaging the stress within the matrix along the center path in each test provides the following benefits:

- The center path records all the data throughout the entire pellet, so averaging the data obtained by this path assists in reducing the maximum and minimum local values within the matrix, and promotes the overall global state of the pellet independent of geometry

- When comparing the resulting data to the yield stress data, the affect of temperature is normalized by taking the yield stress at the surface temperature as recorded in the experiment.
- It can be easily converted for different dispersion fuel materials, like a matrix of zirconium. The only requirement is to acquire the appropriate yield stress data for the material as a function of temperature.

The failure criterion for the proposed PuO_2–Zr fuel is defined in the same manner.

Figures 5.7 and 5.8 provide a visual presentation of the analysis results for each modeled experimental case. As can be seen, the figures depict stress and strain in only the matrix material; the spheres are removed for clarity in interpreting data. Figure 5.7 specifically shows the stresses that occur within the modeled pellet, while figure 5.8 shows the strains. Levels of stress and strain are depicted using color; the color scale for each figure is consistent throughout the six experimental cases, so that each shade represents the same value. The stresses within each case are globally similar. It is clear from inspection of figure 5.7 that the average stress in the failed experiment (#6) is higher than the other cases indicated by the absence of blue coloration (lower stress) in the images. In figure 5.8, the strains are more varied from case to case than the stress. The strains in the high volume loading cases are shown to be quite high in the areas where the spheres are almost touching. This is because the strain state of the fuel is similar to that which is shown in figure 5.5. Theoretically, the fission fragment damage zones are overlapping when the spheres are within 10 microns of each other, as was explained in section 2.3, resulting in local damage to the matrix of the fuel.

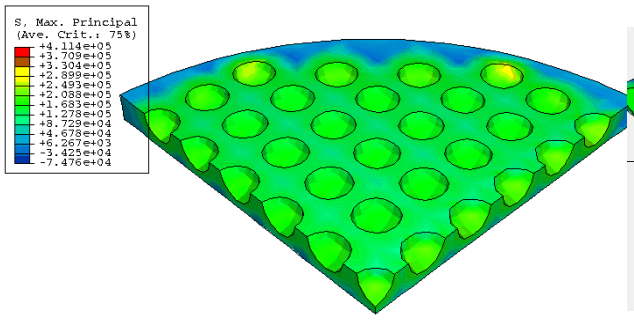

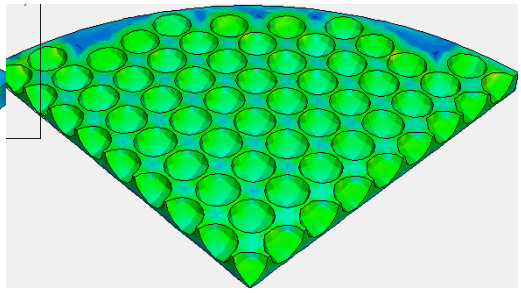

Experiment #1, 16% burnup, 18 vol%

Experiment #2, 6% burnup, 40 vol%

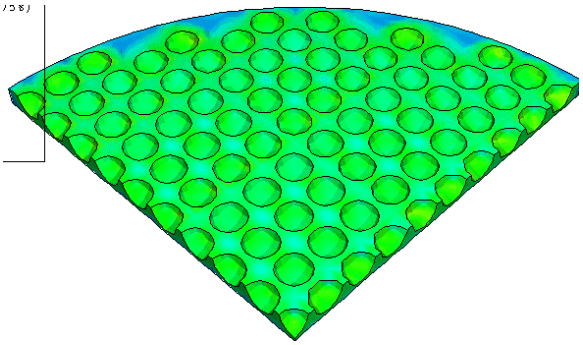

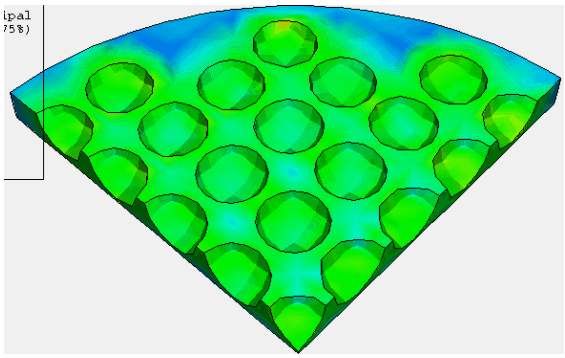

Experiment #3, 9% burnup, 30 vol%

Experiment #4, 11% burnup, 30 vol%

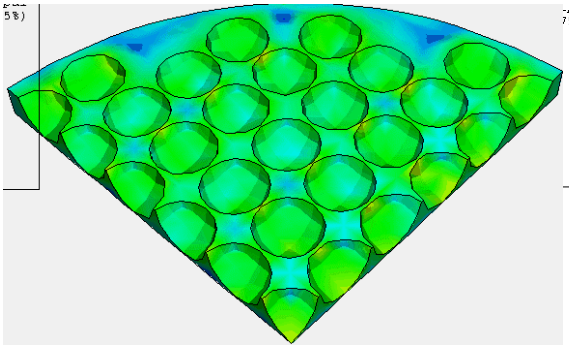

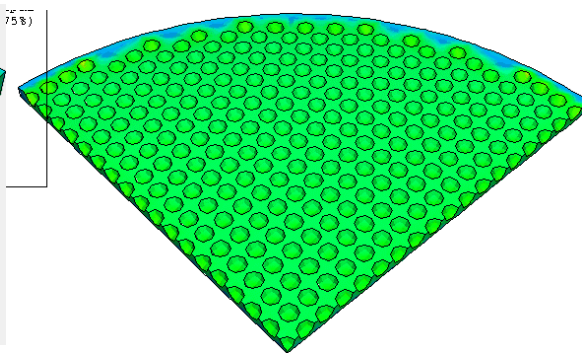

Experiment #5, 9% burnup, 40 vol%

Experiment #6, 35% burnup, 24 vol%

Figure 5.7. Stresses in the pellets for each experimental case (units are kPa)

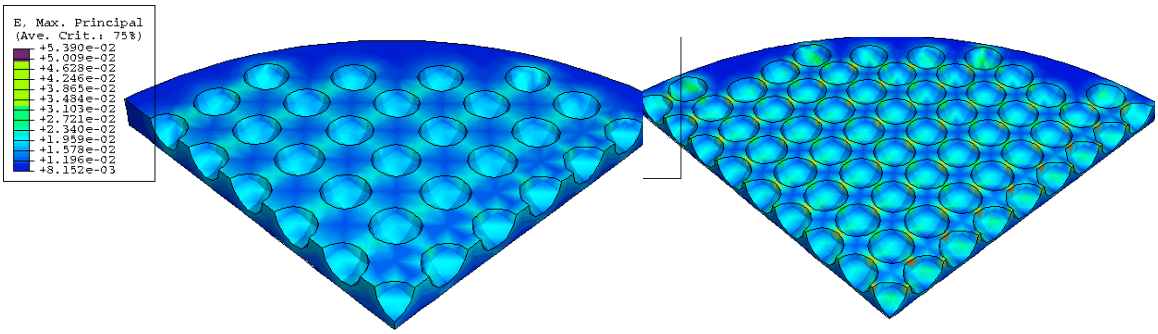

Experiment #1, 16% burnup, 18 vol% Experiment #2, 6% burnup, 40 vol%

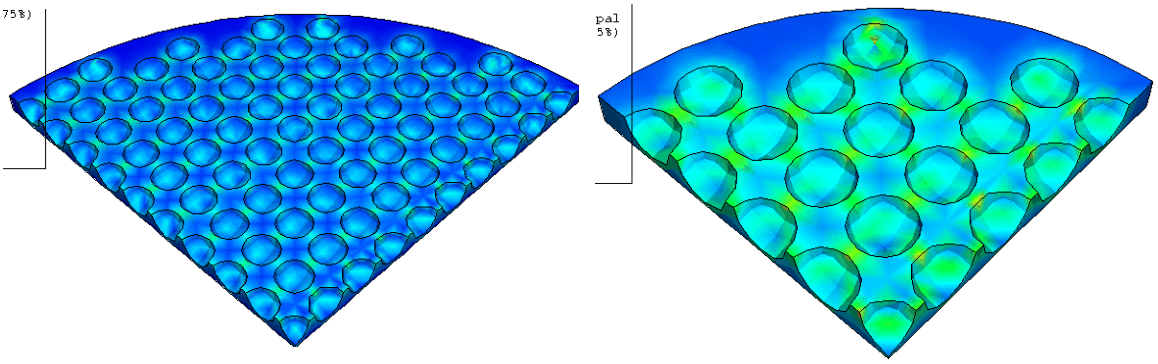

Experiment #3, 9% burnup, 30 vol% Experiment #4, 11% burnup, 30 vol%

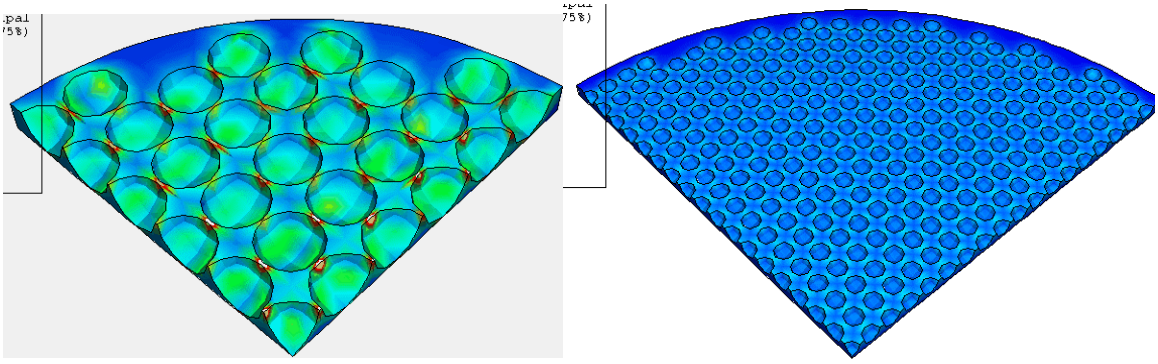

Experiment #5, 9% burnup, 40 vol% Experiment #6, 35% burnup, 24 vol%

Figure 5.8. Strains in the pellets for each experimental case

PuO_2 – Zr Parametric studies

The study of the dispersion fuel PuO_2 – Zr is important because it has great potential to help reduce the current United States plutonium inventory. The PuO_2 – Zr fuel offers many potential advantages (and few disadvantages) that were discussed in section 2.2. It is important that the behavior of this fuel be well understood for application in the commercial power sector, where fuel failure has considerable financial consequences for the operator. Parametric studies in support of understanding fuel design criteria are presented in this section. The material properties used in these parametric studies are tabulated in appendix B.

One of the parametric studies conducted for the proposed PuO_2-Zr dispersion fuel is the effect of particle size on the design of the fuel. This study was completed to verify the theory behind dispersion fuel matrix damage [55] regarding particle size. It was also conducted to determine the specific particle size for a PuO_2 – Zr fuel, containing a cubic array of particles that would be permissible without compromising fuel stability.

This parametric study was conducted by varying particle diameter at a constant fuel radius, volumetric loading, temperature and final burnup. The parameters used in this study were a fuel radius of 3.75 millimeters, volume loading of 25 percent, a surface temperature of 538°C from a 282 MW/m^3 power in each particle, and a burnup of 25 percent. Three different particle sizes were investigated, 300, 200 and a 100-micron radius. Figure 5.9 shows the model geometry. Using these geometries, the affect of particle size on fuel stability was evaluated.

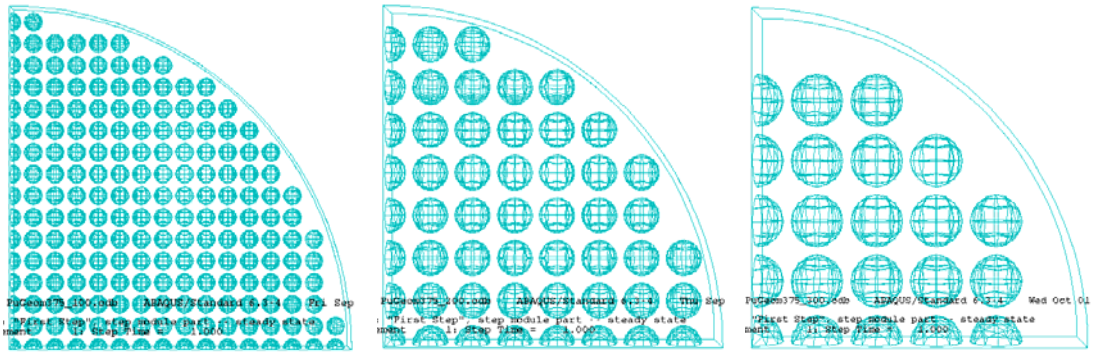

Figure 5.9. The three geometries used in the study of particle size effects

The second parametric study involved examining the effect of volumetric power on fuel stresses, strains, and swelling. This has the net effect of increasing fuel temperature and temperature gradient. This is important because the literature on dispersion fuels [29, 24, 44] indicates the high sensitivity of fuel failure on temperature. It is also important to understand the relationship between temperature, fuel loading, and burnup on fuel performance. This study was completed by taking a constant geometry and burnup, and varying the heat generation rate within the spheres. The geometry used in this study is shown in figure 5.10. The increase in heat generation rate represents an increased fission rate occurring within the particles. The model parameters for the power dependence test includes: a fuel radius of 4.5 millimeters, particles with radius of 200 microns, a volumetric loading of 20 percent, and a burnup of 25 percent. The range of volumetric power within the particles ranged from 50 MW/m^3 to 350 MW/m^3, resulting in surface temperatures ranging from 360°C to 700°C. Since the spheres are small, a large temperature gradient does not exist across the small particles, for most of the heat is conducted through the matrix away to the coolant.

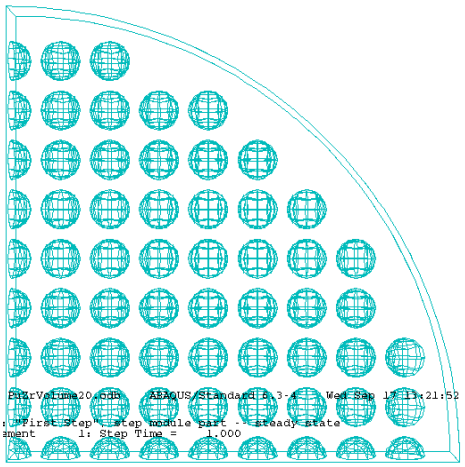

Figure 5.10. Geometry used in temperature dependence study.

The third parametric study investigated the role that volumetric loading plays in the stability of the fuel within the reactor. This study was completed to verify the theory behind dispersion fuel matrix damage [55] regarding volumetric loading. It was also conducted to determine the specific volumetric loading a PuO_2 – Zr fuel, would be allowed before compromising fuel stability. The relationship between the volumetric loading of fissionable particles within a dispersion fuel and the stability is important, because plutonium destruction rate can be increased at higher plutonium loadings. The maximum volumetric loading that can occur with the assumption of perfectly spherical monosize particles is 74 percent. This high loading value is desirable from a plutonium-burning viewpoint, but at that loading, there would no longer be any undamaged matrix material left for structural stability and high thermal conductivity. Few dispersion fuel tests have explored loadings higher than 50 volume percent [29,13, 44]. As a result, the volumetric loading study only tests fuels within the loading range of 5 to 45 percent. The primary microstructural changes that results from increasing the volume fraction of

particles is a decreasing web thickness, resulting in a lower fraction of undamaged matrix material. The model parameters used in these studies includes: a pellet radius equal to 4.5 millimeters, particle radius of 200 microns, a burnup of 25 percent, and a surface temperature equal to 441° C, resulting from a total pellet power of 31.2 MW/m^3. The geometries that result from changing volume loading are shown in figure 5.11.

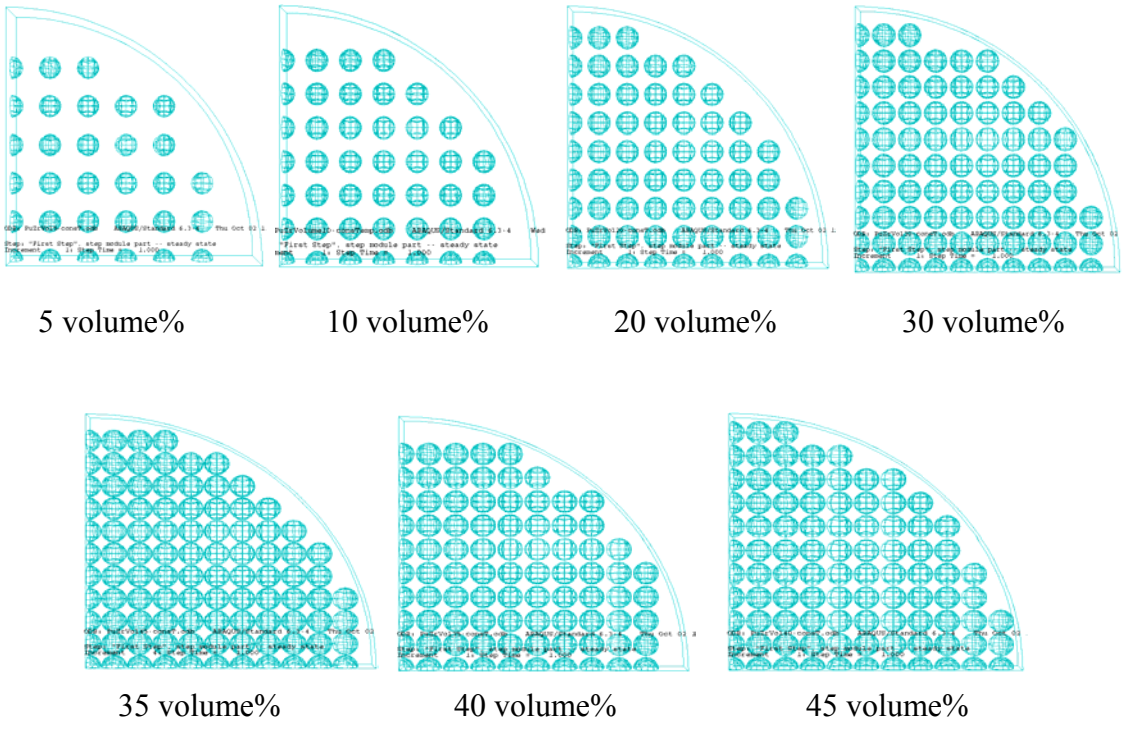

Figure 5.11. The geometries of increasing volumetric loading of particles

The fourth parametric study that was conducted examined the maximum burnup of the PuO_2 in the fuel before it becomes unstable. This particular study is very important because this can determine how much of the plutonium can actually be fissioned before the failure criteria is reached. The stability of this fuel in regard to burnup was modeled using a constant geometry, under constant conditions while varying the burnup. Increasing burnup in the model results in a greater pressure force exerted by

the fission gas on the matrix. The geometry and setup that was used in this study were a pellet radius of 4.5 millimeters, a particle radius of 200 microns, a volumetric loading of 35 percent, and a power in each particles of 120 MW/m^3 resulting in a surface temperature of 480° C. The burnup values that were tested ranged from 10 to 70 percent burnup of the fissionable atoms, or after conversion, from about 95 to 655 megawatt days per kilogram of heavy metal (MWd/kgHM). The geometry that was used for this study is shown in figure 5.12.

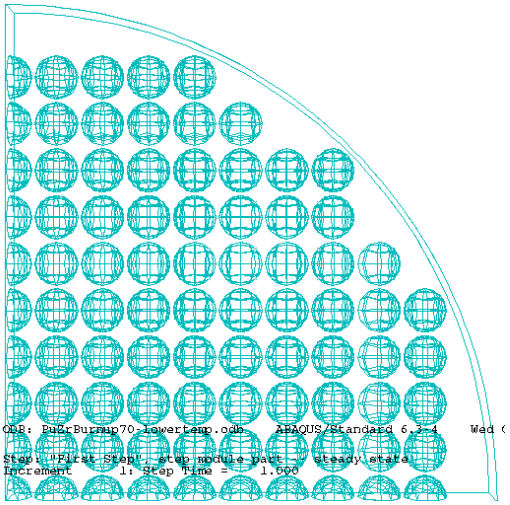

Figure 5.12. Geometry used in the burnup parametric study

These parametric studies offer insight into what variables affect the stability of the PuO_2 – Zr dispersion fuel. When analyzed in comparison to the failure criterion defined in the previous section, further understanding of dispersion fuel operating limits provides input to fuel design criteria.

5.3. Results and Discussion

In this section, results from the parametric modeling studies are presented, discussed and compared to the failure criterion established in section 5.1.

5.3.1. Sphere Size

The theoretical effect of changing the particle size was investigated in the early research on dispersion fuels. As discussed in chapter 2.3, a relationship was obtained by these theoretical studies. For a given volume fraction of fuel particles, decreasing particle size results in overlapping fission fragment damage zones.

Contour plots of the calculated results for the stress and the strain are shown in figure 5.13 as a function of fissile particle size. The color shades correspond to the scale on the left, which for stress is in the units of kilopascals. Inspection of the contour plots of the stress indicates only minor differences on a stress level.

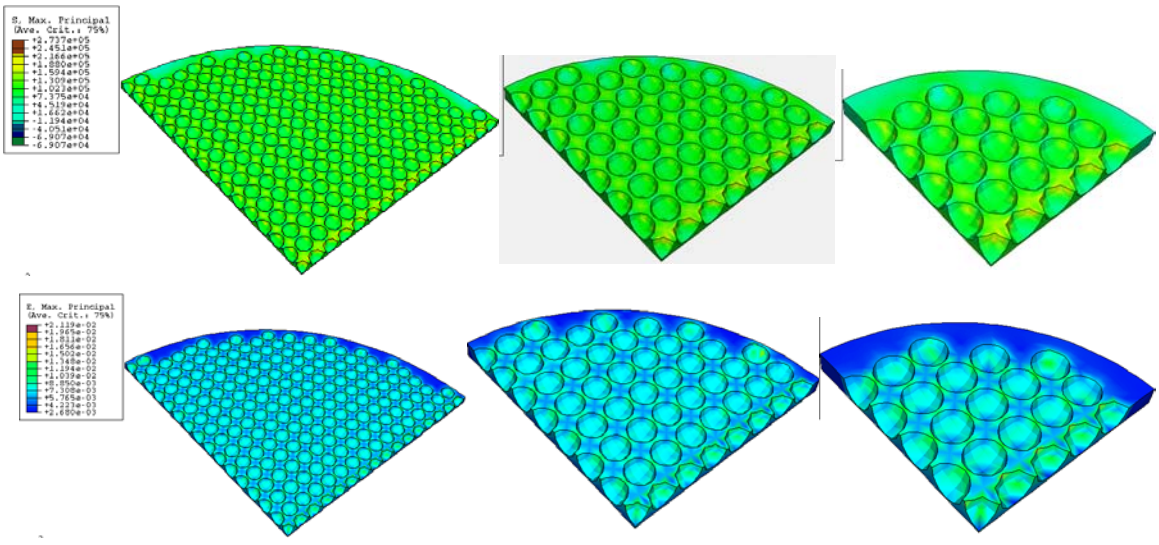

Figure 5.13. Contour plots of the stresses (top) and strains (bottom) within the sphere size test cases of 100, 200, 300 microns

Data acquired through the center and horizontal pathlines is more revealing. The average stress as calculated by the finite element model along the pathlines is plotted for the three different particle sizes in figure 5.14. Also included in figure 5.14 is a horizontal line representing the yield stress of the matrix material at the operating temperature. Stress values above this line indicate fuel failure.

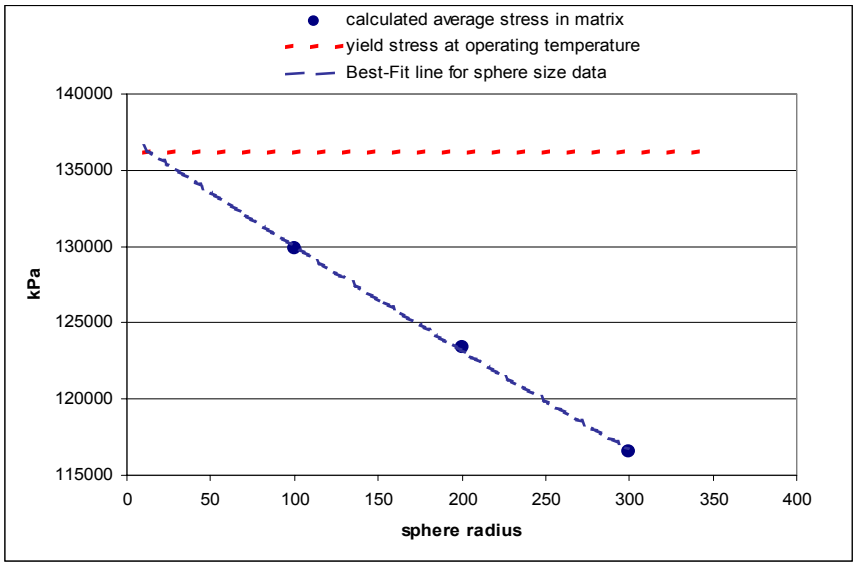

Figure 5.14. sphere size vs. average stress within the matrix

The trend of the stress data is linear in nature, which makes extrapolation of the data possible. The equation that most reasonably fits the data that was used to extrapolate the data on this plot, with an R^2 value of 0.999, is shown below. The variable "P" in the equation represents the particle radius.

$$\sigma_{average} = -66.55 * P + 136604 \qquad (5.1)$$

The yield stress at the operating temperature of 538° C intersects the extrapolated data at a particle size radius of nearly 14 microns. Therefore, according to the failure criterion that was defined in section 5.1, the fuel will be stable for particle radius larger

than 14 microns. Figure 5.15 shows the swelling that occurs in the fuel as the sphere radius is changed. Clearly, swelling is larger at the smaller sphere sizes, and stabilizes at sphere size larger than 200 microns. The results for the study on sphere size shows that larger sphere sizes are more beneficial in maintaining fuel stability, because the matrix stress increases as the particles decrease in size. This is in accordance with previous theoretical predictions. This might be the primary reason why, in the UO_2 – stainless steel experimental database, the one failed fuel data point that was used to define the failure criterion had the smallest particle size among all recorded cases.

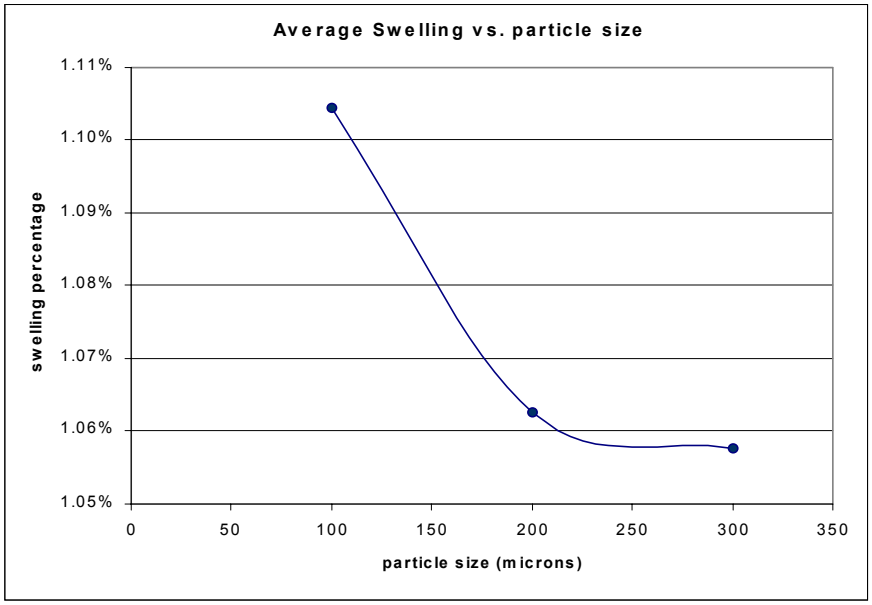

Figure 5.15. Average calculated swelling vs. sphere size

Using the linear stress trend logic shown in figure 5.14, the best fuel geometry would be a fuel with very large particle sizes, but obviously, that cannot be the solution either. Commercial nuclear fuel is essentially one big particle, since it is 100 percent UO_2, with no metal-matrix. The limitations of this approach are already known; dispersion fuel is researched as a candidate for extending the burnup range and safety in

light water reactors. The biggest issue with the very large particles is that heat is poorly conducted out of them, and local hot spots are formed as is seen in figure 5.16. On the other hand, smaller particles produce a much more smooth temperature profile, like the 100-micron case shown in the figure 5.16. Therefore, an intermediate size needs to be used in dispersion fuel production. As a result of this research, the recommended sphere size for the PuO_2 – Zr dispersion fuel is a particle with radius 250 microns ± 50 microns.

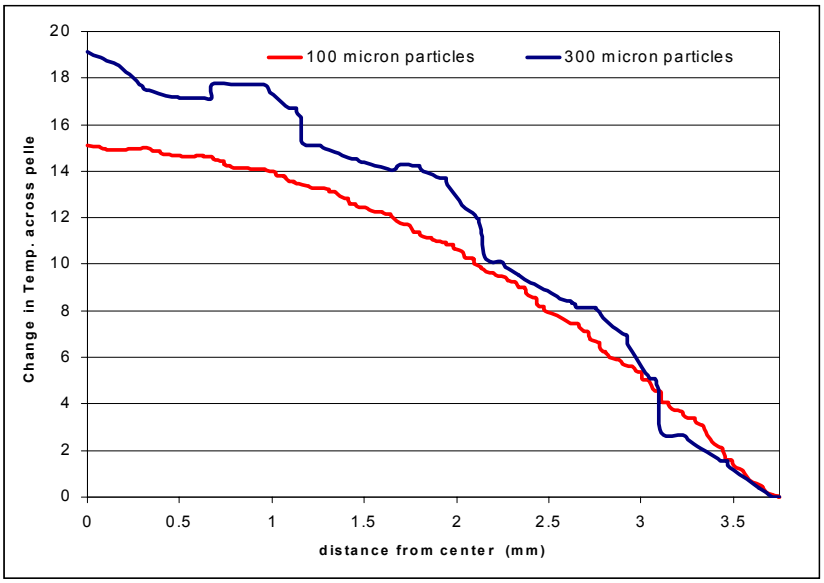

Figure 5.16. Temperature profiles for 100 and 300 micron sphere size

This size is a compromise between being large enough to reduce the amount of fission fragment damage to the matrix, yet still capable of conducting the heat out of the spheres without concern for forming local hot spots in the fuel.

5.3.2. Power

The parametric study that was done on the affect of operating power on the fuel produced the results shown below. Contour plots of the stress are shown in figure 5.17. From these contours, the stress appears to increase quickly beyond 420°C. Beyond 450°C, the stress levels off and increases only slowly. This trend can be seen in figure 5.18. On the other hand, the strain seems to increase with temperature in a linear fashion. This trend is shown in figure 5.19, and the corresponding contours in figure 5.20. In figure 5.18, the stress rapidly increases in the temperature range of 420° to 490°, and asymptotically reaches a constant value at higher temperature. The plot of swelling versus temperature undergoes a similar trend as the stress. The yield stress at each

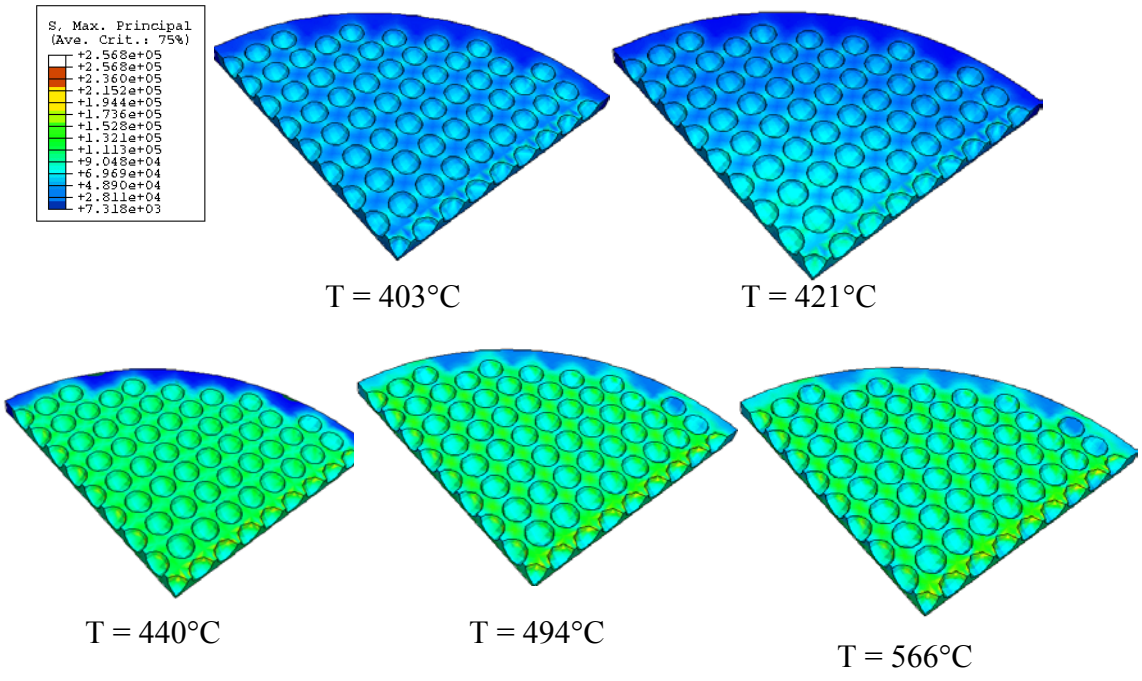

Figure 5.17. Contours of the stresses within the fuel at different surface temperatures (kPa)

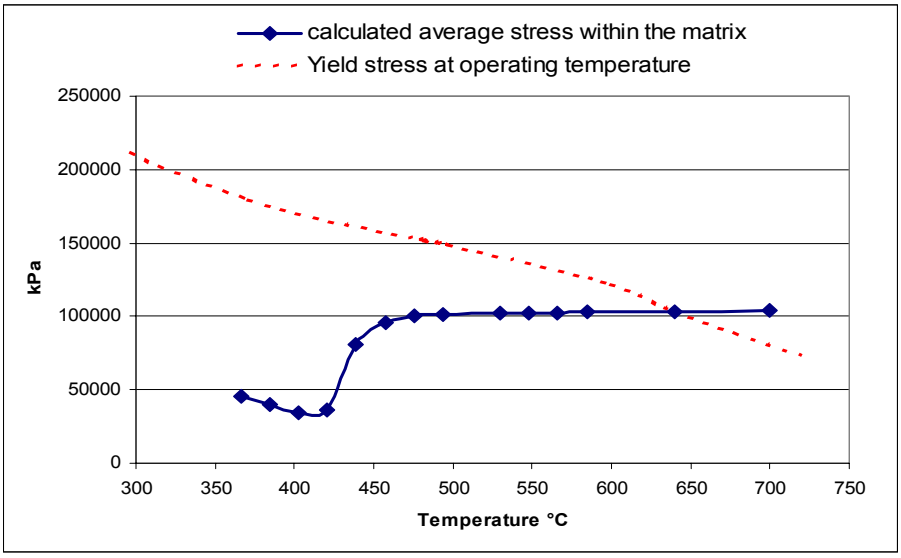

Figure 5.18. Temperature vs. average stress within the matrix

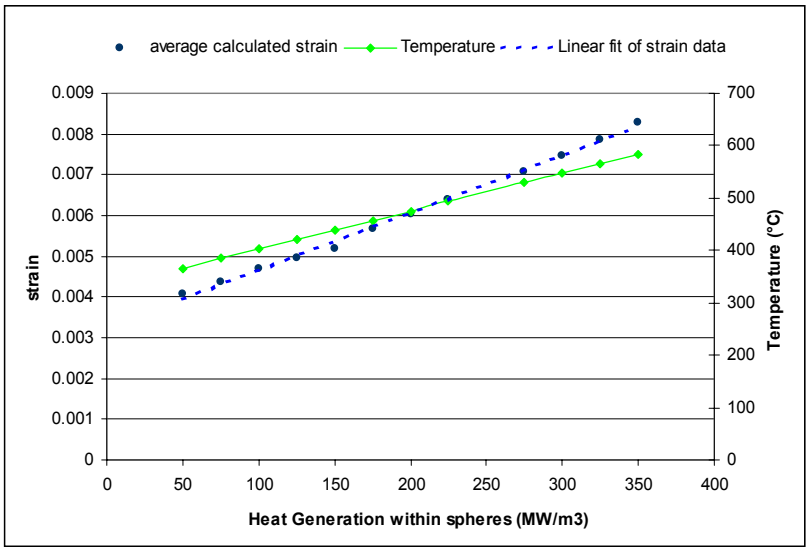

Figure 5.19. Strain and Temperature vs. heat generation within particles

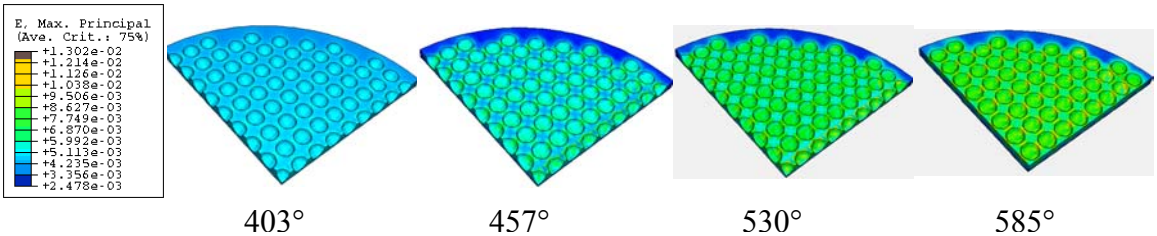

Figure 5.20. Evolution of increasing strain with increasing temperature

separate operating temperature is also included in figure 5.18. This yield stress intersects with the calculated average stress at a temperature of 640° C. Using this data in conjunction with the established failure criterion, results in the prediction that the maximum surface temperature that this particular fuel geometry can operate at is nearly 640°C. The estimated operating temperature for a zirconium fuel in a light water reactor is in the range of 400 to 500°C [22]. The primary reason why the stress jumps in this analysis is that the stress is greatly dependent upon the thermal expansion of zirconium (as seen in appendix B). The plotted strains increase at a constant rate with increasing temperature, as can be seen by the gradual increase in the contour plots for the different temperatures in figure 5.20. The strains are less dependent upon thermal expansion, but instead are more dependent upon the exerted pressures due to fission gases. Overall, the best way to maintain stability in the fuel in regard to temperature is to ideally operate below a surface temperature of 425°C.

One of the primary reasons for using dispersion fuel is to have a fuel that operates at a substantially lower temperature than commercial fuel. This indicates the strong influence that temperature can have on the properties and fuel performance. Temperature also plays a large role in affecting the ability of the dispersion fuel to operate safely, and long-term. The results from the finite element model show that there is a large increase in the stress in that range of temperatures, therefore, the temperature has a large effect on the fuel behavior.

5.3.3. Volumetric Loading

The third study was conducted to focus on the impact of volumetric loading on fuel integrity. The results for these tests are represented by the contour plots generated by ABAQUS, and the individual data points obtained from the pathlines. Figure 5.21 shows the stresses that occur as a function of volumetric loading. As the loading increases, the stresses increase even near the outer edge of the pin; for example, in the 45% loading case, the surface region experiences such a large stress that it is difficult to differentiate it from the middle stresses in the fuel (unlike the 10 and 20% loading cases). The theory associated with this variable is proven by the finite element model, since the calculated stress increases as the volumetric loading increases. The contour of the strain is shown in figure 5.22. Like the stress contours, there is very little strain in the 5% loading case, but as more particles are embedded in the matrix, local strain increases. Figure 5.23 shows the average calculated stress from the center pathline as a function of volumetric loading percentage. Included in figure 5.23 is the yield stress for zirconium at the operating temperature for these tests. The intersection at which the yield stress and the average stress within the matrix occurs, defines the point of maximum volumetric loading while maintaining fuel stability. Since the data behaves in a linear fashion, a linear best-fit line for the data was calculated for extrapolation up to the point of intersection. The equation that describes the data is:

$$\sigma_{average} = 2445.5 * V + 40292 \qquad (5.2)$$

In this equation, "V" represents the volumetric loading of fissionable particles.

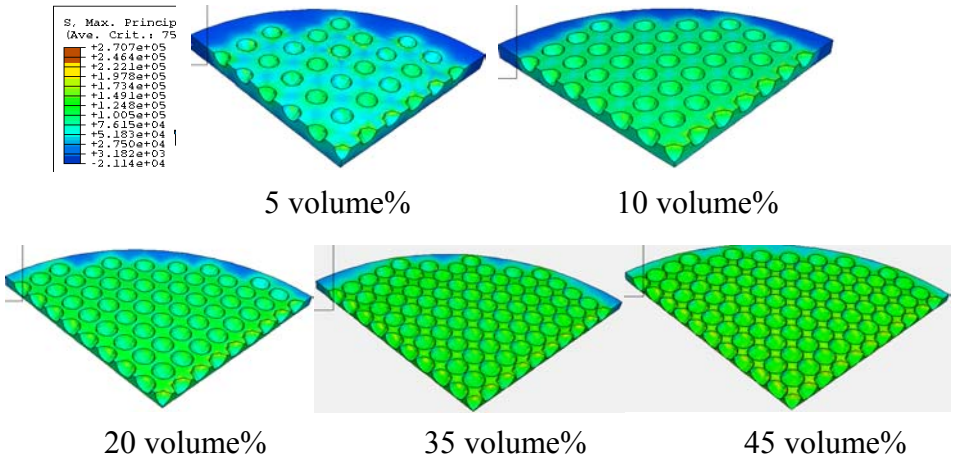

Figure 5.21. Contour plots of stress for different volumetric loadings (kPa)

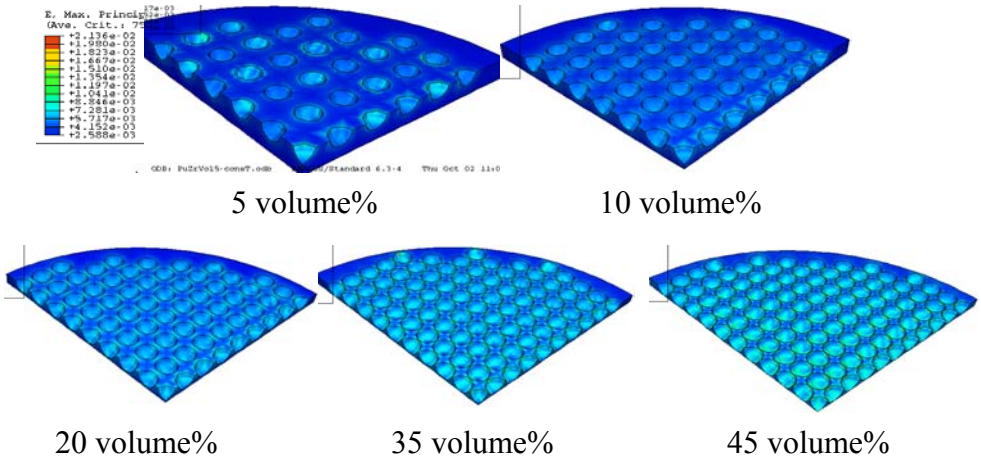

Figure 5.22. Contour plots of strain for different volumetric loadings

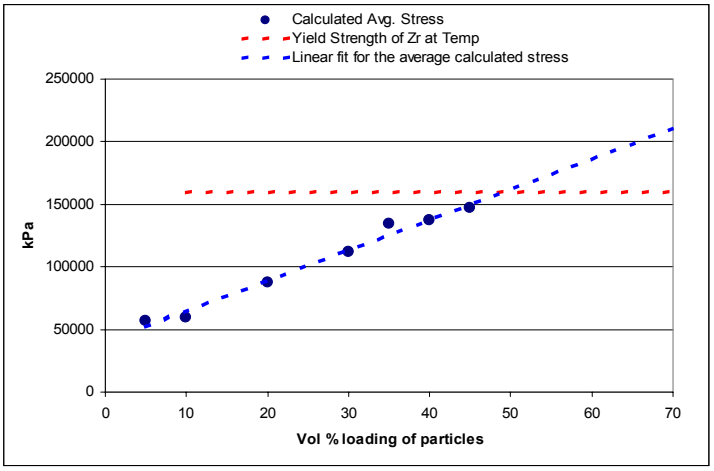

Figure 5.23. Calculated average stress vs. volumetric loading percentage

After using this equation to extrapolate, the intersection occurs at nearly 49% volumetric loading. The calculated swelling follows a trend very similar to the average stress shown in figure 5.23. The average swelling of the pellet is 0.83% for 5 volume percent loading, and increases to 1.134% for 45 volume percent loading. It is seen in figure 5.22 that the strains too, increase as the volumetric loading increases. Figure 5.24 is a plot of the temperature profiles for different volumetric loadings. The magnitudes of the temperatures are all nearly equal (approximately 453°C ± 1° center temperature), but they have been spaced apart vertically to assist in the overall comparison with each other.

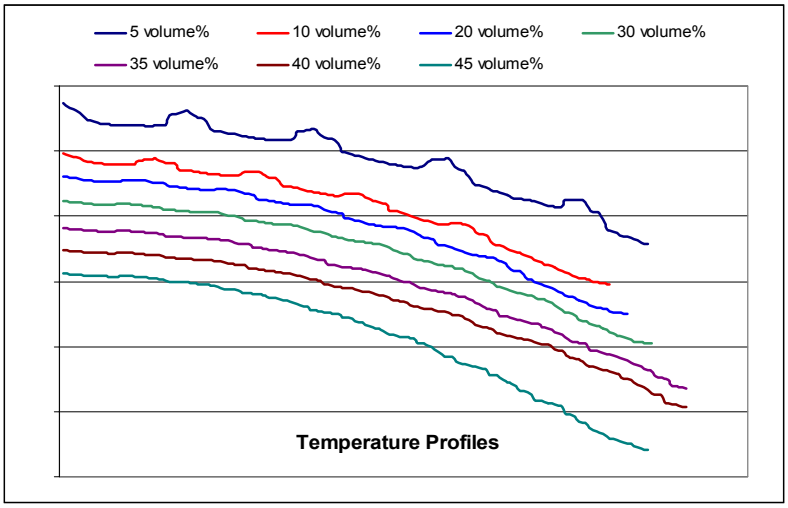

Figure 5.24. Temperature profiles of varying volume loadings

It is seen by the obvious bumps that the lower the volumetric loading, the more obvious the local heating within the spheres. As the volumetric loading increases, the temperature profile becomes smooth. This uniform thermal profile is offset, in the higher volumetric loadings, by a larger temperature gradient. This is to be expected since the volume of highly conductive matrix material decreases as the particle volume increases. Table 5.3 shows the effective thermal conductivity (at 300 K), using equation 4.4 as a function of

volume loading. Due to the decrease in effective thermal conductivity at high loading, higher volume loading cases have a higher temperature gradient from center to surface of the pellet.

Table 5.3. Effective thermal conductivity for various volume loadings

Volumetric loading percentage	Effective conductivity of dispersion fuel (W/m°K)
5	15.3
10	14.5
20	12.9
30	11.4
35	10.7
40	10.1
45	9.42

The compromise involved with the volumetric loading is that in order to efficiently burn the plutonium, the volume fraction of plutonium in the fuel must be high, but if it is too high, the fuel will fail. The recommended volumetric loading for the PuO_2–Zr fuel for maximum plutonium destruction while maintaining a safe distance from the failure point is a volumetric loading between 30 – 35 percent. Increasing the volume density of particles decreases the overall conductivity resulting in a higher temperature drop across the pellet. Overall, in a geometric sense, if there is enough distance between the particles to account for the damage zone formed by the fission fragments, then there will likely be enough matrix material present to keep the fuel structurally sound and thermally suitable for the fuel cycle needs. In summary, according to the finite element dispersion fuel

model, and the failure criterion, as one approaches 49% loading in a PuO_2 – Zr fuel, the fuel will approach its stability threshold for 25 percent burnup and 441°C.

5.3.4. Burnup

The fourth study investigated the amount of burnup that a fuel of this type can withstand while remaining below the failure threshold. Results are presented using the contour plots and specific data acquired from along the pathlines. Figure 5.25 shows contour plots of the 10% and 70% burnup cases. These contour plots show only small changes in matrix stress as a result of burnup increase. The contour plots of the strain are not included since the appearance of the contours does not vary much for each burnup case. The swelling also changes very little with the increase in burnup.

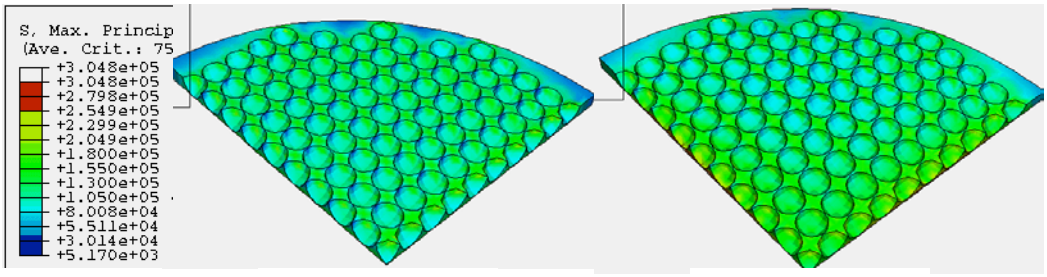

10% burnup 70% burnup

Figure 5.25. Contour plot of the stresses in 10% and 70% burnup cases (kPa)

One reason for the very little change in strain and swelling might be that the particles, that are releasing the fission gases, might be accounting for the some of the strain and swelling since they are experiencing an increase in strain as burnup increases. Figure 5.26 shows a plot of the strain and stress experienced within the particles with increasing burnup. The y-axis on the left corresponds to the strain and the y-axis on the

right corresponds to the stress. Another reason for a smaller change in stress than expected is because the majority of the stresses are thermal stresses, and the fission gas

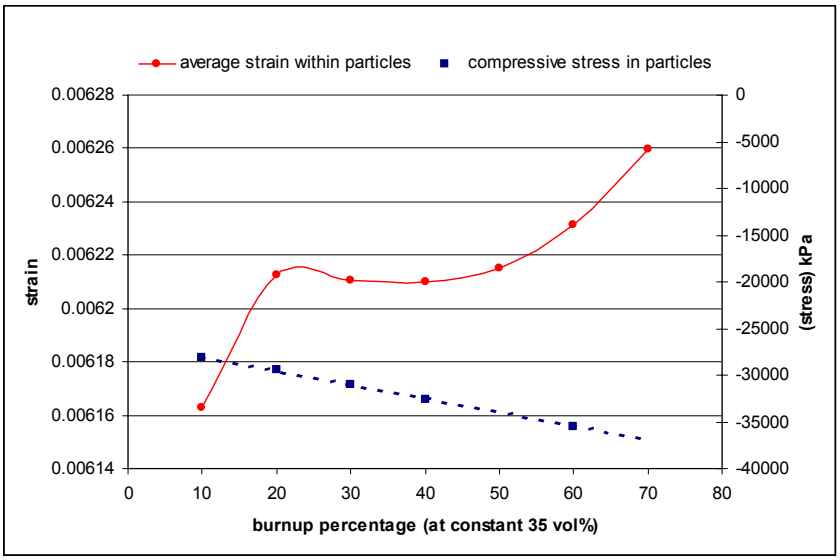

Figure 5.26. Stress and strain within the particle vs. burnup %

swelling stress is less of a factor in this case. Figure 5.27 shows the average stress within the matrix, as taken from the center pathline, as a function of burnup. Included on this plot is the yield stress of zirconium at the operating temperature of the fuel. The two lines intersect at a burnup value of nearly 35%. This value corresponds to the maximum burnup of this particular fuel (temperature of 480°C, and 35 volume percent loading) while maintaining matrix stress values below the failure threshold. The 35% burnup of plutonium atoms converted to the other typical burnup units is approximately 330 megawatt-days per kilogram of heavy metal, which is nearly five times higher than current burnup limits for uranium oxide fuels in light water reactors. Increasing burnup increases the fission gas inventory within the fuel, resulting in an increase in the stresses within the matrix.

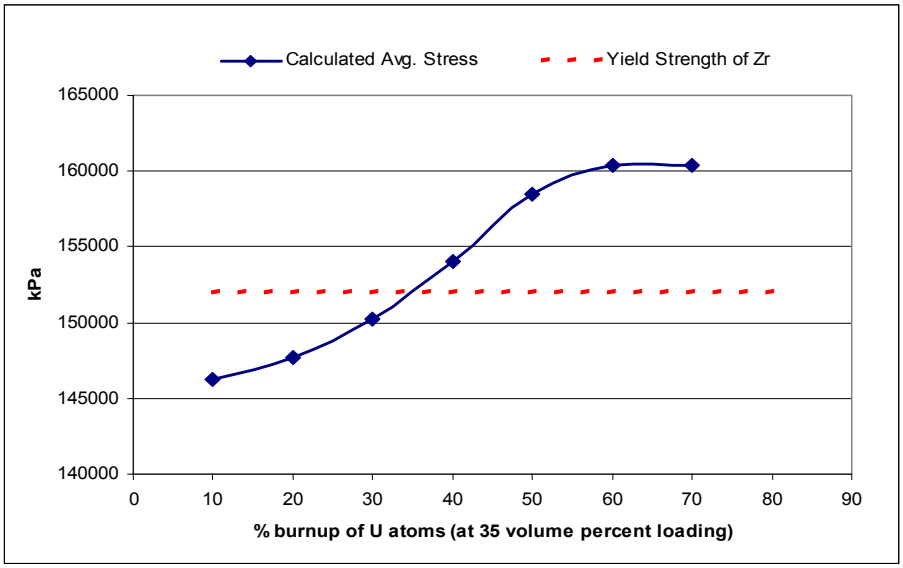

Figure 5.27. Average calculated stress vs. burnup %

The study on the burnup capabilities of the PuO_2–Zr dispersion fuel has led to an increase in understanding of to what extent this fuel can fission, and yet remain safe. The limiting factor in to what extent the fuel can burn in the reactor is whether or not the matrix can withstand the forces that are exerted on it by the production of fission gases in the particles. For this fuel type the objective would be to run the fuel to as high a burnup as possible, without exceeding the proposed failure limit. The ability to predict when the fuel might fail due to burnup is an important result, because maximizing the burnup of the fuel in the reactor maximizes the amount of plutonium destroyed.

Since the stress within the fuel also increases for a higher volumetric loading, these results will also affect the total burnup that can be achieved. There is decision that needs to be made in designing the fuel; higher burnup or higher volumetric loading? The answer to the question depends upon the needs associated with the fuel cycle. Additional comparisons of the burnup to temperature and volume loading will be shown later.

5.3.5. Material Comparison

The last set of data that will be presented is the data that was generated using the experimental geometries and conditions of the experimental tests mentioned in section 5.1, except using the PuO_2–Zr fuel materials instead of the UO_2–stainless steel materials. This is presented as a comparison between zirconium and stainless steel matrices. Figure 5.28 shows three bar graphs comparing the average swelling, the average strain, and the average stress in PuO_2–Zr fuel to the corresponding values in the UO_2–stainless steel fuel. Clearly, these three plots show the benefits of using zirconium as the matrix material, since the swelling, strain and stress is lower in the zirconium matrix than the

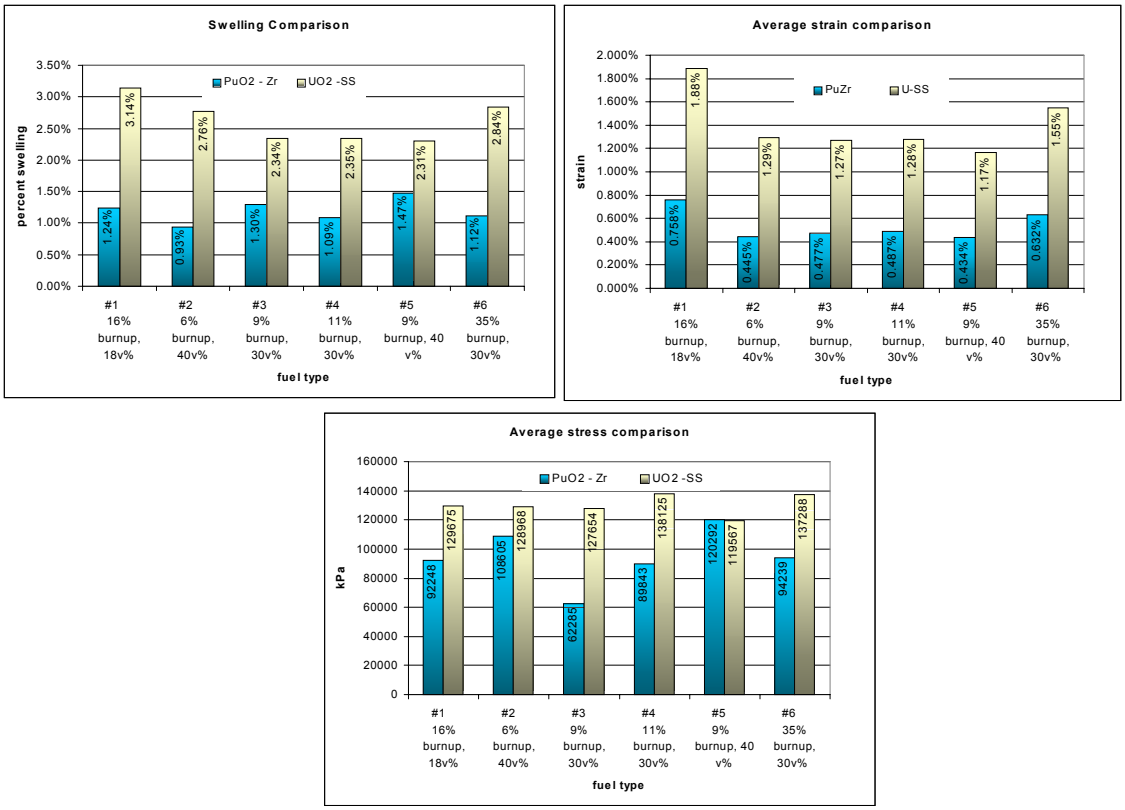

Figure 5.28. Comparisons between the UO_2 – S.S. fuel vs. PuO_2 – Zr fuel in swelling, strain and stress

stainless steel matrix. In addition, the yield stress of zirconium is higher than stainless steel, so according to the defined failure criterion, it should have an extended operating stability range relative to stainless steel fuel. Although, these advantages do not come without any drawbacks, for the cost of zirconium is much higher than that of stainless steel. Further material advantages of zirconium over stainless steel can be seen by looking through the material properties that are included in appendix B.

5.4. Additional Data Studies

An additional data study for the PuO_2 – Zr fuel, involved integrating together all the data from the various tests that were conducted. It is important to know how the different variables that were tested interact with each other. Analyzing the three primary variables of burnup, volumetric loading, and temperature as functions of average stress within the fuel, has led to an understanding of a few particular trends in the data under set conditions. A reasonable assumption has been made that the trends seen at a set temperature, volume loading, or burnup, will continue at each new value of temperature, volume loading or burnup. Previously, two of the three variables had to remain constant while looking at the stress distribution, but with some extrapolation and further data generation, a few new figures can be generated, where only one of the variables must remain constant. This leads to a better understanding of the interaction between variables. Figures 5.29 – 5.31, show two variable surface plots and give an indication of how the variables interact with each other as a function of stress.

Figure 5.29 shows the relationship between the volumetric loading and temperature at a constant burnup of 25%. The plane intersecting the curved surface is the

yield stress of zirconium as a function of surface temperature. The intersection of the plane with the surface is representative of the proposed operating limit, as defined by the failure criterion. This shows that at the lower temperatures, e.g. 400°C, the volumetric loading can be high (over 50%), but as the temperature increases, the loading must be smaller, viz. 37 percent loading at 465°C. The plot also shows that the fuel will not be stable if it has a high loading fraction and it is operating at a high temperature.

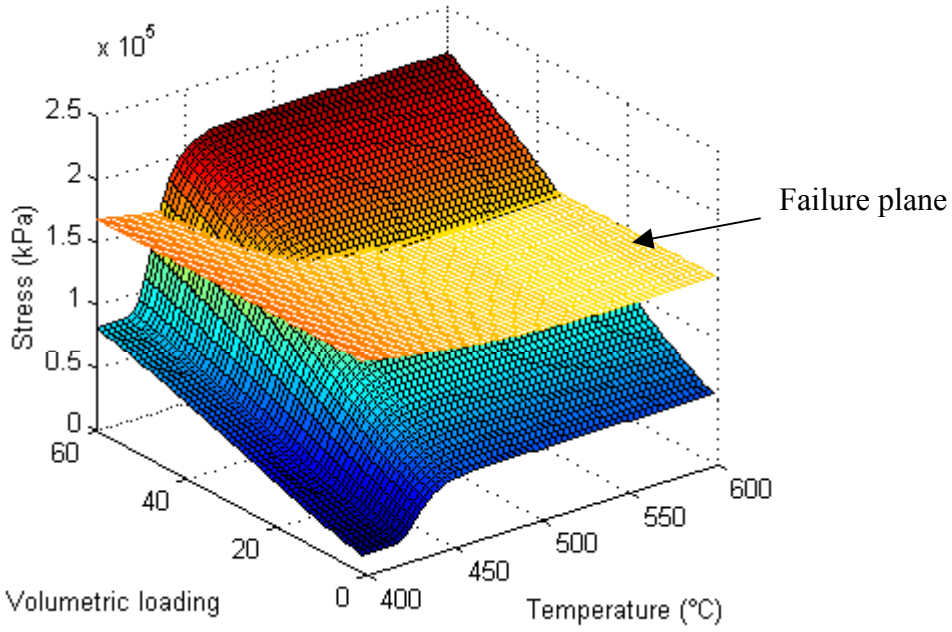

Figure 5.29. Combination plot of Temperature and Volumetric loading vs. Stress, including the failure plane

Figure 5.30 is a plot of the stress within the fuel given a volumetric loading and burnup value, with a constant temperature of 480°C. This plot again shows that the fuel stability is a strong function of volumetric loading. Burnup plays a relatively smaller role in generating matrix stress. The figure shows that a fuel can operate at 480°C with a maximum loading of about 38% if only a small burnup of 8 – 10% is desired. If the goal

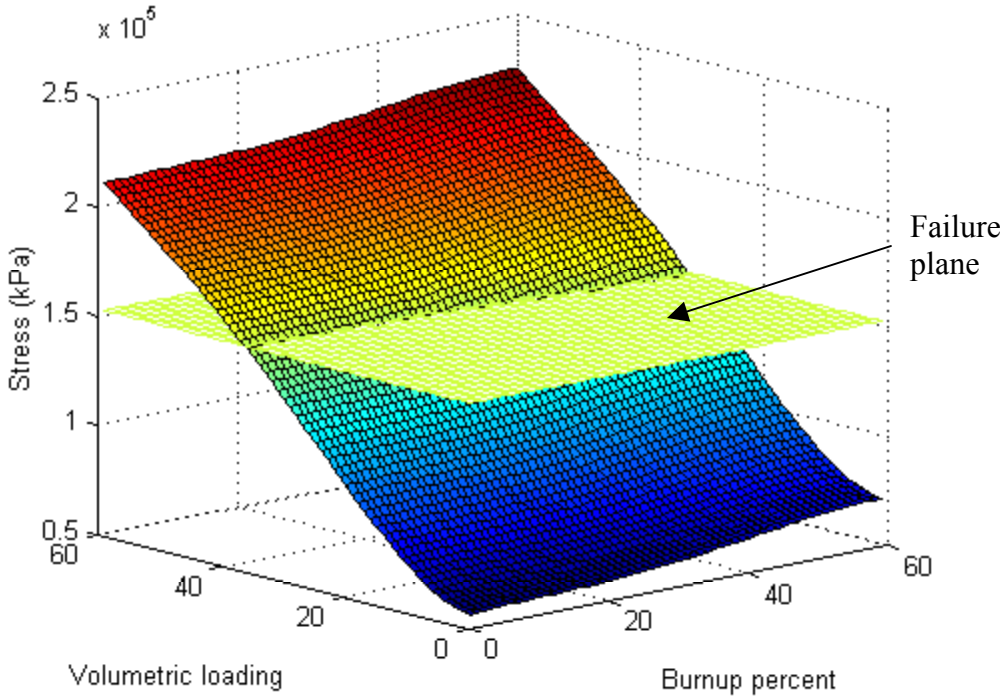

Figure 5.30. Combination plot of Volumetric loading and Burnup percent vs. Stress, including the failure plane

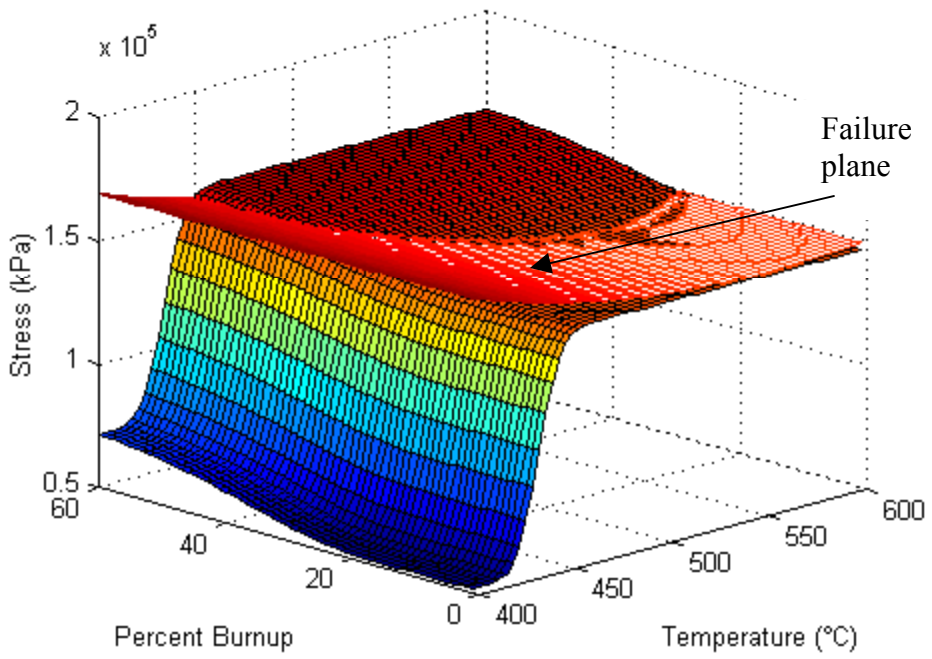

Figure 5.31. Combination plot of Temperature and Burnup percent vs. Stress, including the failure plane

of the fuel is to reach a high burnup, like 50%, then at this temperature, the fuel is limited to only 30 volume percent loading of fissionable particles.

Figure 5.31 shows a plot of stress as a function of burnup and temperature at a volumetric loading of 35 percent for the PuO_2 – Zr dispersion fuel. This plot demonstrates that it is difficult to get to a burnup higher than 30 percent if the fuel is operating above 510°C. If the desired burnup is only 25 percent, then the fuel can operate at almost any temperature below 600°C. This figure also shows that at this loading, temperature has a larger effect on fuel stability than burnup.

The PuO_2–Zr fuel that has been analyzed, is clearly a good candidate for the objective of disposing plutonium using commercial reactors. The primary variables that have been studied include: geometry, burnup, volumetric loading percent, and operating temperature. The results of the studies and how they affect the further design of the fuel has been discussed and analyzed in this section. The comparison of how each variable interacts with the other variables is presented in the plots in figure 5.29 through 5.31.

CHAPTER 6 – CONCLUSION

The primary goal of this research was to further understand the mechanical behavior of the PuO_2–Zr dispersion nuclear fuel, so that it could move one step closer to becoming one of the future fuels responsible for reducing the United States excess plutonium stockpiles. The mechanical interactions were studied by first gaining knowledge and information on all the interactions that occur within the fuel, then implementing them into a finite element model of the fuel. The finite element computer code, ABAQUS, was capable of simulating many of the interactions within the fuel, but several assumptions had to be made. After the model was completed, numerous studies were conducted to validate the accuracy of the model. The second set of studies focused on simulating experimental conditions of tests that were completed previously by nuclear research laboratories on dispersion fuels. As a result of these tests, a failure criterion was decided upon, and the model was converted for use in simulating the proposed PuO_2 – Zr fuel. Next, a number of variables were parametrically investigated as to their effect on the capabilities of the fuel. The results of these tests were analyzed and compiled into a set of helpful guidelines from which the design and performance of the dispersion fuel could be deduced. Using the previously defined failure criterion, it is possible to predict the limits of the PuO_2 – Zr fuel so that safety would not be compromised during operation. This finite element modeling and the studies associated with it, has led to further understanding of the important parameters involved with using a PuO_2 – Zr dispersion fuel.

The failure criterion that was defined using the experimental data from a UO_2–stainless steel dispersion fuel, has made it possible to make a reasonable prediction as to when the PuO_2 – Zr fuel might no longer be stable in the reactor. The results of the parametric studies were compared to the failure criterion after completion of the tests. The effect of the particle size inside the fuel pellet was evaluated using a few different geometries. The results of the study indicated that smaller particles are less desirable for the overall stability of the fuel. Therefore, it is recommended that a larger particle be used in the fuel pellet during manufacturing. Having a particle radius of about 250 microns would keep the particle large enough for fuel stability and small enough that localized hot spots would not be a problem within the fuel. The overall trend seen in varying the particle size is that the smaller a particle gets, the higher will be the stress produced within the matrix.

The effect of varying the reactor power, resulting in different operating temperatures in the fuel, was also investigated. The results from this study showed that the overall stress and strain within the fuel are quite dependent upon the operating temperature. The temperature range from 420° to 490°C is particularly sensitive to large changes in stress and strain for a small change in temperature. Therefore, the recommended operating temperature is around 425°C. Even though this is recommended, the actual operating temperature is a function of the reactor power level and associated power cycle design, so it is dependent upon the needs of the utility.

The last two studies evaluated the effect of burnup on the stability of the fuel as well as volumetric loading. These tests showed that volumetric loading has a great affect on the performance of the fuel. The burnup also has an effect on the stability of the fuel,

but a higher burnup is desired in order to meet the objective of fissioning away the plutonium effectively. If an increased burnup is desired, it can be achieved by either lowering the operating temperature, or lowering the volume fraction of particles in the fuel. Recommendations for the volumetric loading and burnup percentage are not specifically mentioned in this research, since it was determined that a number of different combinations can be successfully implemented for fuel stability. The actual recommendations should be based on the fuel requirements and overall economics of the plutonium disposal / power generation system. The combined effect of the three main variables on the average stress within the matrix is shown in figures 5.29, 5.30, and 5.31. These figures can be used to recommend what fuel design is suitable, and can help predict when the fuel integrity may be compromised while in the reactor.

Despite the abilities of the finite element model, a number of improvements could be made to the investigation of the PuO_2 – Zr dispersion fuel. First, the material properties of PuO_2 could be further researched, so that during the implementation of the model to PuO_2, it can be assured that the model is reacting in the exact way that the material should. Second, the capabilities of the finite element model could be expanded to include a more specific nuclear burnup characteristics. For instance, instead of simulating the fission gases that are produced by using a pressure force, it could be modeled more accurately at the interface of the matrix and particle materials by accounting for the porosity of the particles and the fission gas migration. Another primary area of improvement could be in the documentation of dispersion fuel tests that were done using a pellet geometry. Very few data points exist in that area; hence, more experiments should be conducted. Additionally, much of the data is classified, or has

been lost over the years. This lack of data has limited the confidence level in the predictive capability of the model. Overall, further studies and improvements could have been made to the model if the information had been available to more accurately simulate the PuO_2 –Zr dispersion fuel.

Now that the investigation of the mechanical behavior of the PuO_2–Zr dispersion fuel is complete, a few future suggestions are recommended. Further modeling of the fuel could be done by expanding the model to a full pellet geometry, rather than only a single slice. This also might be dependent upon the computational capabilities of the research organization. The model could also be expanded to include a larger window of the reactor coolant and fuel channels to look at the effects of the proximity of other fuel tubes to each other. The thermochemical stability of the zirconium and the plutonium within a reactor pool should also be further studied, so that the effect of corrosion and fission product chemistry on the strength of the fuel can be understood. A detailed analysis needs to be done on the ability to neutronically control a reactor that is completely made of a non-fertile fuel like plutonium alone. If the fuel successfully passes these analytical tests, the next major step that is recommended is manufacturing a number of fuel pellets in this form, and running experimental tests, to see if the fuel reacts as it should according to this finite element model, and other chemical and neutronic models.

The results of this study show that the PuO_2 – Zr dispersion fuel has a promising outlook in the future. This research alone does not allow the determination of whether or not this fuel will be capable of reducing the excess plutonium stockpile, but it has shown that further research ought to be done on this fuel type to further investigate its

capabilities. One of the major drawbacks of this fuel is the overall cost of manufacturing and production. Since zirconium is relatively costly, it is essential that a cost effective means of production be implemented so that it can compete with other fuels. The advantageous characteristic of plutonium destruction is not, by itself, enough to adopt this fuel type, since if it is too expensive, it would likely no longer be in consideration. However, if the recommended research mentioned above, is followed, there is a good chance that this fuel will be seriously considered as a possibility in the future plutonium disposal plan. There are issues that need to be taken care of before using this dispersion fuel, but the overall use of this fuel to achieve the objective is a feasible goal.

Since one of the primary goals of the advanced fuel cycle initiative, supported by the United States Congress, is to reduce the amount of plutonium that is disposed of in underground storage, it is essential that a new fuel be developed that can be used to burn the excess plutonium, while producing electricity. One possible fuel to achieve this objective is the PuO_2–Zr metal-matrix dispersion fuel. The mechanical behavior of this fuel has been investigated and shown that it can remain stable inside a reactor in order to destroy the plutonium. There are some limitations to the fuel that need to be considered in the manufacturing and reactor operation areas, but overall these studies show that it can withstand the loads that are applied to it while in the reactor. Overall, the results of this research have shown the stability and limitations of this PuO_2 – Zr dispersion fuel, but more studies need to be done before the fuel can be implemented in order to further solidify the safety and design requirements of the fuel.

APPENDIX A

Example PYTHON Scripting Computer Code for Generating the Dispersion Fuel Model

```
"""
Dispersion fuel geometry and model

"""
#**********************Define Geometry parameters (all values in mm)
cyl_rad = 3.0
cyl_depth = 1.25
sph_rad = 0.400
sph_sep = .100
edge_dist = .100

# convection_coeff = 500
# Tinf = 330.0   #convection sink temperature C
pressure = -593.8  #need a negative b/c pressure is on matrix
heat_gen = 100000
tie_dist = 0.005
#**********************

# Create a model.

myModel = mdb.Model(name='pellet')

#--------------------------------------------------
#  BUILD AND CREATE THE MATRIX PART AND THE FUEL PARTS
#--------------------------------------------------

import part  #creates the part

# Create a sketch for the base feature.

mySketch = myModel.Sketch(name='pellet',sheetSize=20.)

# create the quarter arc for pellet extrusion
mySketch.ArcByCenterEnds(center=(0.0,0.0), point1=(0.0, cyl_rad), point2=(cyl_rad,
        0.0))
mySketch.Line(point1=(0.0, cyl_rad), point2=(0.0, 0.0))
mySketch.Line(point1=(0.0, 0.0), point2=(cyl_rad, 0.0))

myBeam = myModel.Part(name='pellet', dimensionality=THREE_D,
         type=DEFORMABLE_BODY)

# Create the part's base feature by extruding the sketch
# through a distance of cyl_depth (mm)
```

```
myBeam.BaseSolidExtrude(sketch=mySketch, depth=cyl_depth)

# while loop partitioning it along the z-axis as many times as the number of spheres
new_edge = cyl_depth
side_one = 3
side_two = 5
delta1 = edge_dist+sph_rad
divisions = cyl_depth/(delta1)
partitions = (cyl_depth-2*(edge_dist+sph_rad))/(2*sph_rad+sph_sep)
#print 'partitions =',  partitions
#print 'side_one =', side_one
param = 0.5
count = 1
while param < 1.0:
        param = 1/divisions
#       print 'param =',param
        myModel.parts['pellet'].PartitionEdgeByParam(edges=(myModel.parts['pellet'].ed
                        ges[1],
                myModel.parts['pellet'].edges[side_one],
                myModel.parts['pellet'].edges[side_two]), parameter= (param))
        side_one = side_one+2
        side_two = side_two+2

#       print 'side_one = ', side_one
        shortened_edge_length = new_edge - delta1
#       print 'shortened_edge_length =' , shortened_edge_length
        delta1 = 2*sph_rad+sph_sep
        new_edge = shortened_edge_length
        divisions = shortened_edge_length/(2*sph_rad+sph_sep)
#       print 'divisions = ', divisions
        param = 1/divisions
        count = count+1
#       print 'count = ', count

print 'The number of sphere layers = ', count-2

myPelletPart = myModel.parts['pellet']
myCutterSketch = mdb.models['pellet']

# Loops to Cut Away the Holes for the Spheres
z = edge_dist+sph_rad
while z < cyl_depth-edge_dist-sph_rad:

        # This Command Creates the Actual Partition Planes at the Sphere Layers
        myPelletPart.PartitionCellByPlaneThreePoints(cells=(
                        myPelletPart.cells.findAt((0,0,z)), ),
```

```
                point1=myPelletPart.vertices.findAt((0,cyl_rad,z),),
                point2=myPelletPart.vertices.findAt((0,0,z),),
                point3=myPelletPart.vertices.findAt((cyl_rad,0,z)))

        deltax = 0   #coordinates at which the sphere cut outs are made
        deltay = 0

        while (deltax**2+deltay**2)**0.5+sph_rad+edge_dist < cyl_rad:  #loop moving
                in the x-direction

                myCutterSketch.Sketch(name='__profile__',sheetSize=20,
                        transform=myPelletPart.MakeSketchTransform(sketchPlane=
                        myPelletPart.faces.findAt((sph_rad+sph_sep/2,sph_rad+sph_sep/2,
                        z),), sketchPlaneSide=SIDE1,
                        sketchUpEdge=myPelletPart.edges.findAt((cyl_rad-0.05,0,z),),
                        sketchOrientation=RIGHT, origin=(0, 0, z)))

                myCutterSketch.sketches['__profile__'].sketchOptions.setValues(
                        constructionGeometry=ON, decimalPlaces=2,
                        dimensionTextHeight=0.5,
                        grid=ON, gridFrequency=2, gridSpacing=0.5, sheetSize=20.0)
                myPelletPart.projectReferencesOntoSketch(
                        filter=COPLANAR_EDGES,
                        sketch=myCutterSketch.sketches['__profile__'])

        while (deltax**2+deltay**2)**0.5+sph_rad+edge_dist < cyl_rad: #loop moving
                in the y-direction
#                       print'(x,y,z) =',deltax,deltay,z

# This part creates the ARC that is CUT out

        myCutterSketch.sketches['__profile__'].ArcByCenterEnds(center=(deltax,deltay),
                point1=(deltax,deltay-sph_rad), point2=(deltax,deltay+sph_rad))

        myCutterSketch.sketches['__profile__'].Line(point1=(deltax,deltay-sph_rad),
                point2=(deltax,deltay+sph_rad))

                        deltay = deltay + 2*sph_rad+sph_sep  #updating the y coordinate

# This part actually REVOLVES the ARC to CUT it out fully

        myCutterSketch.sketches['__profile__'].VerticalConstructionLine(point=(deltax,0
                ))

                myCutterSketch.parts['pellet'].CutRevolve(angle=360.0,
```

```
                        flipRevolveDirection=OFF, sketch=
                        myCutterSketch.sketches['__profile__'],
                        sketchOrientation=RIGHT,
                        sketchPlane=myCutterSketch.parts['pellet'].faces.
                        findAt((sph_rad+sph_sep/2,sph_rad+sph_sep/2,z),),
                        sketchPlaneSide=SIDE1,

        sketchUpEdge=myCutterSketch.parts['pellet'].edges.findAt((cyl_rad-0.05,0,z)))


                deltax = deltax-2*sph_rad-sph_sep   #updating the x value coordinate
                deltay = 0

        del mdb.models['pellet'].sketches['__profile__']
        z = z+(2*sph_rad+sph_sep)

print 'z =',z
print 'The matrix geometrical model has been completed.... Congratulations!'

#-------------------------------------------------------------------------

#  Drawing and partitioning the fourth, half and whole SPHERES for reinsertion
#  into the matrix material...

myFuelSketch = myModel.Sketch(name='fuel1',sheetSize=3.0)

#THIS MAKES THE WHOLE SPHERE WITH PARTITIONS
myModel.sketches['fuel1'].sketchOptions.setValues(
        constructionGeometry=ON, decimalPlaces=2, dimensionTextHeight=0.05,
         grid=ON, gridFrequency=2, gridSpacing=0.05, sheetSize=3.0)
myModel.sketches['fuel1'].ObliqueConstructionLine(point1=(0.0, -1.5), point2=(0.0,
        1.5))
myFuelSketch.ArcByCenterEnds(center=(0.0,0.0), point1=(0.0, -sph_rad), point2=(0.0,
        sph_rad))
myFuelSketch.Line(point1=(0.0, sph_rad), point2=(0.0, -sph_rad))
myModel.Part(dimensionality=THREE_D, name='fuel',type=DEFORMABLE_BODY)
myModel.parts['fuel'].BaseSolidRevolve(angle=360.0,flipRevolveDirection=OFF,
        sketch=myModel.sketches['fuel1'])
del myModel.sketches['fuel1']
myModel.parts['fuel'].PartitionCellByPlaneThreePoints(cells=(myModel.parts['fuel'].cell
        s[0], ),point1=myModel.parts['fuel'].vertices[1], point2=
        myModel.parts['fuel'].InterestingPoint(myModel.parts['fuel'].edges[0], MIDDLE),
        point3=myModel.parts['fuel'].vertices[0])
myModel.parts['fuel'].PartitionCellByPlanePointNormal(cells=(myModel.parts['fuel'].cell
        s[0], myModel.parts['fuel'].cells[1]),normal=myModel.parts['fuel'].datums[1],
```

```
        point=myModel.parts['fuel'].InterestingPoint(myModel.parts['fuel'].edges[1],
        MIDDLE))
myModel.parts['fuel'].PartitionCellByPlaneThreePoints(cells=(
        myModel.parts['fuel'].cells[0],myModel.parts['fuel'].cells[1],
         myModel.parts['fuel'].cells[2],myModel.parts['fuel'].cells[3]),point1
        =myModel.parts['fuel'].InterestingPoint(myModel.parts['fuel'].edges[1],
        MIDDLE), point2=myModel.parts['fuel'].vertices[2],point3
        =myModel.parts['fuel'].InterestingPoint(myModel.parts['fuel'].edges[2],
        MIDDLE))

#THIS MAKES THE HALF FUEL SPHERE WITH PARTITIONS
myModel.Sketch(name='__profile__', sheetSize=20.0)
myModel.sketches['__profile__'].sketchOptions.setValues(
        constructionGeometry=ON, decimalPlaces=2, dimensionTextHeight=0.5,
        grid=ON, gridFrequency=2, gridSpacing=0.5, sheetSize=20.0)
myModel.sketches['__profile__'].ObliqueConstructionLine(point1=(0.0, -1.5),
        point2=(0.0, 1.5))
myModel.sketches['__profile__'].ArcByCenterEnds(center=(0.0,0.0),
        point1=(0.0, sph_rad), point2=(0.0, -sph_rad))
myModel.sketches['__profile__'].Line(point1=(0.0, sph_rad), point2=(0.0, -sph_rad))

myFuelPart_half = myModel.Part(dimensionality=THREE_D, name='fuel_half',
         type=DEFORMABLE_BODY)

myFuelPart_half.BaseSolidRevolve(angle=180.0,flipRevolveDirection=OFF,
        sketch=myModel.sketches['__profile__'])
del myModel.sketches['__profile__']
myFuelPart_half.PartitionCellByPlaneNormalToEdge(cells=(myFuelPart_half.cells[0], ),
        edge=myFuelPart_half.edges[0],
        point=myFuelPart_half.InterestingPoint(myFuelPart_half.edges[0], MIDDLE))
mdb.models['pellet'].parts['fuel_half'].PartitionCellByPlaneThreePoints(cells=(
        mdb.models['pellet'].parts['fuel_half'].cells[0],
        mdb.models['pellet'].parts['fuel_half'].cells[1]),
        point1=mdb.models['pellet'].parts['fuel_half'].vertices[4],
        point2=mdb.models['pellet'].parts['fuel_half'].InterestingPoint(
        mdb.models['pellet'].parts['fuel_half'].edges[0], MIDDLE),
        point3=mdb.models['pellet'].parts['fuel_half'].vertices[3])


#THIS MAKES THE QUARTER FUEL SPHERE (WITH ONE PARTITION)
myModel.Sketch(name='__profile__', sheetSize=20.0)
myModel.sketches['__profile__'].sketchOptions.setValues(
        constructionGeometry=ON, decimalPlaces=2, dimensionTextHeight=0.5,
        grid=ON, gridFrequency=2, gridSpacing=0.5, sheetSize=20.0)
myModel.sketches['__profile__'].ObliqueConstructionLine(point1=(0.0, -1.5),
        point2=(0.0, 1.5))
```

```
myModel.sketches['__profile__'].ArcByCenterEnds(center=(0.0,0.0),
        point1=(0.0, sph_rad), point2=(sph_rad, 0.0))
myModel.sketches['__profile__'].Line(point1=(0.0, sph_rad), point2=(0.0, 0.0))
myModel.sketches['__profile__'].Line(point1=(0.0, 0.0), point2=(sph_rad, 0.0))
myFuelPart_fourth = myModel.Part(dimensionality=THREE_D, name='fuel_fourth',
        type=DEFORMABLE_BODY)

myFuelPart_fourth.BaseSolidRevolve(angle=180.0,flipRevolveDirection=OFF,
        sketch=myModel.sketches['__profile__'])
myModel.parts['fuel_fourth'].PartitionCellByPlaneThreePoints(
         cells=(myModel.parts['fuel_fourth'].cells.findAt((0,0,0)), ),
        point1=myModel.parts['fuel_fourth'].vertices.findAt((0,sph_rad,0),),
        point2=myModel.parts['fuel_fourth'].vertices.findAt((0,0,0),), point3=
        myModel.parts['fuel_fourth'].InterestingPoint(myModel.parts['fuel_fourth'].
        edges.findAt((0,0,sph_rad),), MIDDLE))
del myModel.sketches['__profile__']

print 'The quarter, half and full spheres have been made.....way to go!!'

#-------------------------------------------------
#  MATERIAL PROPERTIES SECTION
#-------------------------------------------------
from material import *
from section import *
myModel.setValues(absoluteZero=-273.15)

# **********************   Fuel Material Properties
myModel.Material('Uranium')
myModel.materials['Uranium'].Density(temperatureDependency=ON,
        table=((0.000010961,27),(0.000010929,127),(0.000010897,227),
        (0.000010865,327),(0.000010832,427),(0.0000108,527),(0.000010766,627),
        (0.000010733,727),(0.000010699,827),(0.000010664,927),(0.000010628,1027),
        (0.00001059,1127),(0.000010551,1227),(0.000010511,1327),(0.000010468,1427)
        ,(0.000010423,1527),(0.000010376,1627),(0.000010327,1727),
        (0.000010275,1827),(0.00001022,1927),(0.000010162,2027),(0.000010101,2127)
        ,(0.000010037,2227),(0.0000099698,2327),(9.8989E-06,2427),(9.8244E-
        06,2527),(9.7462E-06,2627),(9.6644E-06,2727),(9.5787E-06,2827)) )

myModel.materials['Uranium'].Expansion(temperatureDependency=ON,
        table=((9.7555E-06,27),(9.7841E-06,127),(9.8388E-06,227),
        (9.9196E-06,327),(1.0026E-05,427),(1.0159E-05,527),
        (1.0317E-05,627),(1.0515E-05,727),(1.0782E-05,827),
        (1.1120E-05,927),(1.1529E-05,1027),(1.2008E-05,1127),
        (1.2558E-05,1227),(1.3177E-05,1327),(1.3865E-05,1427),
        (1.4622E-05,1527),(1.5447E-05,1627),(1.6341E-05,1727),
        (1.7302E-05,1827),(1.8331E-05,1927),(1.9427E-05,2027),
```

```
        (2.0590E-05,2127),(2.1818E-05,2227),(2.3113E-05,2327),(2.4474E-05,2427),
        (2.5899E-05,2527),(2.7389E-05,2627),(2.8944E-05,2727),(3.0563E-05,2827)) )

myModel.materials['Uranium'].Conductivity(temperatureDependency=ON,
        table=((9760,27),(8058,127),(3850,400),(3570,500),(3430,600),(3350,700),
        (3190,800),(2990,900),(2790,1000),(2610,1100),(2450,1200),(2320,1300),
        (2220,1400),(2140,1500),(2090,1600),(2060,1700),(2060,1800),(2080,1900),
        (2120,2000),(2180,2100),(2260,2200),(2350,2300),(2450,2400),(2560,2500),
        (2680,2600),(2800,2700),(2930,2800)) )

myModel.materials['Uranium'].Elastic(temperatureDependency=ON,
        table=((164127450.9, 0.316, 0),(162280978.6, 0.316, 100),
        (160434506.4, 0.316, 200),(158588034.2, 0.316, 300),
        (156741562, 0.316, 400),(154895089.8, 0.316, 500),(153048617.6, 0.316, 600),
        (151202145.4, 0.316, 700),(149355673.2, 0.316, 800),(147509200.9, 0.316, 900),
        (145662728.7, 0.316, 1000),(143816256.5, 0.316, 1100),
        (141969784.3, 0.316, 1200), (140123312.1, 0.316, 1300),
        (138276839.9, 0.316, 1400),(136430367.7, 0.316, 1500),
        (134583895.5, 0.316, 1600),(132737423.2, 0.316, 1700),
        (130890951, 0.316, 1800),(129044478.8, 0.316, 1900),
        (127198006.6, 0.316, 2000) ))

myModel.materials['Uranium'].SpecificHeat(temperatureDependency=ON,
        table=((236580000, 27),(264320000, 127),(281530000, 227),
        (292990000, 327),(300710000, 427),(305840000, 527),
        (309180000, 627),(311400000, 727),(313060000, 827),
        (314650000, 927),(315660000, 1027),(319500000, 1127),
        (323570000, 1227),(329250000, 1327),(336880000, 1427),(346790000, 1527),
        (359260000, 1627),(374570000, 1727),(392970000, 1827),
        (414680000, 1927),(439890000, 2027),(468780000, 2127),
        (501510000, 2227),(538200000, 2327),(578960000, 2427),(623860000, 2527),
        (672970000, 2627),(726320000, 2727),(783920000, 2827)) )

myModel.materials['Uranium'].Swelling(table=((3.00247E-10, ), ))
myModel.materials['Uranium'].Plastic(table=((490500, 0), ))
#myModel.materials['Uranium'].Creep(law=HYPERBOLIC_SINE, table=((53111.11111
#       ,0.00014234, 0.6198, -100000, 1.987), ))

myModel.HomogeneousSolidSection(material='Uranium',name='uranium-section',
        thickness=1.0)

#**********************  Matrix Material Properties
myModel.Material('ss316L')
myModel.materials['ss316L'].Density(temperatureDependency=ON, table=(
        (7.95683E-06, 20),(7.92609E-06, 93),(7.87935E-06, 204),
        (7.83219E-06, 316),(7.78545E-06, 427),(7.73871E-06, 538),
```

```
        (7.69197E-06, 649),(7.64523E-06, 760),(7.5985E-06, 871),(7.55176E-06, 982)) )

myModel.materials['ss316L'].Expansion(table=((1.9400E-05, ), ))

myModel.materials['ss316L'].Conductivity(temperatureDependency=ON,
        table=((13574.61099, 21),(13887.60218, 38),(14402.9422, 66),
        (14918.05064, 94),(15414.52795, 121),(15929.13464, 149),
        (16443.46205, 177),(16957.4941, 205),(17471.21471, 233),
        (17966.27815, 260),(18479.34016, 288),(18992.04305, 316),
        (19504.37074, 344),(19998.0306, 371),(20509.57444, 399),
        (21020.69539, 427),(21531.37737, 455),(22041.60429, 483),
        (22533.1628, 510),(23042.44903, 538),(23551.23252, 566),
        (24059.49719, 594),(24549.10314, 621),(25056.30187, 649),
        (25562.9341, 677),(26068.98375, 705),(26556.39339, 732),
        (27061.25184, 760),(27565.48002, 788),(28069.06186, 816)) )

myModel.materials['ss316L'].Elastic(temperatureDependency=ON, table=(
        (196249570.5, 0.291472872, 24),(195203578.5, 0.292722205, 38),
        (193100523.7, 0.295195799, 66),(191058598.2, 0.297549392, 93),
        (188926548.3, 0.299957324, 121),(186779737.2, 0.302331827, 149),
        (84618165, 0.304672903, 177),(182519812, 0.306898709, 204),
        (180329244.7, 0.309174122, 232),(178123916.2, 0.311416107, 260),
        (175903826.5, 0.313624663, 288),(173668975.7, 0.315799791, 316),
        (171499961.2, 0.317865578, 343),(169236115.3, 0.319975043, 371),
        (166957508.2, 0.322051081, 399),(164664140, 0.32409369, 427),
        (162438698, 0.32603169, 454),(160116334.7, 0.328008637, 482),
        (157779210.2, 0.329952156, 510),(155427324.5, 0.331862246, 538),
        (153060677.7, 0.326883046, 566),(150764574.2, 0.335516888, 593),
        (148368932.3, 0.337327888, 621),(145958529.2, 0.339105459, 649),
        (143533365, 0.340849603, 677),(141180834, 0.342499796, 704),
        (138726674.7, 0.344178277, 732),(136257754.2, 0.34582333, 760),
        (133774072.5, 0.347434954, 788),(131275629.7, 0.34901315, 816),
        (128852437.2, 0.350503324, 843),(126324999.3, 0.352015857, 871)) )

myModel.materials['ss316L'].SpecificHeat(temperatureDependency=ON,
        table=((453275277.1, 20),(488885356.3, 93),(526386792.4, 204),
        (549252867.4, 316),(563094000, 427),(574145658.2, 538),
        (588381654.1, 649),(611775800.1, 760),(650301908.4, 871)) )


myModel.materials['ss316L'].Plastic(table=((2.32E+05,0, 27.0), ))
#myModel.materials['ss316L'].Creep(law=HYPERBOLIC_SINE, table=((8.09419E-05,
#       1.66793E-05, 1.0,-14000,1.987), ))

myModel.HomogeneousSolidSection(material='ss316L',
        name='ss316L-section', thickness=1.0)
```

```
import section
#  Assigning the Section Properties to the Parts
myModel.parts['pellet'].assignSection(region=Region(
        cells=myModel.parts['pellet'].cells[0:count-1]),sectionName='ss316L-section')
myModel.parts['fuel'].assignSection(region=Region(
        cells=myModel.parts['fuel'].cells[0:8]),sectionName='uranium-section')
myModel.parts['fuel_fourth'].assignSection(region=Region(
        cells=myModel.parts['fuel_fourth'].cells[0:2]),sectionName='uranium-section')
myModel.parts['fuel_half'].assignSection(region=Region(
        cells=mdb.models['pellet'].parts['fuel_half'].cells[0:4]),sectionName='uranium-
        section')

#--------------------------------------
# STEP MODULE, STEP ANALYSIS DEFINITION
#--------------------------------------

import step

#Modify these parameters below to change the step case, transient, s.s., creep, etc....

myModel.CoupledTempDisplacementStep(amplitude=RAMP, cetol=None,
creepIntegration=IMPLICIT_EXPLICIT,
        deltmx=None, description = 'step module part -- steady state',name='First
        Step',previous= 'Initial', response = STEADY_STATE)


#-----------------------------------------------------
#  ASSEMBLY OF SPHERES INTO THE MATRIX HOLES
#  THEN TYING NODES TOGETHER
#  THEN PUTTING A PRESSURE LOAD WITHIN SPHERES
#  THEN PUTTING HEAT GENERATION INTO THE SPHERES
#  ALL IN ONE BIG LOOPING LOOP
#-----------------------------------------------------

import assembly
import interaction
import load

myAssembly = mdb.models['pellet'].rootAssembly

myAssembly.DatumCsysByDefault(CARTESIAN)
myAssembly.Instance(name='matrix',part=mdb.models['pellet'].parts['pellet'])
myMatrix = myAssembly.instances['matrix']
print'matrix instance is placed'
```

```
z_pos = edge_dist+sph_rad
y_pos = 0
x_pos = 0
quarter = 1
half = 1
full = 1
while z_pos < cyl_depth-edge_dist-sph_rad:

        while (y_pos**2+x_pos**2)**0.5+sph_rad+edge_dist < cyl_rad:  # y loop

                while (x_pos**2+y_pos**2)**0.5+sph_rad+edge_dist < cyl_rad:  # x loop
#                       print'x,y,z =', x_pos,y_pos,z_pos
                        if x_pos==0 and y_pos==0:
                                fourth_name = 'fuel_forth-'+str(quarter)
                                myAssembly.Instance(name=fourth_name,part=myModel.
                                        parts['fuel_fourth'])
                                myAssembly.Instance(name=fourth_name,part=myModel.
                                        parts['fuel_fourth'])
                                myAssembly.instances[fourth_name].rotateAboutAxis(
                                        angle=90.0, axisDirection=(0.0, sph_rad, 0.0),
                                        axisPoint=(0.0, 0.0, 0.0))
                                myAssembly.instances[fourth_name].translate(vector=(0,
                                        0.0, z_pos))

                                tieFourth_name='quarter tied nodes-'+str(quarter)
                                myModel.Tie(adjust=ON, master=Region
                                        (side1Faces=myAssembly.instances[fourth_name].
                                        faces[2:4]),name=tieFourth_name,
                                        positionToleranceMethod=SPECIFIED,
                                        positionTolerance=tie_dist, slave=Region
                                        (side1Faces=myMatrix.faces.findAt
                                        (((sph_rad/2,sph_rad/2,z_pos-sph_rad/2**0.5),) )+\
                                        myMatrix.faces.findAt(((sph_rad/2,sph_rad/2,z_pos
                                        +sph_rad/2**0.5),) ),))
# Switch tie surfaces...
                                myModel.constraints[tieFourth_name].swapSurfaces()

                                pressFourth_name ='quarter pressure load-'+str(quarter)

#Pressure on matrix
                                myModel.Pressure(amplitude=UNSET,createStepName=
                                        'First Step',distribution=UNIFORM, magnitude =
                                        -pressure, name=pressFourth_name,region=Region
                                        (side1Faces=myMatrix.faces.findAt
                                        (((sph_rad/2,sph_rad/2,z_pos-sph_rad/2**0.5),) )+\
```

```
                                myMatrix.faces.findAt(((sph_rad/2,sph_rad/2,z_pos
                                +sph_rad/2**0.5),) ),))

#Pressure on spheres
                        #myModel.Pressure(amplitude=
                        #       UNSET,createStepName='First Step',distribution=
                        #       UNIFORM, magnitude = -pressure,
                        #       name=pressFourth_name,region=
                        #       Region(side1Faces=
                        #       myAssembly.instances[fourth_name].faces[2:4]))

                        heatgenFourth_name ='quarter heat gen -'+str(quarter)
                        myModel.BodyHeatFlux(createStepName='First Step',
                                magnitude=heat_gen, name=heatgenFourth_name,
                                region=Region(cells=myAssembly.instances
                                [fourth_name].cells[0:2]))

#                       print'quarter fuel is placed'
                        quarter = quarter + 1
                elif x_pos==0 or y_pos==0:
                        half_name = 'fuel_half-'+str(half)
                        if x_pos == 0:
                                myAssembly.Instance(name=half_name,part=
                                        myModel.parts['fuel_half'])
                                myAssembly.instances[half_name].rotateAboutAxis
                                        (angle=90.0, axisDirection=
                                        (0,2*sph_rad,0), axisPoint=
                                        (0.0, -sph_rad, 0.0))
                                myAssembly.instances[half_name].translate(vector
                                        =(x_pos,y_pos,z_pos))

                                tieHalf_name='half tied nodes-'+str(half)
                                myModel.Tie(adjust=ON,master=Region
                                        (side1Faces=myAssembly.instances
                                        [half_name].faces[2:4]+\myAssembly.
                                        instances[half_name].faces[8:10]),name=tie
                                        Half_name, positionToleranceMethod=
                                        SPECIFIED, positionTolerance=tie_dist,
                                        slave=Region(side1Faces=myMatrix.faces.
                                        findAt(((sph_rad/2**0.5,y_pos,z_pos-
                                        sph_rad/2**0.5),) )+\myMatrix.faces.
                                        findAt(((sph_rad/2**0.5,y_pos,z_pos+
                                        sph_rad/2**0.5),) ),))
                                #Swap tie surfaces
                                myModel.constraints[tieHalf_name].swapSurfaces()
```

```
                    pressHalf_name ='half pressure load '+str(half)
                    #Pressure on Matrix

                    myModel.Pressure(amplitude=UNSET,
                            createStepName='First Step',distribution=
                            UNIFORM, magnitude = -pressure,
                            name=pressHalf_name,region=
                            Region(side1Faces=myMatrix.faces.
                            findAt(((sph_rad/2**0.5,y_pos,
                            z_pos-sph_rad/2**0.5),)
                            )+\myMatrix.faces.findAt
                            (((sph_rad/2**0.5,y_pos,
                            z_pos+sph_rad/2**0.5),) ),))

                    #Pressure on Spheres
                    #myModel.Pressure(amplitude=UNSET,createSte
                            #Name='First Step',distribution=
                            #UNIFORM, magnitude = -pressure,
                            #name=pressHalf_name,region=
                            #Region(side1Faces=myAssembly.instances
                            #[half_name].faces[2:4]+\
                            #myAssembly.instances[half_name].
                            #faces[8:10]))
#                   print'half fuel part1 is placed'
                else:
                    myAssembly.Instance(name=half_name,part=
                            myModel.parts['fuel_half'])myAssembly.
                            instances[half_name].rotateAboutAxis
                            (angle=90.0,,axisDirection=(-2*sph_rad,0,
                            0), axisPoint=(sph_rad,0.0,0.0))
                    myAssembly.instances[half_name].translate(vector
                            =(x_pos,y_pos,z_pos))

                    tieHalf_name='half tied nodes-'+str(half)
                    myModel.Tie(adjust=ON,master=Region
                            (side1Faces=myAssembly.
                            instances[half_name].faces[2:4]+\
                            myAssembly.instances[half_name].faces
                            [8:10]),name=tieHalf_name,
                            positionToleranceMethod=SPECIFIED,
                            positionTolerance=tie_dist,
                            slave=Region(side1Faces=myMatrix.faces.
                            findAt(((x_pos,sph_rad/2**0.5,
                            z_pos-sph_rad/2**0.5),) )+\
```

```
                                    myMatrix.faces.findAt(((x_pos,sph_rad/2**0.5,
                                    z_pos+sph_rad/2**0.5),) ),))
                                    #Swap Tie surfaces
                                    myModel.constraints[tieHalf_name].swapSurfaces()
#                                   print'half fuel part2 is placed'

                                    pressHalf_name ='half pressure load-'+str(half)

                                    #Pressure on matrix

                                    myModel.Pressure(amplitude=UNSET,
                                            createStepName='First Step',distribution=
                                            UNIFORM, magnitude = -pressure,name=
                                            pressHalf_name,region=Region
                                            (side1Faces=myMatrix.faces.
                                            findAt(((x_pos,sph_rad/2**0.5,
                                            z_pos-sph_rad/2**0.5),) )+\

                                    myMatrix.faces.findAt(((x_pos,sph_rad/2**0.5,
                                            z_pos+sph_rad/2**0.5),) ),))

#Pressure on spheres
                                    #myModel.Pressure(amplitude=UNSET,createStep
                                    #       Name='First Step',distribution=
                                    #       UNIFORM, magnitude = -pressure,
                                    #        name=pressHalf_name,region=
                                    #        Region(side1Faces=myAssembly.instances
                                    #        [half_name].faces[2:4]+\
                                    #    myAssembly.instances[half_name].faces[8:10]))

                                heatgenHalf_name ='half heat gen -'+str(half)
                                myModel.BodyHeatFlux(createStepName='First Step',
                                        magnitude=heat_gen, name=heatgenHalf_name,
                                        region=Region(cells=myAssembly.instances
                                        [half_name].cells[0:4]))
                                half = half+1
                            else:
                                full_name = 'fuel_full-'+str(full)

                                myAssembly.Instance(name=full_name,part=myModel.
                                        parts['fuel'])

                                myAssembly.instances[full_name].translate(vector=
                                (x_pos,y_pos,z_pos))
```

```
                    tiefull_name='full tied nodes-'+str(full)
                    myModel.Tie(adjust=ON,master=Region(side1Faces=
                        myAssembly.instances[full_name].faces[4:6]+\
                        myAssembly.instances[full_name].faces[8:9]+\
                        myAssembly.instances[full_name].faces[10:11]+\
                        myAssembly.instances[full_name].faces[14:16]+\
                        myAssembly.instances[full_name].faces[18:20]),
                        name=tiefull_name,positionToleranceMethod=
                        SPECIFIED,positionTolerance=tie_dist,
                        slave=Region(side1Faces=myMatrix.faces.
                        findAt(((x_pos+sph_rad/2**0.5,y_pos,
                        z_pos-sph_rad/2**0.5),) )+\myMatrix.faces.findAt
                        (((x_pos+sph_rad/2**0.5,y_pos,z_pos+
                        sph_rad/2**0.5),) ),))
# Swap tie surfaces..
                    myModel.constraints[tiefull_name].swapSurfaces()

                    pressFull_name ='full pressure load-'+str(full)

#Pressure on Matrix
                    myModel.Pressure(amplitude=UNSET,createStepName=
                        'First Step',distribution=UNIFORM, magnitude =
                        -pressure, name=pressFull_name,region=
                         Region(side1Faces=myMatrix.faces.
                         findAt(((x_pos+sph_rad/2**0.5,y_pos,
                        z_pos-sph_rad/2**0.5),) )+\myMatrix.faces.findAt
                        (((x_pos+sph_rad/2**0.5,y_pos,
                        z_pos+sph_rad/2**0.5),) ),))

#Pressure on Spheres
                    # myModel.Pressure(amplitude=UNSET,createStepName=
                        #'First Step',distribution=UNIFORM, magnitude =
                        #-pressure, name=pressFull_name,region=
                        #Region(side1Faces=myAssembly.instances
                        #[full_name].faces[4:6]+\
                        # myAssembly.instances[full_name]. faces[8:11]+\
                         #myAssembly.instances[full_name].faces[14:16]+\
                         #myAssembly.instances[full_name].faces[18:20]))

                    heatgenFull_name ='full heat gen-'+str(full)
                    myModel.BodyHeatFlux(createStepName='First Step',
                        magnitude=heat_gen, name=heatgenFull_name,
                        region=Region(cells=myAssembly.instances
                        [full_name].cells[0:8]))
#                   print'full fuel sphere is placed'
                    full = full+1
```

```
                        x_pos=x_pos+2*sph_rad+sph_sep
#                       print'end x loop'
                y_pos=y_pos+2*sph_rad+sph_sep
                x_pos = 0
#               print'end y loop'
        z_pos = z_pos+2*sph_rad+sph_sep
        x_pos = 0
        y_pos = 0
#       print'end z loop'
print'You are great, you got it to work!!!'
```

APPENDIX B

Material Properties of UO_2, PuO_2, Zirconium, and Stainless Steel 316L

Table B.1. Thermal Conductivity in terms of Temperature for UO_2, PuO_2, Zr, SS-316L

THERMAL CONDUCTIVITY [41, 33, 18, 7]

Temp. (°C)	UO_2 (W/m°C)	Temp. (°C)	PuO_2 (W/m°C)	Temp. (°C)	Zr (W/m°C)	Temp. (°C)	SS -316L (W/m°C)
27	6.84	0	6.045	0	12.29	21	13.6
127	5.25	100	4.771	100	13.69	38	13.9
400	3.85	200	3.940	200	14.96	66	14.4
500	3.57	300	3.356	300	16.17	94	14.9
600	3.43	400	2.923	400	17.35	121	15.4
700	3.35	500	2.588	500	18.54	149	15.9
800	3.19	600	2.323	600	19.81	177	16.4
900	2.99	700	2.107	700	21.18	205	17.0
1000	2.79	800	1.928	800	22.72	233	17.5
1100	2.61	900	1.780	900	24.45	260	18.0
1200	2.45	1000	1.656	1000	26.44	288	18.5
1300	2.32	1100	1.555	1100	28.72	316	19.0
1400	2.22	1200	1.476	1200	31.35	344	19.5
1500	2.14	1300	1.420	1300	34.36	371	20.0
1600	2.09	1400	1.388	1400	37.81	399	20.5
1700	2.06	1500	1.381	1500	41.73	427	21.0
1800	2.06	1600	1.401	1600	46.19	455	21.5
1900	2.08	1700	1.448	1700	51.21	483	22.0
2000	2.12	1800	1.524	1800	56.85	510	22.5
2100	2.18	1900	1.626	1900	63.16	538	23.0
2200	2.26	2000	1.757	2000	70.17	566	23.6
2300	2.35					594	24.1
2400	2.45					621	24.5
2500	2.56					649	25.1
2600	2.68					677	25.6
2700	2.8					705	26.1
						732	26.6
						760	27.1
						788	27.6
						816	28.1

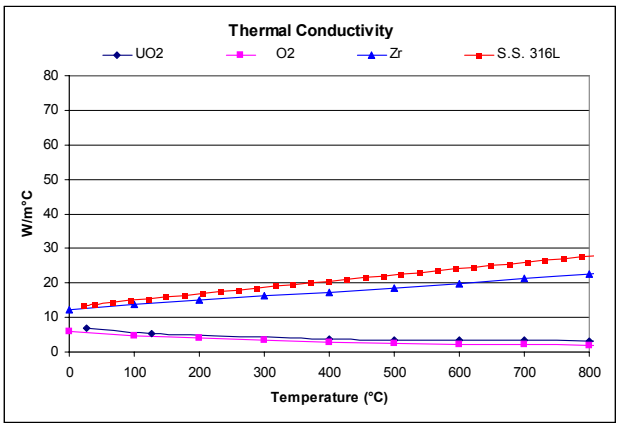

Figure B.1. Thermal Conductivity vs. Temperature

Table B.2. Density of UO_2, PuO_2, Zr, SS-316L in terms of Temperature

DENSITY [41, 51, 7]

Temp. (°C)	UO_2 (kg/m^3)	Temp. (°C)	PuO_2 (kg/m^3)	Temp. (°C)	Zr (kg/m^3)	Temp. (°C)	SS -316L (kg/m^3)
27	10961	0	11460	27	6510	20	7957
127	10929	27	11451	862	6415	93	7926
227	10897	127	11417			204	7879
327	10865	227	11384			316	7832
427	10832	327	11350			427	7785
527	10800	427	11316			538	7739
627	10766	527	11282			649	7692
727	10733	627	11247			760	7645
827	10699	650	11239			871	7599
927	10664	650	11239			982	7552
1027	10628	727	11212				
1127	10590	827	11177				
1227	10551	927	11140				
1327	10511	1027	11103				
1427	10468	1127	11066				
1527	10423	1227	11027				
1627	10376	1327	10988				
1727	10327	1427	10947				
1827	10275	1527	10906				
1927	10220	1627	10863				
2027	10162	1727	10819				
2127	10101	1827	10774				
2227	10037	1927	10727				
2327	9969.8	2027	10679				
2427	9898.9						
2527	9824.4						
2627	9746.2						
2727	9664.4						
2827	9578.7						

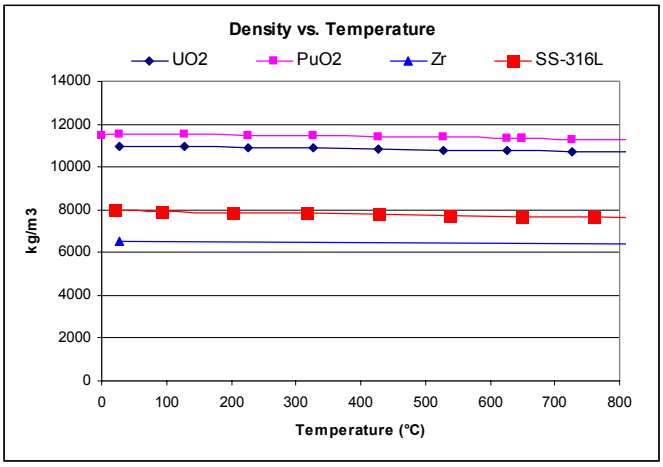

Figure B.2. Density vs. Temperature

Table B.3. Thermal Expansion of UO_2, PuO_2, Zr, SS-316L as a function of Temperature

THERMAL EXPANSION [41, 59, 53, 7]

Temp. (°C)	UO_2 ($°C^{-1}$)	Temp. (°C)	PuO_2 ($°C^{-1}$)	Temp. (°C)	Zr ($°C^{-1}$)	Temp. (°C)	SS -316L ($°C^{-1}$)
27	9.756E-06	-73	9.42E-06	117	5.64E-06	59	1.540E-05
127	9.784E-06	127	1.02E-05	160	5.55E-06	93	1.559E-05
227	9.839E-06	327	1.15E-05	212	5.74E-06	149	1.579E-05
327	9.920E-06	527	1.27E-05	243	5.69E-06	204	1.598E-05
427	1.003E-05	727	1.44E-05	286	5.97E-06	260	1.618E-05
527	1.016E-05			326	7.22E-06	316	1.639E-05
627	1.032E-05			364	8.28E-06	371	1.658E-05
727	1.052E-05			402	9.61E-06	399	1.678E-05
827	1.078E-05			425	1.01E-05	427	1.696E-05
927	1.112E-05			428	9.60E-06	454	1.713E-05
1027	1.153E-05			432	8.42E-06	482	1.730E-05
1127	1.201E-05			437	7.38E-06	510	1.745E-05
1227	1.256E-05			442	6.57E-06	538	1.758E-05
1327	1.318E-05			447	5.79E-06	566	1.770E-05
1427	1.387E-05			452	5.44E-06	593	1.780E-05
1527	1.462E-05			460	5.03E-06		
1627	1.545E-05			480	4.80E-06		
1727	1.634E-05						
1827	1.730E-05						
1927	1.833E-05						
2027	1.943E-05						
2127	2.059E-05						
2227	2.182E-05						
2327	2.311E-05						
2427	2.447E-05						
2527	2.590E-05						
2627	2.740E-05						
2727	2.894E-05						
2827	3.056E-05						

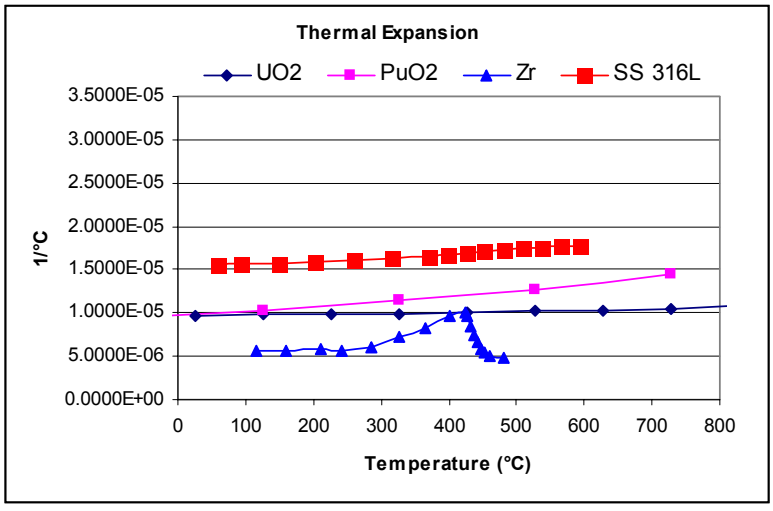

Figure B.3. Thermal Expansion vs. Temperature

Table B.4. Young's Modulus and Poisson's ratio of UO_2, PuO_2, Zr, SS-316L

YOUNG'S MODULUS [18, 51, 7]

Temp. (°C)	UO_2 (GPa)	Temp. (°C)	PuO_2 (GPa)	Temp. (°C)	Zr (GPa)	Temp. (°C)	SS -316L (GPa)
0	164	0	172	27	95.8	24	196
100	162	100	170	93	90.3	38	195
200	160	200	168	205	83.4	66	193
300	158	300	167	316	75.8	93	191
400	157	400	165	427	68.9	121	189
500	155	500	163	537	61.4	149	187
600	153	600	161	649	53.8	177	185
700	151	700	159			204	183
800	149	800	157			232	180
900	148	900	156			260	178
1000	146	1000	153			288	176
1100	144	1100	151			316	174
1200	142	1200	149			343	172
1300	140	1300	147			371	169
1400	138	1400	145			399	167
1500	136	1500	143			427	165
1600	135	1600	141			454	162
1700	133	1700	139			482	160
1800	131	1800	137			510	158
1900	129	1900	135			538	155
2000	127	2000	134			566	153
						593	151
						621	148
						649	146
						677	144
						704	141
						732	139
						760	136
						788	134
						816	131
						843	129
						871	126

POISSON'S RATIO (all temps)

UO_2	0.316
PuO_2	0.276
Zr	0.340
SS316L	0.323

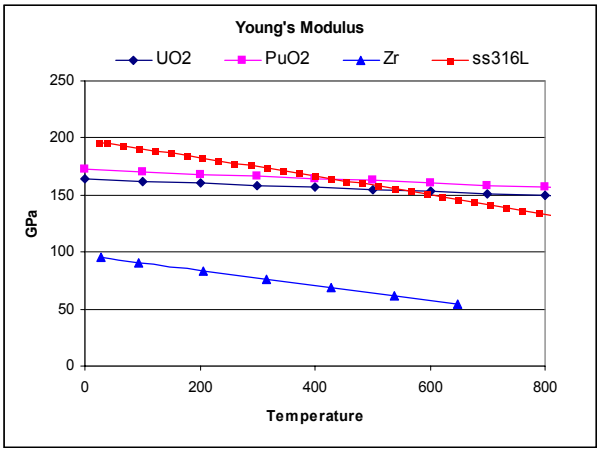

Figure B.4. Young's Modulus vs. Temperature

Table B.5. Yield Strength of UO_2, PuO_2, Zr ,SS-316L as a function of temperature

YIELD STRENGTH [7, 51, 49, 2]

Temp. (°C)	Zr (MPa)	UO_2 (all Temps)	Temp. (°C)	SS -316L (MPa)
37.77	468.8	490.5 MPa	25	231.9
148.9	330.9		50	216.3
260.0	234.4	PuO_2 (all Temps)	75	202.9
371.1	179.3	490.5 MPa	100	191.4
482.2	151.7		125	181.4
			150	172.7
			175	165.1
			200	158.6
			225	152.8
			250	147.8
			275	143.4
			300	139.6
			325	136.2
			350	133.3
			375	130.6
			400	128.3
			425	126.1
SWELLING OF UO_2 [32]			450	124.2
(and assumed for PuO_2)			475	122.4
			500	120.7
0.77 ΔV/V per 10 GWd/MTU			525	119.1
			550	117.5
			575	115.9
			600	114.3
			625	112.6
			650	110.8

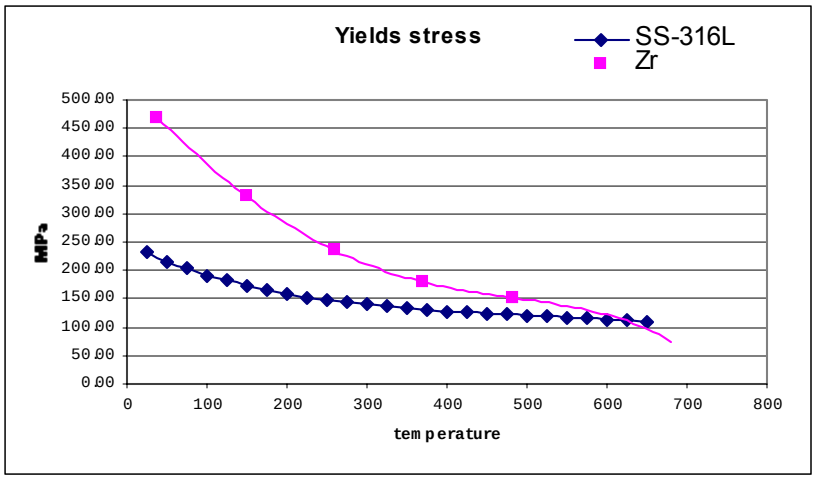

Figure B.5. Yield Stress vs. Temperature

Table B.6. Specific Heat of UO2, PuO2, Zr, SS-316L in terms of Temperature

SPECFIC HEAT [18, 7, 41]

Temp. (°C)	UO_2 (J/kg°C)	Temp. (°C)	PuO_2 (J/kg°C)	Temp. (°C)	Zr (J/kg°C)	Temp. (°C)	SS -316L (J/kg°C)
27	236.6	127	259.2	27	281	20	453.3
127	264.3	227	294.1	127	302	93	488.9
227	281.5	327	312.2	367	331	204	526.4
327	293.0	427	322.6	817	375	316	549.3
427	300.7	527	329.0	820	502	427	563.1
527	305.8	627	333.3	840	590	538	574.1
627	309.2	727	336.3	860	615	649	588.4
727	311.4	827	338.5	880	719	760	611.8
827	313.1	927	340.1	900	816	871	650.3
927	314.7	1027	341.4	920	770		
1027	315.7	1127	342.4	940	619		
1127	319.5	1227	343.2	960	469		
1227	323.6	1327	343.9	975	356		
1327	329.3	1427	344.5				
1427	336.9	1527	345.1				
1527	346.8	1627	345.8				
1627	359.3	1727	346.5				
1727	374.6	1827	347.5				
1827	393.0	1927	348.7				
1927	414.7	2027	350.4				
2027	439.9						
2127	468.8						
2227	501.5						
2327	538.2						
2427	579.0						
2527	623.9						
2627	673.0						
2727	726.3						
2827	783.9						

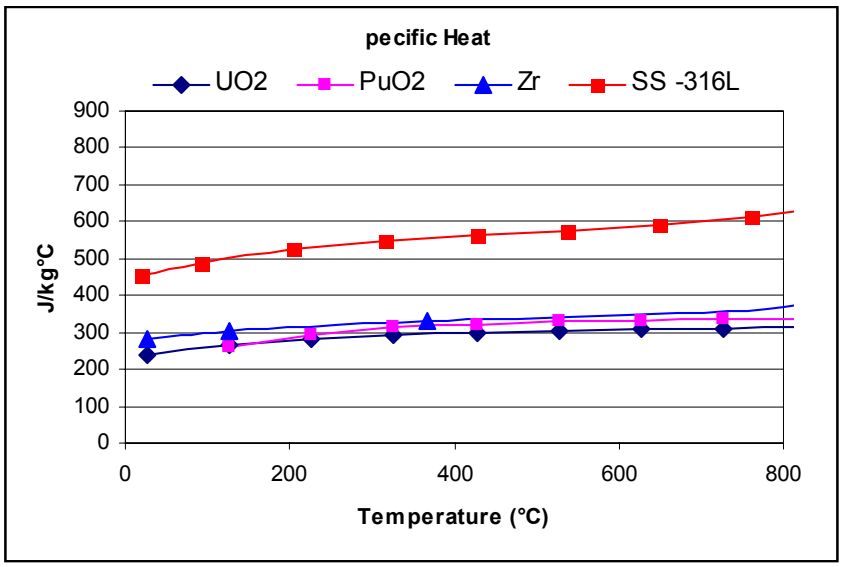

Figure B.6. Specific Heat vs. Temperature

REFERENCES

1. ABAQUS Help Manual. 2002.

2. Bocek, M., Faisst, G., and C. Petersen. "Examination of the Plastic Properties of Zircaloy-4 at Elevated Temperatures in Air Atmosphere." Journal of Nuclear Materials. Vol. 62, 1976: pp 26 – 36.

3. Bement, A.L., and Franklin, and Lucas (Eds.). Creep of Zirconium Alloys in Nuclear Reactors. American Society for Testing and Materials. 1983.

4. Berna, G.A., et al. "FRAPCON-3: A Computer Code for the Calculation of Steady State, Thermal Mechanical Behavior of Oxide Fuel Rods for High Burnup." NUREG / CR – 6534, Vol. 2, PNNL – 11513. December 1997.

5. Callister, William. Materials Science and Engineering: An Introduction. New York: John Wiley and Sons Inc. 2000. 5th ed.

6. Canon, R.F., and J.T.A. Roberts and R.J. Beals. "Deformation of UO_2 at High Temperatures." Journal of the American Ceramic Society. Vol. 54, no. 2. Feb. 1971: p105 – 112.

7. Cullen, David. Material Properties of Stainless Steel 316L. Argonne National Laboratory – West. July 2003.

8. Downar, Thomas, et al. "Thoria – Based Cermet Nuclear Fuel: Neutronics Fuel Design and Fuel Cycle Analysis." Proceedings of ICONE10. Arlington, VA; April 14 – 18, 2002.

9. Duderstadt, James, and Louis Hamilton. Nuclear Reactor Analysis. New York: John Wiley and Sons Inc. 1976.

10. Frost, Brian, R.T. (ed.). Material Science and Technology: A Comprehensive Treatment. Volume 10A: Nuclear Materials, Part 1. April 1994.

11. Frost, B.R.T. "Fast Reactor Fuels." Nuclear Engineering. Vol 9, no. 93. Feb. 1964: pp 55 – 67.

12. Frost, B.R.T. Nuclear Fuel Elements. Oxford: Pergamon Press, 1982.

13. Frost, B.R. T. and Wait. "Research on the Fabrication Properties and Irradiation Behavior of Plutonium Fuels for the UK Reactor Program." Plutonium as a Power Reactor Fuel. Proceedings of the ANS topical meeting; Richland, MA. Sept. 13 – 14, 1962: pp 4.1 – 4.38.

14. "Fuel Design Data." Nuclear Engineering International. September, 2002, p. 20 – 23.
15. Gibby, R.L. "The Effect of Plutonium Content on the Thermal Conductivity of (U,Pu)O2 Solid Solutions." Journal of Nuclear Materials. Vol. 38, 1971: pp163 – 177.

16. Glasstone, S. and Sesonske, A. Nuclear Reactor Engineering. New York: Chapman and Hall, Inc. 1994, 5th ed, Vol. 1.

17. Goslee, David, E. "Improving Performance of Stainless Steel – UO_2 Cermet Fuels." Nucleonics. Vol. 21, no. 7. July 1963: pp. 48 – 52.

18. Hagrman, D.L., and G.A. Reymann, and R.E. Mason. MATPRO Version 11 (Revision 2): A Handbook of Materials Properties for Use in the Analysis of Light Water Reactor Fuel Rod Behavior. NUREG / CR – 0479 rev 2. Idaho National Engineering Laboratory: Idaho Falls. August 1981.

19. Hayes, V.O., Neill, F.H., Schaffer, L.D., "Summary of UO_2 – stainless steel dispersion irradiation experiments. ORNL–CF–58–2–71. (March 18, 1958).

20. Higgy, H.R. and F.H. Hammad. "Effect of Neutron Irradiation on the Tensile Properties of Zircaloy-2 and Zircaloy-4." Journal of Nuclear Materials. Vol. 44. 1972: pp 215 – 227.

21. Hilbert, R.F., et al. "Mechanisms of Swelling and Gas Release in Uranium Dioxide." Journal of Nuclear Materials. Vol. 38. 1971: pp 26 – 34.

22. Hilton, B. Argonne National Laboratory – West. Personal Communication. October 1, 2003.

23. Holden, A.N. Ceramic Fuel Elements. New York: Gordon and Breach Science Publishers, Inc. 1966.

24. Holden, A.N. Dispersion Fuel Elements. New York: Gordon and Breach Science Publishers, Inc., 1967.

25. Ibrahim, I.A., Mohammed, F.A., Lavernia, E.J. "Particulate reinforced metal matrix composites – a review." Journal of Materials Science. Vol. 26, 1991: pp 1137 – 1156.

26. Ivans, W. "Neutronics Feasibility Study of Plutonium Oxide Dispersion Fuel in an Inert Zirconium Matrix." Office of Science, SULI Program. Argonne National Laboratory – West. August 1, 2003.

27. Kasemeyer, U., et al. "The Irradiation of Inert – Matrix Fuel in comparison to Uranium Plutonium Mixed Oxide Fuel at the Halden Reactor." Progress in Nuclear Energy. Vol. 38, no. 3–4. 2001: pp 309 – 312.

28. Keller, Donald, L., et al. "High Temperature Irradiation Test of UO_2 Cermet Fuels." BMI – 1608 (Jan. 7, 1963).

29. Keller, Donald, L. "Predicting Burnup of Stainless – UO_2 Cermet Fuels." Nucleonics. Vol. 19, no. 6. June 1961: pp. 45 – 48.

30. Lambert, J.D.B. "Irradiation Stability of Dispersion Fuels." Transactions of the British Ceramic Society. Vol. 62, no. 247. 1963: pp. 247 – 255.

31. Lambert, J.D.B. "Irradiation Study of UO_2–Stainless Steel and $(U,Pu)O_2$–Stainless Steel Cermet Fuels in Rod and Plate Geometry." High Temperature Nuclear Fuels. Metallurgical Society Conferences. Vol. 42, pp 237 – 254. New York: Gordon and Breach Science Publishers, 1966

32. Lanning, D.D. and C.E. Beyer, and C.L. Painter. "FRAPCON-3: Modifications to Fuel Rod Material Properties and Performance Models for High Burnup Application." NUREG / CR – 6534, Vol. 1, PNNL – 11514. December 1997.

33. Long, Y., and Y. Zhang, and M.S. Kazimi. "Inert Matrix Materials as Hosts of Actinide Nuclear Fuels." (Report MIT-NFC-TR-055). Dept. Nuclear Engineering, Massachusetts Institute of Technology. March 2003.

34. Manzel, R, and C.T. Walker. "EPMA and SEM of Fuel Samples from PWR Rods with an Average Burn-up of around 100 MWd/kgHM." Journal of Nuclear Materials. Vol. 301. 2002: pp 170 – 182.

35. McDeavitt, Sean, et al. "Thoria – Based Cermet Nuclear Fuel: Cermet Fabrication and Behavior Estimates." Proceedings of ICONE10. Arlington, VA; April 14 – 18, 2002.

36. Meyer, M. Personal Communication. Argonne National Laboratory – West. July 2003.

37. Morris, R.N., et al. "MOX Average Power 30 GWd/MT PIE: Final Report – Chapter 3." ORNL / MD / LTR – 212. 2002.

38. Olander, D. Fundamental Aspects of Nuclear Reactor Fuel Elements. Oak Ridge, TN: Technical Information Center, 1976.

39. Paprocki, Stan, J., et al. "Fabrication and Irradiation of SM-2 Core Materials." BMI – 1528 (July 12, 1961).

40. Perrin, J.S. "Effect of Irradiation on Creep of UO_2–PuO_2." Journal of Nuclear Materials. Vol. 42. 1972: pp 101 – 104.

41. Popov, S.G., et al. "Thermophysical Properties of MOX and UO2 Fuels Including the Effects of Irradiation." ORNL / TM – 2000 / 351. November 2000.

42. Reynaud, S.M. "Nitride Fuel Performance." Masters Thesis. Dept. of Nuclear Engineering, Texas A & M University. May 2002.

43. Roberts, J.T.A. and Y. Ueda. "Influence of Porosity on Deformation and Fracture of UO_2. Journal of the American Ceramic Society. Vol. 55, no. 3. 1972: p117 – 124.

44. Samoilov, A.G., and A. Kashtanov, and V. Volkov. Dispersion-Fuel Nuclear Reactor Elements. Translated from Russian. Jerusalem: Israel Program for Scientific Translations, 1968

45. Seltzer, M.S., et al. "A Review of Creep Behavior of Ceramic Nuclear Fuels." Reactor Technology. Vol. 14, no. 2. 1971: pp 99 -133.

46. Solomon, A.A., and J.L. Routbort, and J.C. Voglewede. "Fission Induced Creep of UO_2 and its Significance to Fuel-Element Performance." ANL-7857, Metals, Ceramics and Materials. September 1971.

47. Stehle, H., and H. Assmann and F. Wunderlich. "Uranium Dioxide Properties for LWR Fuel Rods." Nuclear Engineering and Design. Vol. 33. 1975: pp 230 – 260.

48. Stora, J.P. "Thermal Conductivity of Two Phase Solid Bodies." Nuclear Technology. Vol. 17, March 1973.

49. Tachibana, Toshimichi, and H. Furuya and M. Koizumi. "Dependence on Strain Rate and Temperature Shown by Yield Stress of Uranium Dioxide." Journal of Nuclear Science and Technology. Vol. 13, no. 9. Sept. 1976: pp 497-502.

50. Thurber, W.C., et al. "Irradiation Testing of Fuel for Core B of the Enrico Fermi Fast Breeder Reactor." ORNL – 3709 (Nov. 27, 1964)

51. Tipton, C.R. (Ed.) Reactor Handbook. Vol. 1 "Materials," 2nd ed. Interscience Publishers Inc., New York, 1960.

52. Todreas, N. and Kazimi, M. Nuclear Systems 1 – Thermal Hydraulic Fundamentals. Hemisphere Publishing Co., 1990.

53. Touloukian, Y.S., et al. "Thermal Expansion – Metallic Elements and Alloys." Thermophysical Properties of Matter. IFI/Plenum, New York, Vol 12, p1316.

54. Weber, C.E. and H. H. Hirsch. "Dispersion-Type Fuel Elements." International Conference on the Peaceful Uses of Atomic Energy. Vol. 9, p196 (United Nations, New York, 1956).

55. Weber, C.E. "Progress on Dispersion Elements." Progress in Nuclear Energy. Series 5. *Metallurgy and Fuels.* Vol. 2. 1959.

56. Weber, C.E. "Fuel Element Design." Journal of Metals. May 1956: pp 651 – 654.

57. Weir, J.R. "A Failure Analysis for the Low-Temperature Performance of Dispersion Fuel Elements." ORNL – 2902 (Jun 15, 1960).

58. White, D.W., and A.P. Beard and A.H. Willis. "Irradiation Behavior of Dispersion Fuels." Paper presented at the Fuels Elements Conference. KAPL–P – 1849: Paris, (Nov. 18-23, 1957).

59. Yemel'yanov, V.S., and Yevstyukhin, A.I. The Metallurgy of Nuclear Fuel. Pergamon Press, Oxford, 1969.

60. Young, Warren, C. Roark's Formulas for Stress and Strain. McGraw – Hill Inc., New York, 6th ed., 1989.

61. Yuan, Y., and H.C. No, and M.S. Kazimi. "A Preliminary Investigation of Performance of Rock-like Oxide Fuel for High Burnup in LWRs." (Report MIT-NFC-TR-037). Dept. of Nuclear Engineering, Massachusetts Institute of Technology. December 2001.